EUROPEAN ORGANISATION FOR NUCLEAR RESEARCH (CERN)

Submitted to: JHEP

CERN-EP-2018-334
6th March 2019

Constraints on mediator-based dark matter and scalar dark energy models using $\sqrt{s} = 13$ TeV pp collision data collected by the ATLAS detector

The ATLAS Collaboration

Constraints on selected mediator-based dark matter models and a scalar dark energy model using up to 37 fb^{-1} $\sqrt{s}$ = 13 TeV pp collision data collected by the ATLAS detector at the LHC during 2015–2016 are summarised in this paper. The results of experimental searches in a variety of final states are interpreted in terms of a set of spin-1 and spin-0 single-mediator dark matter simplified models and a second set of models involving an extended Higgs sector plus an additional vector or pseudo-scalar mediator. The searches considered in this paper constrain spin-1 leptophobic and leptophilic mediators, spin-0 colour-neutral and colour-charged mediators and vector or pseudo-scalar mediators embedded in extended Higgs sector models. The results are also interpreted for the first time in terms of light scalar particles that could contribute to the accelerating expansion of the universe (dark energy).

Contents

1 Introduction

The existence of a non-luminous component of matter and the origin of the accelerating expansion of the universe are two major unknowns in our current understanding of the universe.

The existence of dark matter (DM) is supported by a variety of astrophysical measurements, ranging from the rotational speed of stars in galaxies, over precision measurements of the cosmic microwave background [1, 2], to gravitational lensing measurements [3–5]. However, the nature and properties of the DM remain largely unknown. Searches for particle DM are performed using different complementary approaches: the measurement of elastic scattering of DM by nuclei and electrons in a detector [6–14], the detection of Standard Model (SM) particles produced in the annihilations or decays of DM in the universe [15–19], the production of DM particles at colliders [20–38], and the study of the effect of DM interactions on astrophysical systems [39, 40]. Another major unknown in the physics of our universe, beside the nature of DM, is the origin of its accelerating expansion [41, 42]. In the context of a homogeneous and isotropic universe, this implies the existence of a repulsive force, which causes the universe to expand at an accelerating rate [43]. Assuming general relativity, one of the simplest explanation for this repulsive force is a new type of matter which mimics a constant energy density, thus dubbed dark energy (DE). The effect of DE on cosmological scales is studied by measuring the redshift–distance relation using supernovae, baryon acoustic oscillations, the matter power spectrum and the cosmic microwave background, as well as gravitational lensing [44]. On microscopic scales, DE is probed by laboratory experiments searching for additional gravitational forces that would lead to deviations from the $1/r^2$ law [45–53]. Multi-messenger astronomical observations also provide important information for understanding the nature of DE [54–56].

The work reported in this paper considers the hypothesis that the DM is composed of a weakly interacting massive particle (WIMP) [57]. For some parameter choices and assumptions, WIMPs can account for the relic density of non-relativistic matter in the early universe [58] measured in data from the Planck [2] and WMAP [1] experiments. For benchmarking purposes it is assumed that WIMPs are Dirac fermions in all models considered in this paper. For most of these models, WIMPs are pair-produced in pp collisions at the Large Hadron Collider (LHC) [59]. These particles, denoted by the symbol χ throughout this paper, are stable over cosmological scales and do not interact with the detector. To identify events with DM, additional particle(s), X = jet, γ, W, Z, h, $(t)\bar{t}$, $(b)\bar{b}$, need to be produced in association with DM in a pp collision, in order to tag the event and measure the recoiling WIMPs as missing transverse momentum (with magnitude $E_{\mathrm{T}}^{\mathrm{miss}}$). If the DM candidates can be produced at the LHC via an s-channel exchange of a new particle, then this mediator could also decay back into SM final states: resonance searches can therefore also be used to constrain DM models. The interplay of resonance and $X + E_{\mathrm{T}}^{\mathrm{miss}}$ searches depends on the specific model choice and is further outlined in this paper. In the models considered, some of which are new with respect to previous ATLAS publications, one or more new particles mediate the interaction of DM with the SM particles. The first category considers simplified models mediated by a vector, axial-vector, scalar or pseudo-scalar mediator. In the case of simplified vector and scalar mediators, different types of interactions are explored (baryon-charged, neutral-flavour-changing and coloured interactions). The second category considers less simplified models involving an extended Higgs sector plus an additional mediator, either a vector or a pseudo-scalar particle. The assumptions and choices of the considered models closely follow the work of the DM Forum/LHC DM Working Group [60–63].

Theories such as R-parity-conserving supersymmetry [64–67] can also provide a viable WIMP DM candidate. These models are examined using a wide range of experimental signatures [68–75] in searches performed by the ATLAS Collaboration and are not included in this paper.

Furthermore, analyses focusing on signatures compatible with (unstable) long-lived particles decaying in the detector volume are also not considered in this paper [76].

Results from particle physics experiments may be used to help elucidate the microscopic nature of DE [77, 78]. Hadron collider data considering $X + E_{\mathrm{T}}^{\mathrm{miss}}$ final states are used to constrain Horndeski models of DE [79] in an effective field theory (EFT) framework [80].

This paper aims to provide an overview of the experimental programme of ATLAS searches [81] for mediator-based DM production performed to date using 13 TeV proton–proton collisions delivered by the LHC in 2015 and 2016. The studies presented in this paper use public ATLAS results. Since no significant excess over the expected SM background was found in any of these analyses, the results are used to constrain the available phase space for DM models. Furthermore, DE models are also constrained using these analyses.

The paper is structured as follows. The DM and DE models considered in this paper are outlined in Section 2, while the data and simulation samples are described in Section 3. The data analyses for each different signature are briefly described in Section 4, where the complementarity of different final states is also discussed. Finally, the dominant systematic uncertainties affecting the modelling of the signal samples are highlighted in Section 5 and the results are presented in Section 6, followed by the conclusions (Section 7).

2 Theoretical framework

All DM results presented in this paper are interpreted in the framework of simplified DM models [60, 63, 82–85], where a new particle (or set of particles) mediates the interaction of DM with the SM particles. These DM simplified models, which overcome some of the shortcomings of previous EFT-based DM models [84, 86–90], can be classified according to content and properties of the particles that mediate the interaction between DM and SM particles (mediator sector), giving rise to collider signatures with different kinematic characteristics and topologies.

Two classes of models are considered: the case where the mediator sector is composed of a single particle, either of spin-1 (Section 2.1) or of spin-0 (Section 2.2), and the case where the mediator sector is composed of an extended Higgs sector plus an additional mediator, either a spin-1 (Section 2.3.1) or spin-0 (Section 2.3.2) particle.

Finally, a Horndeski model of DE [91] is studied within an EFT framework and is used to interpret the results (Section 2.4).

All models described in this section are summarised in Table 1. For all models, the width of the mediator is always assumed to be the smallest width that can be calculated from all other parameters [60] (minimal width assumption). Furthermore this paper assumes DM to be a Dirac fermion.[1]

[1] The alternative assumption that DM is a Majorana fermion changes not only the set of allowed interactions, but also the total cross-section for the ones that are allowed. Aside from these, changing the choice of Dirac fermions, Majorana fermions, or scalars is expected to produce minor changes in the kinematic distributions of the visible particles in the final state. However, these assumptions have not been considered further in terms of simplified DM models [60].

Table 1: Summary of the mediator-based simplified models considered in this paper, along with the associated model acronym (2nd column, defined in the text) and mediator symbol (3rd column) used throughout. The 4th and 5th columns indicate the quantum numbers of the mediator. The "-" indicates the cases where no other charge than the new mediator's interaction is present. The 6th column the final-state signatures considered, and the 7th column gives the reference to the interpretation.

Short description	Acronym	Symbol	J^P	Charge	Signatures	Results Section:
Vector/axial-vector mediator	V/AV	$Z'_{\mathrm{V}}/Z'_{\mathrm{A}}$	$1^{\mp}$	-	jet/$\gamma/W/Z$+$E_{\mathrm{T}}^{\mathrm{miss}}$, difermion resonance	6.1.1
Vector baryon-number-charged mediator	VBC	Z'_{B}	1^-	baryon-number	$h + E_{\mathrm{T}}^{\mathrm{miss}}$	6.1.2
Vector flavour-changing mediator	VFC	Z'_{VFC}	1^-	flavour	tt, $t + E_{\mathrm{T}}^{\mathrm{miss}}$	6.1.3
Scalar/pseudo-scalar mediator	S/PS	ϕ/a	$0^{\pm}$	-	jet+$E_{\mathrm{T}}^{\mathrm{miss}}$, $t\bar{t}/b\bar{b}$+$E_{\mathrm{T}}^{\mathrm{miss}}$	6.2.1
Scalar colour-charged mediator	SCC$_{q/b/t}$	$\eta_{q/b/t}$	0^+	colour, 2/3 electric-charge	jet+$E_{\mathrm{T}}^{\mathrm{miss}}$, $b + E_{\mathrm{T}}^{\mathrm{miss}}$, $t + E_{\mathrm{T}}^{\mathrm{miss}}$	6.2.2
Two-Higgs-doublet plus vector mediator	2HDM+Z'_{V}	Z'_{V}	1^-	-	$h + E_{\mathrm{T}}^{\mathrm{miss}}$	6.3.1
Two-Higgs-doublet plus pseudo-scalar mediator	2HDM+a	a	0^-	-	$W/Z/h + E_{\mathrm{T}}^{\mathrm{miss}}$, $t\bar{t}/b\bar{b}$+$E_{\mathrm{T}}^{\mathrm{miss}}$, h(inv), $t\bar{t}t\bar{t}$	6.3.2
Dark energy	DE	ϕ_{DE}	0^+	-	jet+$E_{\mathrm{T}}^{\mathrm{miss}}$, $t\bar{t}$ +$E_{\mathrm{T}}^{\mathrm{miss}}$	6.4

2.1 Vector or axial-vector dark matter models

The first category of models considered in this paper consists of a set of simplified models with a single spin-1 particle that acts as the mediator. This category of models that assume the existence of new gauge symmetries is among the most commonly studied extensions of the SM [92] and provides a convenient framework to describe the interaction between the SM and DM. Three types of simplified models involving a single spin-1 particle are investigated: a neutral mediator [90, 93–99], a baryon-number charged mediator [100–103] and a flavour-changing neutral-current mediator [104–106].

2.1.1 Neutral interaction

One vector or axial-vector simplified model (V/AV) [60] consists of a simple extension of the SM with an additional U(1) gauge symmetry under which the DM particles are charged. The new mediator (Z') is either a vector (Z'_{V}) or an axial-vector (Z'_{A}) boson. The model has five parameters [60]: the masses of the mediator and the DM particle ($m_{Z'_{\mathrm{V/A}}}$ and m_χ, respectively), the flavour-universal coupling of the Z' boson to all flavour quarks, g_q; the coupling to all lepton flavours, g_ℓ; and the coupling to DM, g_χ. Representative

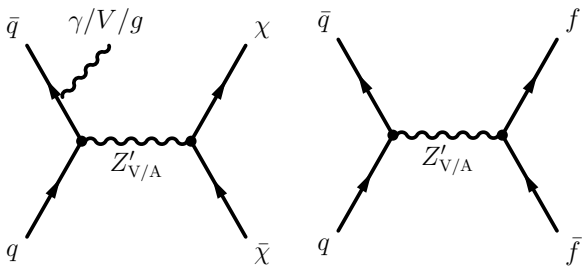

(a) (b)

Figure 1: Schematic representation of the dominant production and decay modes for the V/AV model.

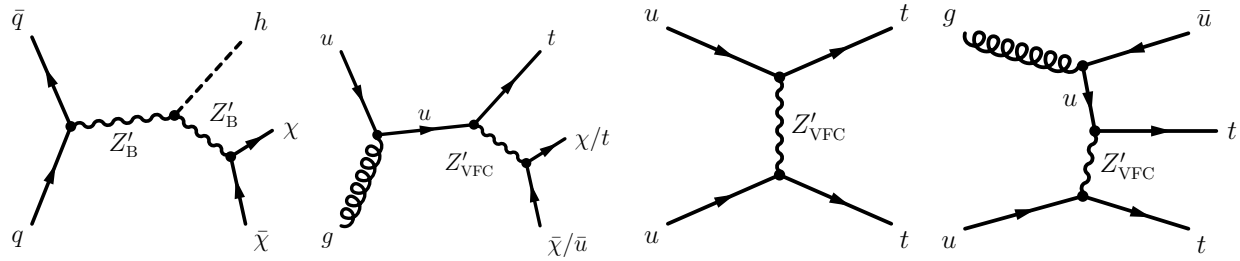

(a) (b) (c) (d)

Figure 2: Schematic representation of the dominant production and decay modes for the (a) VBC model and (b,c,d) VFC model.

diagrams for this model are shown in Figure 1. The Z' mediator can decay into a pair of quarks, a pair of leptons, or a pair of DM particles. In the latter case, an additional visible object has to be produced in association with the mediator as initial-state radiation (ISR), as shown in Figure 1(a). The visible object can either be a jet, a photon or a W or Z boson. In order to highlight the complementarity of dedicated searches based on different final states [62], two coupling scenarios, a leptophobic and a leptophilic Z' mediator, respectively, are considered for the interpretation of these models (see Section 6.1.1).

2.1.2 Baryon-number-charged interaction

The baryon-number-charged mediator simplified model [60, 103] (VBC) considers a spin-1 vector mediator. It also assumes that the charge of the U(1) symmetry coincides with the baryon number and it is spontaneously broken by a baryonic Higgs scalar. The DM candidate in this model is a stable baryonic state and it is neutral under the SM gauge symmetry. While the model can provide an ISR signature through s-channel Z'_{B}-mediator production subsequently decaying into a pair of DM candidates as for the V/AV models described in the previous section (Figure 1(a)), it can also exhibit a distinctive $h + E_{\mathrm{T}}^{\mathrm{miss}}$ signature [103], as shown in Figure 2(a). The model has five parameters [103], whose values are chosen to enhance the cross-section for $h + E_{\mathrm{T}}^{\mathrm{miss}}$ final states relative to traditional ISR signatures. The mixing angle between the baryonic and the SM Higgs bosons, θ, is fixed to $\sin\theta = 0.3$ in order to comply with the current Higgs boson coupling measurements. The coupling of the mediator Z'_{B} with the quarks, g_q, and the DM, g_χ, are set to $1/3$ and 1, respectively. The coupling of the mediator with the Higgs boson, $g_{Z'_{\mathrm{B}}}$, is set to the ratio of the mediator mass to the vacuum expectation value (VEV) of the baryonic Higgs

boson: $m_{Z'_B}/v_B$. The mediator is naturally leptophobic, thus evading the current constraints coming from the dilepton resonance searches. Different mediator and DM masses are investigated.

2.1.3 Flavour-changing interaction

The flavour-changing vector mediator model (VFC) [106] permits the interaction of the DM candidate with the top quark. A spin-1 colour-neutral mediator Z'_{VFC} enables a flavour-changing interaction of the DM with ordinary matter, for instance between the top quark and the up quark. For simplicity, the mediator is allowed to couple only to the right-handed component of the top-quark field [106]. This model predicts flavour-changing neutral current (FCNC) processes which are suppressed in the SM. A representative diagram of the on-shell production of the new mediator Z'_{VFC} is shown in Figure 2(b). The mediator can either decay invisibly, leading to a final state involving a single top quark and large missing transverse momentum, or decay visibly, producing a distinctive final state containing two top quarks with the same electric charge ($tt/\bar{t}\bar{t}$). A similar topology arises from the t-channel exchange of the Z'_{VFC} mediator, as depicted in Figs. 2(c) and 2(d).

The model is fully predictive once the four main parameters are specified [107]: the mass of the mediator $m_{Z'_{VFC}}$, the DM mass m_χ, and the couplings of the mediator to the DM particles and to the quarks, g_χ and g_{ut}, respectively. In the context of the analyses described in this paper, the mass of the DM candidate m_χ has negligible impact on the kinematics, provided that $m_{Z'_{VFC}} > 2m_\chi$, and it is fixed to 1 GeV. This reduces the number of dimensions of the parameter space to three. The sensitivity of the experimental analyses to this model is explored in three scenarios that investigate different parameter planes as a function of $m_{Z'_{VFC}}$, $g_{ut}$and the invisible branching ratio of the Z'_{VFC}mediator, $\mathcal{B}(\chi\bar{\chi})$.

2.2 Scalar or pseudo-scalar dark matter models

The second category of models considered in this paper consists of a set of simplified models with a single spin-0 particle that composes the mediator sector. In simplified models the mediator couples to SM fermions proportionally to the Higgs Yukawa couplings. These models can therefore be easily included in the extended Higgs boson sectors of ultraviolet-complete (UV-complete) theories. The various models considered can be grouped in two broad categories: colour-neutral [108–117] or colour-charged mediators [104–106, 118–132]. The latter category is divided into three further models with different final states.

2.2.1 Colour-neutral interaction

In the scalar or pseudo-scalar simplified models (S/PS) a new spin-0 gauge mediates the interaction, at tree level, with a DM particle [60, 110]. The mediator is considered to be either a scalar (ϕ) or a pseudo-scalar (a). This model has four parameters [25]: the mass of the mediator m_ϕ or m_a; the DM mass; the DM-mediator coupling, g_χ; and the coupling of the mediator with the SM fermions. The latter is composed of a flavour-universal term, g_q, which is a free parameter of the model and multiplies the SM-Yukawa coupling for each of the fermions [110]. This particular form of interaction, common to all models with spin-0 mediators considered in this paper, is typically referred to as the minimal flavour violation (MFV) ansatz and by construction, it relaxes the severe restrictions on the coupling of new spin-0 colour-neutral particles to the SM fermions imposed by flavour measurements [133–135]. Furthermore, it

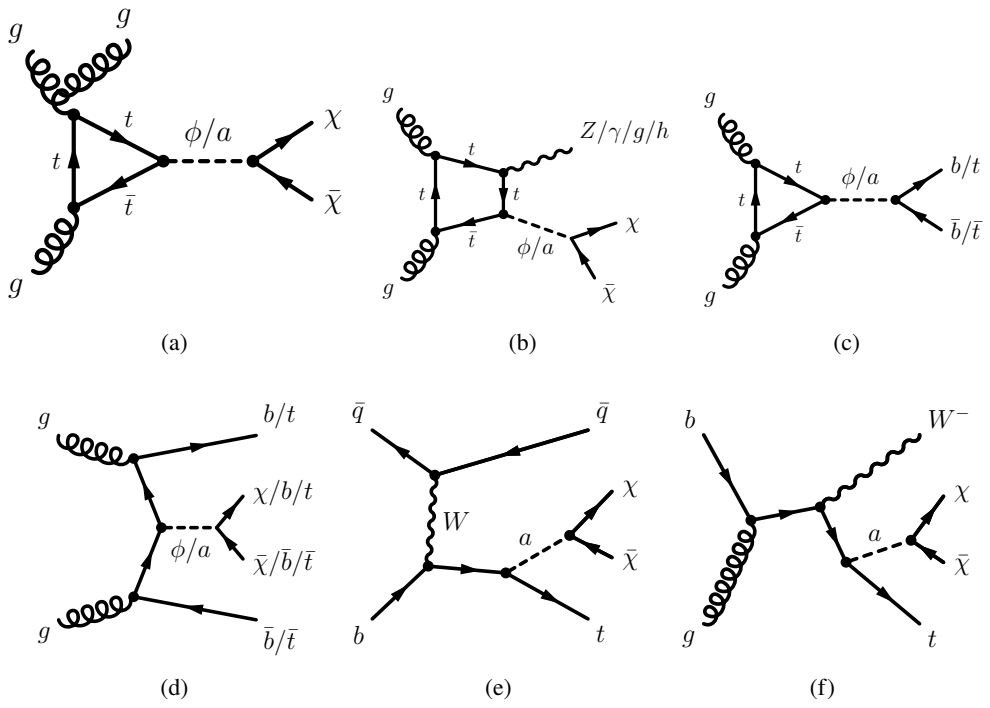

Figure 3: Schematic representation of the dominant production and decay modes for the S/PS models.

implies that these mediators are sizeably produced through loop-induced gluon fusion or in association with heavy-flavour quarks (see Figure 3). According to whether the mediator decays into a pair of DM or SM particles, different final states are sensitive to these models. Due to the Yukawa-like structure of the couplings, visible final states with two or four top quarks are particularly important signatures. Final states involving a single top quark and $E_{\mathrm{T}}^{\mathrm{miss}}$ may also play an important role in constraining these models [136–141]. Despite the absence of a dedicated parameter that regulates the relative importance of up-type and down-type quark couplings (otherwise present in UV completions of these models as in Section 2.3.2), it is also important to study final states involving bottom quarks separately, since these become a relevant signature if the up-type couplings are suppressed.

2.2.2 Colour-charged interaction

The scalar colour-charged interaction model (SCC) assumes that the scalar mediator couples to left- or right-handed quarks and it is a colour triplet. The DM particle(s) is produced via a t-channel exchange of the mediator which leads to a different phenomenology from that of colour-neutral interactions. These models have a strong connection with the minimal supersymmetric Standard Model (MSSM) [142, 143] with a neutralino DM and first- and second-generation squarks with universal masses. They share with it the same cross-sections and phenomenology when the mediator is pair-produced via strong interaction. Nevertheless, additional production diagrams are considered in this scenario, since values assumed for the couplings of the mediator to quarks and DM differ from those of the MSSM.

As in the case of the MSSM, it is reasonable to decouple the first two generations from the third, considering the different mass scales. For this purpose, three different models are considered:[2]

[2] These three scenarios provide benchmarks for each signature considered and do not aim to be an exhaustive set of models

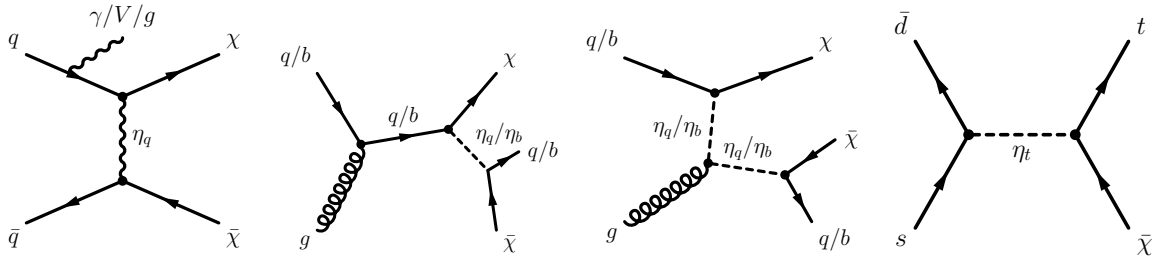

(a) (b) (c) (d)

Figure 4: Schematic representation of the dominant production and decay modes for the SCC models.

1. In the SCC$_q$ model, the mediator, η_q, couples to the left-handed quarks of the first and second generation and is a SU(2) singlet under the SM. The mediator decays into a quark–DM pair, so that the strongest sensitivity for these models is provided by searches involving jets and missing transverse momentum. The three model parameters are the mediator mass, the DM mass, and the flavour-universal coupling to quarks and DM, λ_q. This model is described in detail in Refs. [26, 98] and representative diagrams are shown in Figures. 4(a), 4(b) and 4(c).

2. In the SCC$_b$ model, the mediator, η_b, couples to the right-handed bottom quark. Following previous publications [25, 144], the specific realisation of this model is obtained within the framework of "flavoured" DM, where the DM candidate is the lightest component of a flavour triplet [128]. With these assumptions, the mediator always decays into a b-quark–DM pair. Of the three parameters of the model, the mediator and DM masses and the coupling, λ_b, only the first two are varied, while the last one is set to the value predicting a DM relic density compatible with astrophysical observations [133]. Representative diagrams for these models are presented in Figures. 4(b) and 4(c).

3. In the SCC$_t$ model, the mediator, η_t, consists of a SU(2)$_\mathrm{L}$-singlet field that couples to right-handed quarks, and is produced by down-type quark–anti-quark fusion, and it decays into a top quark and a DM particle. The representative diagram is shown in Figure 4(d). This specific realisation of the model [106], which gives rise to a characteristic signature composed of a single top quark and an invisible particle, can be related to the MSSM if an additional R-parity violating interaction of the top squark with the down-type quarks is assumed. The coupling strength of the mediator to DM and top quarks, denoted by λ_t, and the coupling strength to light-flavour down-type quarks, g_{ds}, are free parameters of the model.

2.3 Extended Higgs sector dark matter models

The third category of models aims to extend the simplified DM mediator models by involving an extended two-Higgs-doublet sector (2HDM) [145–153], together with an additional mediator to DM, either a vector or a pseudo-scalar. This embeds the simplified models in a UV-complete and renormalisable framework and allows the investigation of a broad phenomenology predicted by these types of models. In both models, the 2HDM sector has a CP-conserving potential and a softly broken $\mathbb{Z}_2$ symmetry [154], and the alignment limit is assumed, so that the lightest CP-even state, h, of the Higgs sector can be identified with the SM Higgs boson.

involving colour-charged interactions

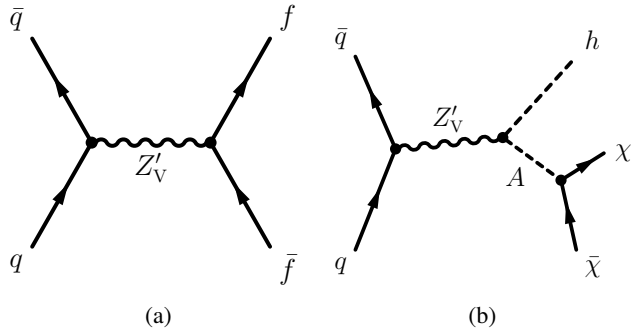

Figure 5: Schematic representation of the dominant production and decay modes for the 2HDM+Z'_{V} model.

2.3.1 Two-Higgs-doublet models with a vector mediator

The first two-Higgs-doublet model [155], denoted for brevity 2HDM+Z'_{V} in the following, is based on a type-II 2HDM [154, 156] with an additional U(1) gauge symmetry, which gives rise to a new massive Z'_{V} gauge boson state. The Z'_{V} boson, which can mix with the Z boson, couples only to right-handed quarks and only to the Higgs doublet that couples to the up-type fermions. The CP-odd scalar mass eigenstate, A, from the extended Higgs sector couples to DM particles and complies with electroweak precision measurement constraints. The phenomenology of this model is extended with respect to the simplified case due to the presence of a new decay mode $Z'_{\mathrm{V}} \to hA$, as shown in Figure 5, with the A boson decaying into a pair of DM particles with a large branching ratio (when kinematically possible), as long as the decay into a pair of top quarks is kinematically forbidden [32]. Additional signatures involving decays of the Z'_{V} boson into SM particles or the H and $H^{\pm}$ bosons are possible in the model. However, the model parameters are chosen in order to be consistent with the constraints from searches for heavy-boson resonances on this model [157], and therefore these signatures are not considered further in the context of this interpretation. The model has six parameters [157]: $\tan\beta$, the ratio of the vacuum expectation values of the two Higgs doublets, is set to unity; m_{χ}, the DM mass, is set to 100 GeV; and g_Z, the coupling of the new Z'_{V} U(1) gauge symmetry, is set to 0.8. The masses m_h and $m_H = m_{H^{\pm}}$ of the two CP-even and charged Higgs bosons are set to 125 GeV, and 300 GeV, respectively, while m_A, the mass of the CP-odd Higgs partner and $m_{Z'_{\mathrm{V}}}$ are free parameters and varied in the interpretation.

2.3.2 Two-Higgs-doublet models with a pseudo-scalar mediator

The second 2HDM model [149], 2HDM+a, includes an additional pseudo-scalar mediator, a. In this case also, the 2HDM coupling structure is chosen to be of type-II, although many of the interpretations considered in this paper hold for a type-I case too. The additional pseudo-scalar mediator of the model couples the DM particles to the SM and mixes with the pseudo-scalar partner of the SM Higgs boson. The physics of the model is fully captured by 14 parameters: the masses of the CP-even (h and H), CP-odd (a and A) and charged ($H^{\pm}$) bosons; the mass of the DM particle (m_{χ}); the three quartic couplings between the scalar doublets and the a boson (λ_{P1}, λ_{P2} and λ_3); and the coupling between the a boson and the DM, y_{χ}; the electroweak VEV, v; the ratio of the VEVs of the two Higgs doublets, $\tan\beta$; and the mixing angles of the CP-even and CP-odd weak eigenstates, α and θ, respectively. The alignment and decoupling limit ($\cos(\beta-\alpha)=0$) is assumed, thus h is the SM Higgs boson and $v = 246$ GeV. The quartic coupling $\lambda_3 = 3$ is chosen to ensure the stability of the Higgs potential for our choice of the masses of the heavy Higgs

bosons which are themselves fixed to the same value ($m_A = m_{H^\pm} = m_H$) to simplify the phenomenology and evade the constraints from electroweak precision measurements [149]. The other quartic couplings are also set to 3 in order to maximise the trilinear couplings between the CP-odd and the CP-even neutral states. Finally, $y_\chi = 1$ is chosen, having a negligible effect on the kinematics in the final states of interest.

This model is characterised by a rich phenomenology. The production of the lightest pseudo-scalar is dominated by loop-induced gluon fusion, followed by associated production with heavy-flavour quarks or associated production with a Higgs or Z boson (Figures 6(a)-6(c)). Furthermore, according to the Higgs sector's mass hierarchy, Higgs and Z bosons can be produced in the resonant decay of the heavier bosons into the lightest pseudo-scalar (Figures 6(d)-6(f)). The pseudo-scalar mediator can subsequently decay into either a pair of DM particles or a pair of SM particles (mostly top quarks if kinematically allowed), giving rise to very diverse signatures. The four-top-quark signature [158] is particularly interesting in this model if the neutral Higgs partner masses are kept above the $t\bar{t}$ decay threshold, since, when kinematically allowed, all heavy neutral bosons can contribute to this final state, as depicted in the diagram of Figure 6(c). Four benchmark scenarios [63] that are consistent with bounds from electroweak precision, flavour and Higgs observables are chosen to investigate the sensitivity to this model as a function of relevant parameters: $m_a, m_A, \tan\beta, \sin\theta$ and m_χ.

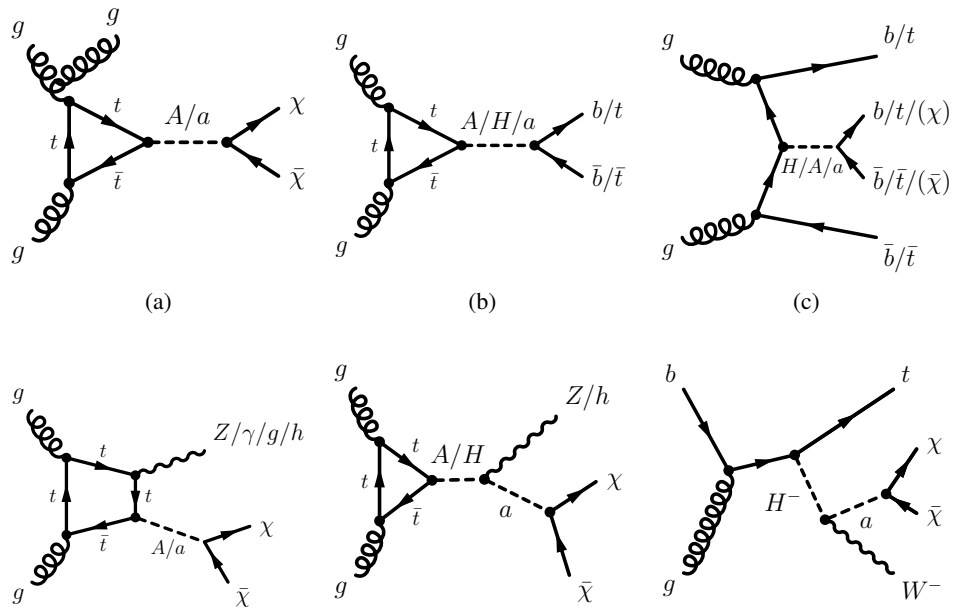

Figure 6: Schematic representation of the dominant production and decay modes for the 2HDM+a model.

2.4 EFT model of scalar dark energy

The Horndeski theories [91] introduce a dark energy scalar which couples to gravity and provide a useful framework for constraining the cosmological constant problem and the source of the acceleration of the expansion of the universe. The model considered in this paper is an EFT implementation of these theories [79]. In this model, the dark energy field is assumed to couple to matter universally. The model contains two classes of effective operators: operators which are invariant under shift-symmetry

$\phi_{\mathrm{DE}} \rightarrow \phi_{\mathrm{DE}}$ + constant, where ϕ_{DE} denotes the DE scalar field, and operators which break this symmetry. Shift-symmetric operators contain derivative interactions of ϕ_{DE} with the SM particles, while operators that break the shift-symmetry contain direct interactions of ϕ_{DE} with the SM. In the former case the DE scalar is pair-produced and does not decay within the volume of collider experiments, thereby resulting in $E_{\mathrm{T}}^{\mathrm{miss}}$ in the detector, while the latter case includes Yukawa-type interactions $\phi_{\mathrm{DE}}\bar{\psi}\psi$, which allow the scalar to decay into SM fermions, thereby changing the expected signatures. The interactions arising from the shift-symmetry breaking operators are tightly constrained [159] and are not considered here.

There are nine shift-symmetric Lagrangian effective operators in the model, each suppressed by powers of a characteristic energy scale M according to the operator's dimensionality:

$$\mathcal{L} = \mathcal{L}_{\mathrm{SM}} + \sum_{i=1}^{9} c_i \mathcal{L}_i = \mathcal{L}_{\mathrm{SM}} + \sum_{i=1}^{9} \frac{c_i}{M_i^{d-4}} O_i^{(d)},$$

where d is the operator's dimension and c_i are the Wilson coefficients. Operators $\mathcal{L}_1$–$\mathcal{L}_5$ correspond to interactions of the DE field with SM fields. The leading, i.e. least suppressed, operators of dimension eight are

$$\begin{aligned} \mathcal{L}_1 &= \frac{\partial_\mu \phi_{\mathrm{DE}} \partial^\mu \phi_{\mathrm{DE}}}{M_1^4} T_\nu^\nu \\ \mathcal{L}_2 &= \frac{\partial_\mu \phi_{\mathrm{DE}} \partial_\nu \phi_{\mathrm{DE}}}{M_2^4} T^{\mu\nu}, \end{aligned}$$

where $T^{\mu\nu}$ is the energy-momentum tensor corresponding to the SM Lagrangian. The $\mathcal{L}_1$ operator corresponds to a derivative coupling of the DE field to the conformal anomaly, T_ν^ν (= $m\bar{\psi}\psi$ for a Dirac field), and is therefore proportional to the mass of the SM fermions to which DE couples. Signatures which probe DE production in association with $t\bar{t}$ are therefore the most sensitive to this type of coupling and are used here. The $\mathcal{L}_2$ operator involves derivatives of the SM fields and is therefore proportional to their momenta. Final states involving large momentum transfers, such as the jet+$E_{\mathrm{T}}^{\mathrm{miss}}$ signature, offer the highest sensitivity to this type of coupling. The $\mathcal{L}_1$ and $\mathcal{L}_2$ operators are referred to as (kinetically dependent) conformal [160] and disformal, respectively. Operators $\mathcal{L}_3$–$\mathcal{L}_5$ correspond to higher-order versions of $\mathcal{L}_1$ and $\mathcal{L}_2$. The operator $\mathcal{L}_6$ corresponds to a generalised kinetic term for the DE scalar and operators $\mathcal{L}_7$–$\mathcal{L}_9$ correspond to the non-trivial Galilean terms [161]. In this paper, only $\mathcal{L}_1$ and $\mathcal{L}_2$ are considered. Due to the absence of terms allowing the decay of the DE scalars into SM particles, the DE particles (ϕ_{DE}) are considered stable and they escape the detector producing a missing-momentum signature.

The validity of the EFT approach in the context of collider data [162–164] is assessed with the procedure described in Ref. [60], imposing the condition $\sqrt{\hat{s}} < g_* M$, where $\sqrt{\hat{s}}$ is the centre-of-mass energy of the hard interaction and g_* is the effective coupling associated with the UV completion of the EFT.

Representative Feynman diagrams corresponding to the $\mathcal{L}_1$ and $\mathcal{L}_2$ operators for the $t\bar{t} + E_{\mathrm{T}}^{\mathrm{miss}}$ and mono-jet signatures are shown in Figure 7.

3 Dataset and Signal simulation

This paper interprets analyses of pp collision data recorded at a centre-of-mass energy of $\sqrt{s}$ = 13 TeV by the ATLAS detector during 2015 and 2016. Unless otherwise specified, the integrated luminosity of the

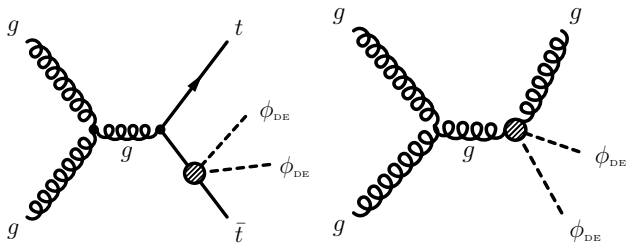

Figure 7: Schematic representation of representative production modes for the DE model for the Lagrangian effective operators (a) $\mathcal{L}_1$ and (b) $\mathcal{L}_2$.

dataset, after requiring that all detector subsystems were operational during data recording, amounts to 36.1 ± 0.8 fb^{-1}.

Monte Carlo (MC) simulated event samples were used to aid in the estimation of the background from SM processes and to model the DM and DE signals. Simulated events were processed either through a detector simulation [165] based on Geant4 [166] or through a fast simulation [165] with a parameterisation of the calorimeter response and Geant4 for the other parts of the detector [167]. Either of these ATLAS detector simulations were used for background processes (details in the specific analysis references) and most of the signal processes, as detailed in the following.

Two sets of samples were used for the modelling of the signal processes considered in this paper. One set of samples is based on signal events processed through the ATLAS detector simulation, referred to as "reconstructed" samples. The second set of samples consists of signal events composed of particle-level objects, defined according to the guiding principles outlined in Ref. [168], and not including any resolution effect due to the ATLAS detector. These are referred to as "particle-level" samples. Particle-level samples were used to define a rescaling procedure specifically designed to broaden the range of signal models and parameter choices considered in the interpretation of the results. The procedure allows the use of less extensive computational resources that would be needed to provide a full detector simulation for the large set of considered signals, while providing a complete picture of the current experimental coverage for these models. The rescaling procedure calculated a set of correction weights for a reference model as the ratio of the acceptance for a baseline signal sample to the acceptance of the signal sample of interest. Both of these acceptances are derived in a particle-level simulation. These weights were then applied to the reconstructed baseline signal sample of the reference model, assuming similar detector effects for the two models. The same procedure was used in some cases to rescale between signal samples of the same reference model but for different parameter choices which affect the kinematics of the final state. Closure-tests were performed to determine the reliability of this procedure and assign specific systematic uncertainties when needed. Further details about the rescaling used in the V/AV, VFC and the 2HDM+a signal samples are given in Appendix A.

The generation settings for signal models considering a spin-1 mediator are summarised in Table 2. For each model the table indicates the Universal FeynRules Output (UFO) model [169] implementation, the matrix element (ME) generator, the parton shower (PS), and the cross-section normalisation, at QCD leading-order or next-to-leading order accuracy (LO and NLO, respectively). Following the notation of the previous section, the simplified models are indicated with $Z'_{\mathrm{V/A}}$, while the baryon-charged and flavour-changing interactions are indicated as Z'_{B} and Z'_{VFC}, respectively. The 2HDM model with an

Table 2: Details of the generation setup and Universal FeynRules Output (UFO) model used for the spin-1 mediator simplified models, for each signature considered in this paper.

Model and Final State	UFO	Generator and Parton Shower	Cross-section	Additional details
$Z'(\chi\bar{\chi}) + j$	DMV [26, 170]	POWHEG-BOX v2 [171] + PYTHIA 8.205 [172]	NLO	Particle-level rescaling of leptophobic Z'_A scenario of Ref. [26] (see Appendix A.1)
$Z'(\chi\bar{\chi}) + \gamma$	DMSimp [113, 173]	MG5_aMC@NLO 2.4.3 (NLO) [174] + PYTHIA 8.212	NLO	Leptophobic Z'_A scenario simulated, other scenarios obtained by cross-section rescaling (see Appendix A.1)
$Z'(\chi\bar{\chi}) + V$	DMSimp	MG5_aMC@NLO 2.5.3 (NLO) + PYTHIA 8.212	NLO	Particle-level rescaling of LO samples of Ref. [20] to each of the four NLO scenarios (see Appendix A.1)
$Z'(qq)$ or $Z'(qq)$+ISR	DMSimp	MG5_aMC@NLO 2.2.3 (NLO) + PYTHIA 8.210	NLO	Leptophobic Z'_A scenario simulated, other scenario obtained by Gaussian resonance limits and cross-section rescaling [175]
$Z'(b\bar{b})$	DMSimp	MG5_aMC@NLO 2.2.3 (NLO) + PYTHIA 8.210	NLO	Leptophobic Z'_A scenario simulated, other scenario obtained by Gaussian resonance limits and cross-section rescaling [175]
$Z'(\ell\ell)$	DMSimp	MG5_aMC@NLO 2.2.3 (NLO)	NLO	Gaussian resonance limits and cross-section rescaling [175]
$Z'(t\bar{t})$	DMSimp	MG5_aMC@NLO 2.4.3 (LO) + PYTHIA 8.186	LO	Particle-level rescaling of the topcolour-assisted technicolour samples of Ref. [176] (see Appendix A.1)
$Z'_{\text{VFC}}(\chi\bar{\chi})/Z'_{\text{VFC}}(\bar{u}t)$	MonotopDMF [177]	MADGRAPH 2.2.3 (LO) +PYTHIA 8.210	LO	Ref. [30] and Appendix A.2
$Z'_B(\chi\bar{\chi}) + h$	Higgs_scalar [103, 178]	MADGRAPH 2.2.3 (LO) +PYTHIA 8.186	LO	Ref. [22], simulated for $h(b\bar{b}) + E_T^{\text{miss}}$
2HDM+Z'_V	Zp2HDM [155, 179]	MADGRAPH 2.2.3 (LO) +PYTHIA 8.186	LO	Ref. [22, 23]

additional vector mediator is indicated as 2HDM+Z'_V. When relevant for the generations settings, each separate final state considered in this paper is indicated for each model.

The generation settings for signal models considering a spin-0 mediator are summarised in Table 3. Following the notation of the previous section, the colour-neutral (colour-charged) simplified models are indicated with ϕ/a (η). The 2HDM with additional pseudo-scalar mediator is indicated as 2HDM+a.

The model implementations, settings and parameter scans follow the prescriptions of the DM Forum/LHC DM Working Group [60–63].

Finally, the generation settings for the DE model are also indicated in Table 4.

4 Experimental signatures

Dark matter searches are an important component of the ATLAS physics programme. Several final-state signatures are targeted to maximise the discovery potential. This section presents summaries of the different

Table 3: Details of the generation setup and Universal FeynRules Output (UFO) model used for the spin-0 mediator models, for each signature considered in this paper.

Model and Final State	UFO	Generator and Parton Shower	Cross-section	Additional details
$a(\chi\bar{\chi}) + j$	DMS_tloop [110, 180]	POWHEG-BOX v2 + PYTHIA 8.205	NLO	Ref. [26]
$\phi(\chi\bar{\chi}) + t\bar{t}$	DMScalarMed_loop [110, 181]	MADGRAPH 2.3.3 (LO) + PYTHIA 8.186	NLO [113]	Ref. [25]
$\phi(\chi\bar{\chi}) + b\bar{b}$	DMScalarMed_loop	MADGRAPH 2.3.3 (LO) + PYTHIA 8.186	NLO [182]	Ref. [25]
η_q	dmS_T [98, 183]	MADGRAPH 2.3.3 (LO) + PYTHIA 8.186	LO	Ref. [26, 98]
η_b	DM_Bflavored [128, 184]	MADGRAPH 2.3.3 (LO) + PYTHIA 8.186	LO	Ref. [25]
η_t	MonotopDMF [30, 177]	MADGRAPH 2.3.3 (LO) +PYTHIA 8.210	LO	Ref. [30]
2HDM+a: $\chi\bar{\chi} + t\bar{t}/b\bar{b}$	Pseudoscalar_2HDM [149, 185]	MADGRAPH 2.3.3 (LO)	LO	Cross-section based rescaling from simplified model samples of Ref. [25]
2HDM+a: $\chi\bar{\chi} + Z$	Pseudoscalar_2HDM	MG5_aMC@NLO 2.4.3 (LO) + PYTHIA 8.212	LO	Only gluon-initiated production considered [149]
2HDM+a: $\chi\bar{\chi} + h$	Pseudoscalar_2HDM	MG5_aMC@NLO 2.4.3 (LO) + PYTHIA 8.212	LO	b-quark-initiated production considered only for $\tan\beta \geq 10$
2HDM+a: $4t$	Pseudoscalar_2HDM	MG5_aMC@NLO 2.4.3 (LO) + PYTHIA 8.212	LO	Ref. [149]

Table 4: Details of the generation setup and Universal FeynRules Output (UFO) model used for the dark energy model.

Model	UFO	Generator and Parton Shower	Cross-section
Dark Energy	Standard_Model_cosmo_no_c10 [79]	MADGRAPH 2.6.1 (LO) + PYTHIA 8.212	LO

searches for DM and is not intended to be exhaustive. More details are available in the reference papers.

Electrons, muons, photons and jets are reconstructed by combining the signals from the different components of the ATLAS detector[3] [186–190]. Leptons (ℓ) in the following refers to electrons or muons. In several analyses, events with identified leptons are rejected from the signal region selection. This is referred to as a lepton veto. The analyses may implement different lepton and photon selection criteria for particle identification [186, 188, 189, 191], isolation [186, 188, 192], and kinematic requirements (p_{T}, η). Small-R and large-R jets are reconstructed from energy deposits in the calorimeters using the anti-k_t jet algorithm [193, 194] and using a radius parameter of $R = 0.4$ and $R = 1.0$, respectively. Reclustered large-R jets are reconstructed from small-R jets using a radius parameter of either $R = 0.8$ or $R = 1.2$. Multivariate algorithms are used to identify small-R jets with $p_{\mathrm{T}} > 20$ GeV containing b-hadrons (b-jets) [195, 196]. This is referred to as b-tagging. For large-R jets, b-tagging is applied to their associated track-jets, which are constructed from tracks reconstructed in the inner detector using the anti-k_t jet algorithm with $R = 0.2$. The missing transverse momentum $\vec{p}_{\mathrm{T}}^{\,\mathrm{miss}}$ (with magnitude $E_{\mathrm{T}}^{\mathrm{miss}}$) is calculated from the negative vector sum of transverse momenta (p_{T}) of electrons, muons and jet candidates and an additional soft term [197]

[3] ATLAS uses a right-handed coordinate system with its origin at the nominal interaction point (IP) in the centre of the detector and the z-axis along the beam pipe. The x-axis points from the IP to the centre of the LHC ring, and the y-axis points upwards. Cylindrical coordinates (r, ϕ) are used in the transverse plane, ϕ being the azimuthal angle around the z-axis. The pseudorapidity is defined in terms of the polar angle θ as $\eta = -\ln\tan(\theta/2)$. Angular distance is measured in units of $\Delta R \equiv \sqrt{(\Delta\eta)^2 + (\Delta\phi)^2}$. The rapidity is defined at $y = 1/2\ln[(E + p_z)/(E - p_z)]$, where E is the energy and p_z is the component of its momentum along the z-axis. The rapidity difference between two jets is defined as $y^* = (y_1 - y_2)/2$.

which includes activity in the tracking system originating from the primary vertex but not associated with any reconstructed particle. Some analyses may also consider photons in the $E_{\mathrm{T}}^{\mathrm{miss}}$ reconstructions.

4.1 Searches for invisible final states

Searches for WIMP candidates at the LHC are characterised by the requirement of large $E_{\mathrm{T}}^{\mathrm{miss}}$ since WIMPs escape detection. Therefore, final states with additional visible particles are considered in the selection of the events. These additional particles may come from initial-state radiation or from associated production. Several signatures that are listed in the following are exploited and optimised to enhance the sensitivity to different DM models.

Jet $+E_{\mathrm{T}}^{\mathrm{miss}}$ The jet$+E_{\mathrm{T}}^{\mathrm{miss}}$ analysis [26], commonly referred to as the mono-jet analysis, is characterised by the presence of an energetic jet and large $E_{\mathrm{T}}^{\mathrm{miss}}$. The analysis selects events with $E_{\mathrm{T}}^{\mathrm{miss}} > 250$ GeV, at least one jet with $p_{\mathrm{T}} > 250$ GeV, and at most three additional jets with $p_{\mathrm{T}} > 30$ GeV. Events are required to pass a lepton veto. To reduce the contribution from multi-jet background where large $E_{\mathrm{T}}^{\mathrm{miss}}$ can originate from jet energy under-measurement, a minimum separation in the azimuthal angle between each selected jet and the $E_{\mathrm{T}}^{\mathrm{miss}}$ direction is also required: $\Delta\phi(\text{jet}, \vec{p}_{\mathrm{T}}^{\,\mathrm{miss}}) > 0.4$. The W+jets, Z+jets, and top-quark-related backgrounds are constrained using MC event samples normalised to data in selected control regions containing leptons. In the case of W+jets and Z+jets events, MC predictions are reweighted to account for higher-order QCD and electroweak corrections as a function of the vector-boson p_{T} [198]. The normalisation factors for these backgrounds are extracted simultaneously using a binned likelihood fit of the $E_{\mathrm{T}}^{\mathrm{miss}}$ distributions in all control and signal regions that includes systematic uncertainties. The remaining SM backgrounds from diboson processes are determined using MC simulated samples, while the multi-jet background contribution is extracted from data.

***h*(inv)** Searches for invisible Higgs boson decays have been performed using several production and decay channels at a centre-of-mass energy of $\sqrt{s} = 8$ TeV [29]. Results of searches in the vector-boson fusion (VBF) production channel and in associated production of a Higgs boson with a W/Z boson are statistically combined with the measured production and decay rates of the Higgs boson in the $\gamma\gamma$, ZZ, WW, $Z\gamma$, bb, $\tau\tau$, and $\mu\mu$ channels to set an upper limit on the Higgs boson's invisible branching ratio of 0.23 at 95% confidence level (CL). This combined limit is used in the results quoted in Section 6. Among the direct searches, the VBF production of Higgs bosons decaying into invisible particles [199] is the most sensitive one, setting an upper limit on the invisible branching ratio of 0.28. The VBF$+E_{\mathrm{T}}^{\mathrm{miss}}$ analysis requires $E_{\mathrm{T}}^{\mathrm{miss}} > 150$ GeV and two jets with $p_{\mathrm{T}} > 35$ GeV. Three orthogonal signal regions are defined by varying the threshold imposed on the leading jet p_{T} and the invariant mass of the two jets. Additional requirements on the angular separation of the two jets are applied to enhance the sensitivity to VBF production. In particular, the two leading jets are required to be well separated in pseudorapidity. Lepton and b-jet vetoes are applied to reduce contamination from $W(\tau\nu)$+jets and top-quark backgrounds, respectively. Dedicated control regions with one and two leptons in the final state are used to constrain the contributions from dominant Z/W+jets backgrounds, through a simultaneous fit together with the signal region. The multi-jet background is estimated using a data-driven technique. Searches for Zh(inv) [24] and Vh(inv) [20] have been performed at centre-of-mass energy $\sqrt{s} = 13$ TeV. A new VBF$+E_{\mathrm{T}}^{\mathrm{miss}}$ analysis is also available using $\sqrt{s} = 13$ TeV pp collision data [200]. However, the 8 TeV combination gives more stringent limits, thus it is used here.

$\gamma + E_{\mathrm{T}}^{\mathrm{miss}}$ Events in the $\gamma + E_{\mathrm{T}}^{\mathrm{miss}}$ analysis [21] are required to pass the lepton veto and to have a photon with $E_{\mathrm{T}} > 150$ GeV. Events with more than one jet ($p_{\mathrm{T}} > 30$ GeV) or with a jet fulfilling $\Delta\phi(\text{jet}, \vec{p}_{\mathrm{T}}^{\,\mathrm{miss}}) < 0.4$ are rejected. Three exclusive signal regions with $E_{\mathrm{T}}^{\mathrm{miss}}$ ranges between 150 GeV, 225 GeV, 300 GeV and above are defined. The $W\gamma$, $Z\gamma$, and γ+jets backgrounds are normalised in control regions using a simultaneous likelihood fit of all $E_{\mathrm{T}}^{\mathrm{miss}}$ regions, but with independent normalisation factors for each region. The backgrounds due to photons from the misidentification of electrons or jets in processes such as W/Z+jets, diboson, and multi-jet events are estimated using data-driven techniques.

$Z(\ell\ell) + E_{\mathrm{T}}^{\mathrm{miss}}$ The event selection criteria in this analysis [24] require large $E_{\mathrm{T}}^{\mathrm{miss}}$ and a pair of high-p_{T} leptons. Two opposite-sign, same-flavour leptons satisfying $p_{\mathrm{T}} > 30$ GeV and $p_{\mathrm{T}} > 20$ GeV are required. The lepton pair is required to have an invariant mass between 76 GeV and 106 GeV to be consistent with originating from a Z boson. Events with an additional lepton with $p_{\mathrm{T}} > 7$ GeV or a b-jet with $p_{\mathrm{T}} > 20$ GeV are vetoed. To target events consistent with a boosted Z boson produced in the direction opposite to $\vec{p}_{\mathrm{T}}^{\,\mathrm{miss}}$, additional requirements are imposed on the azimuthal angle between the dilepton system and $\vec{p}_{\mathrm{T}}^{\,\mathrm{miss}}$ and on the angular distance between leptons. A single inclusive $E_{\mathrm{T}}^{\mathrm{miss}}$ signal region is defined with $E_{\mathrm{T}}^{\mathrm{miss}} > 90$ GeV for each of the ee and $\mu\mu$ channels. The dominant background in this analysis, ZZ production, is estimated from MC simulation. The WZ background is normalised to data in a three-lepton control region. The contributions from Z+jets and non-resonant-$\ell\ell$ backgrounds are estimated using data-driven techniques. A statistical combination of the two decay channels is used for the final results.

$W(qq')/Z(q\bar{q}) + E_{\mathrm{T}}^{\mathrm{miss}}$ This analysis [20] selects events with $E_{\mathrm{T}}^{\mathrm{miss}} > 150$ GeV and a hadronically decaying W or Z boson candidate. The vector-boson candidate is defined with one large-R jet with $p_{\mathrm{T}} > 250$ GeV in a boosted topology ($E_{\mathrm{T}}^{\mathrm{miss}} > 250$ GeV) or with two small-R jets with $p_{\mathrm{T}} > 20$ GeV in a resolved topology. In both cases, a lepton veto is applied. Additional requirements are applied to the invariant mass of the boson candidate. Several signal regions are defined according to the b-jet multiplicity. Similarly, several control regions are defined according to lepton and b-jet multiplicity. The normalisation of the $t\bar{t}$ and W/Z+jets background processes are constrained using a simultaneous fit of all control and signal regions of the $E_{\mathrm{T}}^{\mathrm{miss}}$ distribution. The subdominant contribution from diboson and single-top-quark production is obtained from simulation. Multi-jet contributions are estimated with a data-driven technique.

$h(b\bar{b}) + E_{\mathrm{T}}^{\mathrm{miss}}$ The $h(b\bar{b}) + E_{\mathrm{T}}^{\mathrm{miss}}$ analysis [23] is defined by the requirement of $E_{\mathrm{T}}^{\mathrm{miss}} > 150$ GeV, a lepton veto, and the presence of a Higgs boson candidate decaying to two b-jets with suitable invariant mass. Events with mis-measured $E_{\mathrm{T}}^{\mathrm{miss}}$ are rejected by imposing constraints on $\Delta\phi(\text{jet}, \vec{p}_{\mathrm{T}}^{\,\mathrm{miss}})$, between the missing momentum direction and the direction of any selected jet in the event. Two sets of signal regions are defined targeting moderate-momentum (resolved) and high-momentum (boosted) Higgs boson candidates. In each case, the regions are further split according to whether there are one or two b-jets. The resolved regime, defined in three exclusive $E_{\mathrm{T}}^{\mathrm{miss}}$ regions between 150 GeV and 500 GeV, selects a Higgs boson candidate reconstructed from the two leading b-tagged small-R jets (or from a b-tagged and a non-b-tagged small-R jet) with $p_{\mathrm{T}} > 20$ GeV. In the boosted regime, defined by $E_{\mathrm{T}}^{\mathrm{miss}} > 500$ GeV, the leading large-R jet with $p_{\mathrm{T}} > 200$ GeV is the Higgs boson candidate. The b-jet multiplicity is defined by the number of b-tagged track-jets associated with the large-R jet. Backgrounds involving the production of W/Z bosons in association with heavy-flavour quarks or top-quark pairs are normalised in dedicated control regions distinct from the signal regions by requiring one or two leptons. A simultaneous binned likelihood fit to the invariant mass of the Higgs boson candidate is performed in all signal and control regions. The multi-jet

background is obtained with a data-driven technique. Other subdominant backgrounds are estimated from simulation.

$h(\gamma\gamma) + E_{\mathrm{T}}^{\mathrm{miss}}$ The $h(\gamma\gamma) + E_{\mathrm{T}}^{\mathrm{miss}}$ events in this analysis [22] are selected by requiring at least two photons with $p_{\mathrm{T}} > 25$ GeV. The two leading photons are chosen to reconstruct the Higgs candidate, which is required to satisfy 105 GeV $< m_{\gamma\gamma} <$ 160 GeV. The leading (sub-leading) photon is also required to have $E_{\mathrm{T}}^{\gamma}/m_{\gamma\gamma} > 0.35$ (0.25). Events with leptons are vetoed. Events with $p_{\mathrm{T}}(\gamma\gamma) > 90$ GeV and $E_{\mathrm{T}}^{\mathrm{miss}}/\sqrt{\sum E_{\mathrm{T}}} > 7$ GeV$^{1/2}$ in Ref. [22] are used for the interpretation of DM models, where $\sum E_{\mathrm{T}}$ is the scalar sum of the transverse momentum of all reconstructed objects in the event. The backgrounds are extracted by fitting an analytic function to the diphoton invariant mass distribution. In the case of the non-resonant background, the normalisation and shape are obtained by fitting the invariant mass distribution in data to an exponential function. The SM Higgs boson background shape is modelled with a double-sided Crystal Ball function and fitted to the MC simulation.

$t + E_{\mathrm{T}}^{\mathrm{miss}}$ The $t + E_{\mathrm{T}}^{\mathrm{miss}}$ analysis [30] searches for events with one top quark and relatively large $E_{\mathrm{T}}^{\mathrm{miss}}$. Two signal regions are defined depending on the decay channel of the top quark. The leptonic channel selects events with a positively charged lepton with $p_{\mathrm{T}} > 30$ GeV, $E_{\mathrm{T}}^{\mathrm{miss}} > 50$ GeV, and transverse mass of the lepton and the $E_{\mathrm{T}}^{\mathrm{miss}}$, m_{T}^{W}, larger than 260 GeV. One b-jet with $p_{\mathrm{T}} > 30$ GeV is additionally required. The hadronic channel is optimised to select events with a top quark produced with a large boost. Events are selected with $E_{\mathrm{T}}^{\mathrm{miss}} > 200$ GeV and one large-R jet with $p_{\mathrm{T}} > 250$ GeV with one b-tagged track-jet associated with it. Events failing the lepton veto are rejected. Dedicated control regions are defined to constrain the $t\bar{t}$ and W/Z+jets backgrounds from data. The multi-jet background is estimated from data, whereas other remaining backgrounds are taken from simulation. All signal and control regions for the two decay channels are fitted simultaneously to extract the background normalisation. In the case of the hadronic channel, the transverse mass of the large-R jet and the $E_{\mathrm{T}}^{\mathrm{miss}}$ are the discriminating variables, while for the leptonic channel, the $E_{\mathrm{T}}^{\mathrm{miss}}$ distribution is used to discriminate signal from background.

$b(\bar{b}) + E_{\mathrm{T}}^{\mathrm{miss}}$ The $b + E_{\mathrm{T}}^{\mathrm{miss}}$ analysis [25] selects events with two energetic jets ($p_{\mathrm{T}} > 160$ GeV), at least one of which is b-tagged, $E_{\mathrm{T}}^{\mathrm{miss}} > 650$ GeV, and additional total hadronic energy restricted to be less than 100 GeV. This last requirement rejects top-quark background. The dominant background for this analysis, Z+jets events, is constrained from data in a dedicated control region, which is fitted together with the signal region. The $b\bar{b}$ $+E_{\mathrm{T}}^{\mathrm{miss}}$ analysis [25] instead exploits a selection with at least two b-jets and a considerably lower $E_{\mathrm{T}}^{\mathrm{miss}}$ requirement, $E_{\mathrm{T}}^{\mathrm{miss}} > 180$ GeV. The azimuthal separations between the b-jets and $\vec{p}_{\mathrm{T}}^{\,\mathrm{miss}}$ are exploited to enhance the separation between the signal and the irreducible background in this channel ($Z(\nu\bar{\nu})$+$b\bar{b}$), which is constrained from data in a dedicated control region. The results are extracted by fitting an observable that relies on the pseudorapidity difference between the two b-jets: $\cos\theta^{*}_{bb} = |\tanh(\Delta\eta_{bb}/2)|$.

$t\bar{t} + E_{\mathrm{T}}^{\mathrm{miss}}$ The $t\bar{t}$ $+E_{\mathrm{T}}^{\mathrm{miss}}$ analysis [25, 27, 28] is split into three channels according to the decays of the W bosons from the top-quark decays: 0-lepton, where both W bosons decay hadronically, 1-lepton, where one of the two W bosons decays leptonically and 2-leptons where both W bosons decay leptonically. The analyses targeting the 0-lepton channel exploit two sets of signal topologies: spin-0 DM models [25], used for the DM interpretations presented in this paper, and top-squark decays into a top quark and a neutralino [28], used for the DE interpretation in this paper. Both analyses are characterised by a set of

signal regions which select events with at least four energetic jets, at least two of which are b-tagged, and relatively high $E_{\mathrm{T}}^{\mathrm{miss}}$. Requirements on the invariant mass of reclustered large-R jets are imposed to identify events where a W boson or a top quark are boosted. The dominant backgrounds (Z+jets, top-quark processes and $t\bar{t}+Z$) are constrained in dedicated control regions. The three signal regions used for the DE interpretation are statistically combined, while the two signal regions considered in the DM analysis are not. The analysis targeting the 1-lepton channel selects events with at least four energetic jets, at least one of which is b-tagged, one isolated lepton and high $E_{\mathrm{T}}^{\mathrm{miss}}$. The events are also required to have at least one hadronic top candidate with invariant mass loosely compatible with the mass of the top quark. Requirements on the transverse and asymmetric stransverse masses [27] are used to suppress semileptonic and dileptonic $t\bar{t}$ events, respectively. Requirements on the azimuthal angle between the lepton and $\vec{p}_{\mathrm{T}}^{\,\mathrm{miss}}$ and on $\Delta\phi(\text{jets}, \vec{p}_{\mathrm{T}}^{\,\mathrm{miss}})$ are also exploited to further suppress the background contamination of the signal regions. All top-quark background processes are estimated in dedicated control regions. Finally, the analysis targeting the 2-lepton channel selects events with two opposite-sign leptons which are inconsistent with being produced in the decay of a Z boson. At least one b-jet is also required in the selections. The $E_{\mathrm{T}}^{\mathrm{miss}}$ and the stransverse mass ($m_{\mathrm{T2}}^{\ell\ell}$ [25]) requirements are such that $m_{\mathrm{T2}}^{\ell\ell} + 0.2 \cdot E_{\mathrm{T}}^{\mathrm{miss}} > 170$ GeV. The dominant backgrounds in this channel ($t\bar{t}$ and $t\bar{t}+Z$) are estimated in dedicated control regions.

Table 5 summarises the DM searches for invisible final states. None of these analyses shows a significant deviation from the expected SM background, and thus exclusion limits can be set for the relevant models. These limits are discussed in Section 6. The observed $E_{\mathrm{T}}^{\mathrm{miss}}$ distributions compared with the background predictions are shown in Figure 8 for the $h(b\bar{b}) + E_{\mathrm{T}}^{\mathrm{miss}}$ and $Z(\ell\ell) + E_{\mathrm{T}}^{\mathrm{miss}}$ analyses, with representative 2HDM+a signal distributions shown in each case. These two analyses have the strongest sensitivity for this model, as discussed in Section 6.3.2. The observed $m_{\mathrm{T2}}^{\chi^2}$ and $E_{\mathrm{T}}^{\mathrm{miss}}$ distributions compared with the background predictions are shown in Figure 9 for the $t\bar{t}$ +$E_{\mathrm{T}}^{\mathrm{miss}}$ (0-lepton channel) and jet+$E_{\mathrm{T}}^{\mathrm{miss}}$ analyses, respectively, with representative DE signal distributions shown in each case. Figures 8 and 9 show background predictions after the corresponding fit in each analysis.

4.2 Searches for visible final states

Several searches for narrow resonances are interpreted in terms of the DM models described in Section 2. These searches explore several final-state signatures by selecting different visible particles, thus requiring the presence of reconstructed objects such as jets or leptons, covering a variety of kinematic regions. In some of the analyses described below, further identification techniques are employed to select final states with top quarks.

Dijet For this analysis [201] events with at least two small-R jets are selected if the p_{T} of the leading (sub-leading) jet is greater than 440 (60) GeV. The dijet selection requires a rapidity difference $|y^*| < 0.6$ and the invariant mass of the dijet system to be $m_{jj} > 1.1$ TeV. The background estimation is obtained by fitting the falling m_{jj} distribution. Bin widths are chosen to approximate the m_{jj} resolution, and thus are wider for higher masses. A sliding-window fitting technique is used, where restricted regions of the spectrum are fitted with a functional form. The background is constructed bin-by-bin by performing a likelihood fit to the data in each window and using the fit value in the central bin for the background estimate. The values from the full set of windows are then combined to create the background estimate for the full mass range. Model-independent limits on the visible cross-section for a hypothetical signal that produces a Gaussian contribution to the m_{jj} distribution (for several signal widths) are provided for

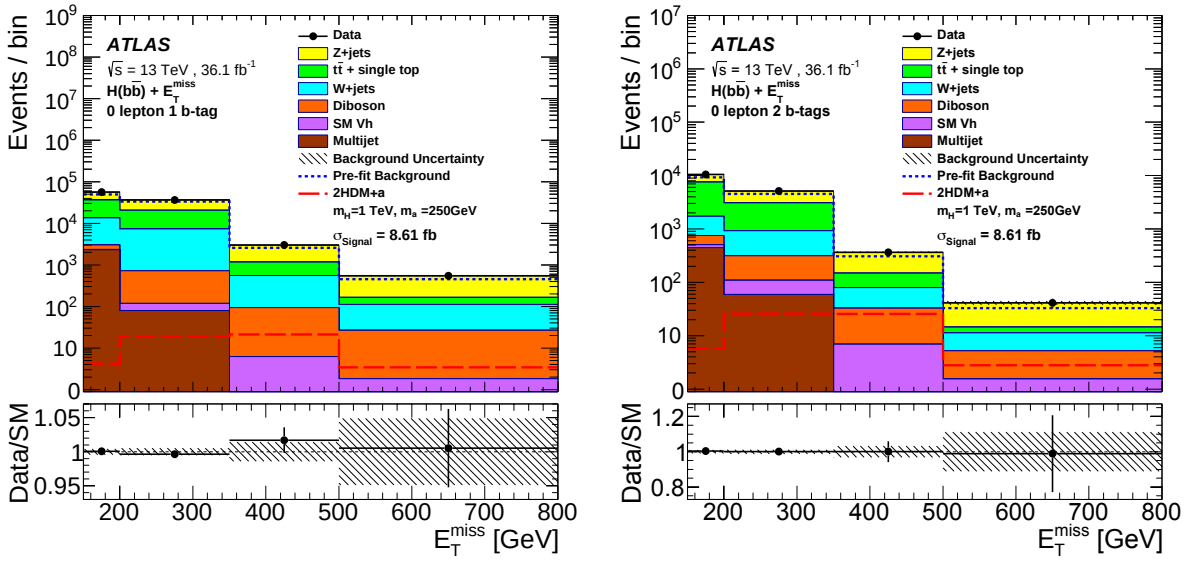

(a) (b)

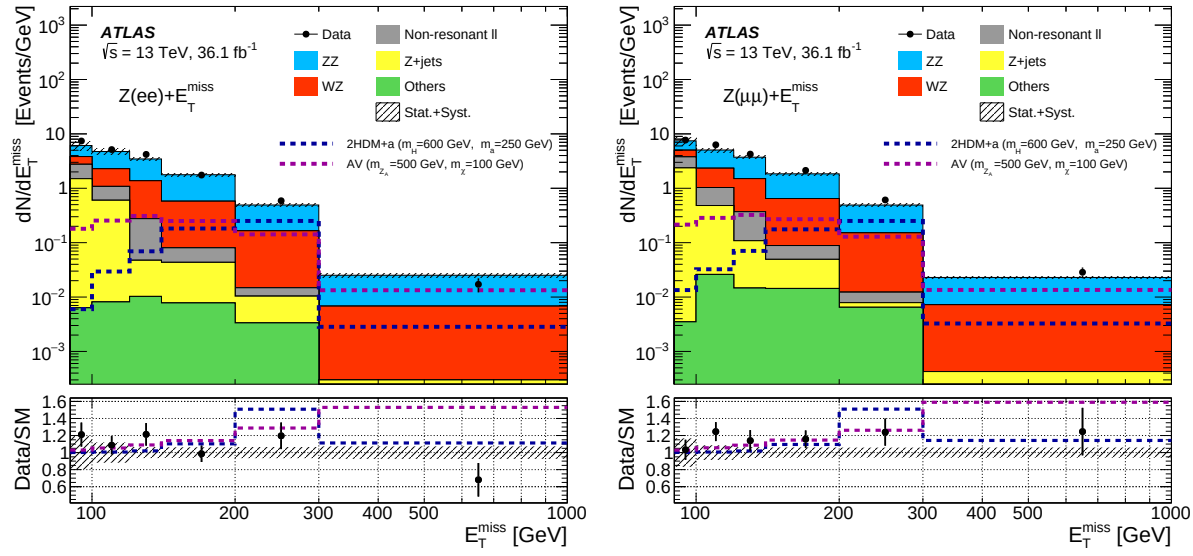

(c) (d)

Figure 8: Observed $E_{\mathrm{T}}^{\mathrm{miss}}$ distribution in the $h(b\bar{b}) + E_{\mathrm{T}}^{\mathrm{miss}}$ analysis in the (a) 1-b-tag and (b) 2-b-tag signal regions compared with the background predictions. The error bands show the total statistical and systematic uncertainties of the background predictions. The expected $E_{\mathrm{T}}^{\mathrm{miss}}$ distribution for a representative signal model is also shown. It corresponds to a 2HDM+a signal with $m_a = 250$ GeV, $m_H = m_{H^\pm} = m_A = 1000$ GeV, $\tan\beta = 1.0$, $\sin\theta = 0.35$, $g_\chi = 1.0$ and $m_\chi = 10$ GeV. Observed $E_{\mathrm{T}}^{\mathrm{miss}}$ distribution in the $Z(\ell\ell) + E_{\mathrm{T}}^{\mathrm{miss}}$ analysis in the (c) ee and (d) $\mu\mu$ signal regions compared with the background predictions. The expected $E_{\mathrm{T}}^{\mathrm{miss}}$ distribution for representative signal models are also shown. They correspond to a 2HDM+a signal with $m_a = 250$ GeV, $m_H = m_{H^\pm} = m_A = 600$ GeV, $\tan\beta = 1.0$, $\sin\theta = 0.35$, $g_\chi = 1.0$ and $m_\chi = 10$ GeV, and an AV signal with $m_{Z'_{\mathrm{A}}} = 500$ GeV, $m_\chi = 100$ GeV, $g_q = 0.25$, $g_\ell = 0$, and $g_\chi = 1.0$. The background predictions are after the corresponding fit in each analysis.

Table 5: Summary of searches for invisible final states used to constrain the different DM models defined in Section 2. The $(*)$ indicates models which were presented in the original publication, all others are either new or updated.

Analysis	Models targeted	Final-state signature	Key Characteristics	Results
Jet $+E_{\mathrm{T}}^{\mathrm{miss}}$ [26]	V/AV$(*)$, S/PS$(*)$, SCC$_q(*)$, DE	1–4 jets, $E_{\mathrm{T}}^{\mathrm{miss}}$, 0 ℓ.	Binned likelihood fit of $E_{\mathrm{T}}^{\mathrm{miss}}$.	Section 6.1.1, 6.2.1, 6.2.2, 6.4
h(inv) [29, 199]	2HDM+a	2 jets, $E_{\mathrm{T}}^{\mathrm{miss}}$, m_{jj}, $\Delta\eta_{jj}$.	Single-bin likelihood fit.	Section 6.3.2
$\gamma + E_{\mathrm{T}}^{\mathrm{miss}}$ [21]	V/AV$(*)$	1 photon, 0–1 jets, $E_{\mathrm{T}}^{\mathrm{miss}}$, 0 ℓ.	Binned likelihood fit of $E_{\mathrm{T}}^{\mathrm{miss}}$.	Section 6.1.1
$Z(\ell\ell) + E_{\mathrm{T}}^{\mathrm{miss}}$ [24]	V/AV, 2HDM+a	2 ℓ, $E_{\mathrm{T}}^{\mathrm{miss}}$, $m_{\ell\ell} \sim m_Z$.	Binned likelihood fit of $E_{\mathrm{T}}^{\mathrm{miss}}$	Section 6.1.1, 6.3.2
$W/Z(qq') + E_{\mathrm{T}}^{\mathrm{miss}}$ [20]	V/AV, 2HDM+a	$E_{\mathrm{T}}^{\mathrm{miss}}$, W/Z candidate (resolved and boosted topologies).	Binned likelihood fit of $E_{\mathrm{T}}^{\mathrm{miss}}$.	Section 6.1.1, 6.3.2
$h(b\bar{b}) + E_{\mathrm{T}}^{\mathrm{miss}}$ [23]	VBC, 2HDM+$Z'_{\mathrm{V}}(*)$, 2HDM+a	$E_{\mathrm{T}}^{\mathrm{miss}}$, h candidate (resolved and boosted topologies).	Binned likelihood fit of m_h in bins of $E_{\mathrm{T}}^{\mathrm{miss}}$.	Section 6.1.2, 6.3.1, 6.3.2
$h(\gamma\gamma) + E_{\mathrm{T}}^{\mathrm{miss}}$ [22]	VBC, 2HDM+$Z'_{\mathrm{V}}(*)$, 2HDM+a	2 photons, $m_{\gamma\gamma} \sim m_h$, $E_{\mathrm{T}}^{\mathrm{miss}}$.	Analytic function fit of $m_{\gamma\gamma}$.	Section 6.1.2, 6.3.1, 6.3.2
$t + E_{\mathrm{T}}^{\mathrm{miss}}$ [30]	VFC	$E_{\mathrm{T}}^{\mathrm{miss}}$, t candidate (all decay channels).	Binned likelihood fit of $E_{\mathrm{T}}^{\mathrm{miss}}$ ($m_{\mathrm{T}}(E_{\mathrm{T}}^{\mathrm{miss}}$, large-$R$ jet)) in the leptonic (hadronic) channel.	Section 6.1.3
$b(\bar{b}) + E_{\mathrm{T}}^{\mathrm{miss}}$ [25]	S/PS$(*)$, SCC$_b(*)$, 2HDM+a	1–2 b-jets, $E_{\mathrm{T}}^{\mathrm{miss}}$, 0 ℓ.	Binned likelihood fit of $\cos\theta^*_{bb}$.	Section 6.2.1, 6.2.2, 6.3.2
$t\bar{t} + E_{\mathrm{T}}^{\mathrm{miss}}$ [25, 27]	S/PS$(*)$, SCC$_t(*)$, 2HDM+a, DE	0–2ℓ, 1–2 b-jets, $\geq 1-4$ jets, $E_{\mathrm{T}}^{\mathrm{miss}}$, $m_{\mathrm{T2}}^{\ell\ell}$.	Binned likelihood fit.	Section 6.2.1, 6.2.2, 6.3.2, 6.4

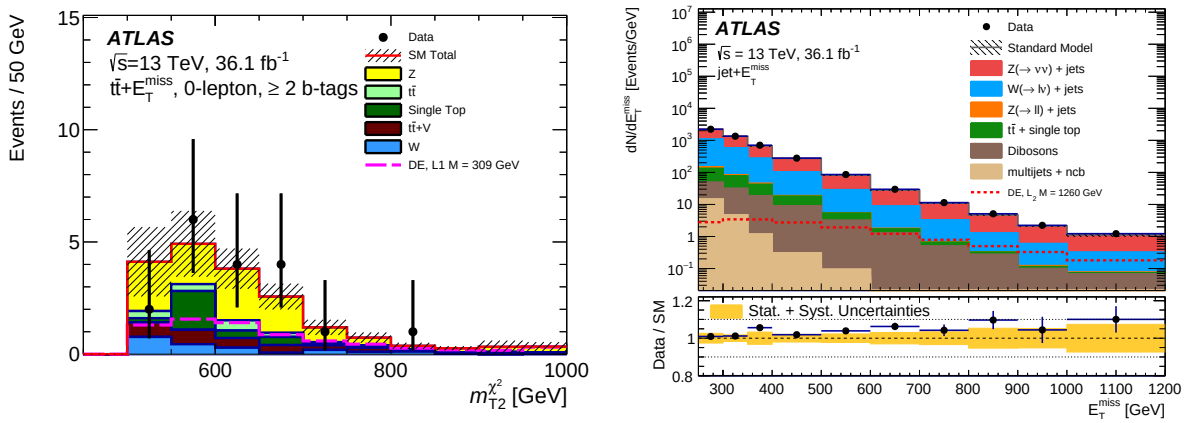

(a) (b)

Figure 9: Observed $m_{\mathrm{T2}}^{\chi^2}$ and $E_{\mathrm{T}}^{\mathrm{miss}}$ distributions in the (a) $t\bar{t}(0L) + E_{\mathrm{T}}^{\mathrm{miss}}$ and (b) jet+$E_{\mathrm{T}}^{\mathrm{miss}}$ analyses, respectively, compared with a representative DE signal and the post-fit background predictions. The error bands show the total statistical and systematic uncertainties of the background predictions. Representative DE signal distributions are shown for $\mathcal{L}_1$ and $\mathcal{L}_2$ operators in (a) and (b), respectively.

this analysis (see Appendix A of Ref. [202]). This analysis was performed in data corresponding to an integrated luminosity of 37.0 fb^{-1}.

Dijet angular A dijet selection can also be exploited to search for deviations from the SM expectation in angular distributions, characteristic of wider resonances where the nominal dijet search would lose sensitivity. A dijet angular analysis [201] is performed in events with two jets following the p_{T} requirements of the dijet search, but relaxing the $|y^*|$ requirement to 1.7. Due to different kinematics in this loosened selection, the mass of the dijet pair is required to be $m_{jj} > 2.5$ TeV. The analysis makes use of the variable $\chi_{jj} = \text{e}^{2|y^*|} \sim (1 + \cos\theta^*)/(1 - \cos\theta^*)$[4], constructed so that, in the limit of massless parton scattering and when only the t-channel scattering contributes to the partonic cross-section, the angular distribution $\text{d}N/\text{d}\chi_{jj}$ is approximately independent of χ_{jj}. MC events from multi-jet production are modelled at LO in QCD, and reweighted to NLO predictions from NLOJET++ [203, 204] using mass- and angle-dependent correction factors. Additional electroweak mass- and angle-dependent correction factors are applied. The data are compared with a SM template in different m_{jj} ranges, and different χ_{jj} bins.

Trigger-object-level dijet For the dijet analysis described before, the high p_{T} threshold imposed on the leading jet is limited by the trigger selection driven by the bandwidth available for single-jet triggers, thus it only targets $m_{jj} > 1.5$ TeV. The limitation from the high-level trigger selection is overcome by recording only high-level trigger jet information, rather than the full detector readout, to a dedicated data stream, reducing the storage needs per event. This strategy allows to record all events passing the single-jet level-one (L1) trigger (with lower threshold than in the high-level trigger) with minimal bandwidth increase. The dataset collected corresponds to an integrated luminosity of 29.3 fb^{-1}. This trigger-object-level dijet analysis (TLA dijet) [205] selects events with at least two trigger-level jets with $p_{\text{T}} > 85$ GeV. Two selection criteria are used: $|y^*| < 0.6$ in the mass range 700 GeV $< m_{jj} <$ 1.8 TeV and $|y^*| < 0.3$ for 450 GeV $< m_{jj} <$ 700 GeV. The leading trigger-level jet is required to have $p_{\text{T}} > 185$ GeV and $p_{\text{T}} > 220$ GeV for the $|y^*| < 0.3$ and $|y^*| < 0.6$ selections, respectively, to ensure full efficiency for the L1 triggers. The search is then interpreted in terms of resonances with a mass between 450 GeV and 1.8 TeV. The background strategy used in the dijet search is also used here.

Resolved dijet + ISR Another alternative strategy to search for low-mass dijet resonances is to select events with a pair of jets recoiling against a photon or an additional jet from ISR. The resolved dijet + ISR analyses [206] select events with a high-p_{T} ISR object (γ or jet), used to trigger the event, and a relatively low mass dijet resonance. Dijet+γ events contain at least one photon with $p_\gamma > 150$ GeV and at least two jets with $p_{\text{T}} > 25$ GeV. The two leading jets must satisfy $|y^*| < 0.8$, which allows to probe of dijet invariant masses between 170 GeV and 1.5 TeV. The three-jet selection requires at least one jet with $p_{\text{T}} > 430$ GeV as well as two additional jets with $p_{\text{T}} > 25$ GeV. The leading jet is chosen as the ISR candidate, and the second- and third-highest-p_{T} jets are required to satisfy $|y^*| < 0.6$. This selection probes a mass range between about 300 GeV and 600 GeV. The background contribution is estimated by fitting the m_{jj} distribution. This analysis was performed in 13 TeV collision data corresponding to an integrated luminosity of 15.5 fb^{-1}.

[4] θ^* is defined as the polar angle with respect to the direction of the initial partons in the dijet centre-of-mass frame.

Boosted dijet + ISR In the case of a dijet+ISR selection, if the associated ISR photon or jet has large transverse momentum, the dijet resonance candidate is reconstructed as a large-R jet [207] of radius 1.0 with mass m. To enhance the sensitivity to quark pair decays, jet substructure techniques are used to discriminate between a two-particle jet from a decay of a boosted resonance and a single-particle jet [208]. Events are required to have a large-R jet, the resonance candidate, and at least one ISR object candidate. The azimuthal angular separation between the resonance candidate and the ISR object is required to satisfy $\Delta\phi > \pi/2$. A $p_{\mathrm{T}} > 2m$ requirement ensures sufficient collimation of the resonance candidate. In the ISR jet (photon) channel, the large-R jet satisfies $p_{\mathrm{T}} > 450$ (200) GeV and the ISR jet (photon) has $p_{\mathrm{T}} > 450$ (155) GeV. A data-driven technique is used to model the expected background in the signal region via a transfer factor that extrapolates from a control region with inverted jet substructure requirements.

Dibjet The dibjet search [209] targets dijet resonances with one or two jets identified as b-jets. Two different analyses cover both the low and high invariant mass regions. Events in the high invariant mass region are selected with at least two jets, one of which has $p_{\mathrm{T}} > 430$ GeV and passes an inclusive jet trigger. The rapidity difference is required to be $|y^*| < 0.8$. This analysis covers the region with $m_{jj} > 1.2$ TeV. The low invariant mass region uses a trigger targeting events with two jets containing b-hadrons, which provides access to lower dibjet invariant masses (m_{jj}) compared to the single jet trigger: 570 GeV $< m_{jj} <$ 1.5 TeV. The rapidity difference requirement is tightened to $|y^*| < 0.6$. In this case, only the two-b-jets selection is considered. Because the double b-jet trigger was not available during the full data-taking period, the total integrated luminosity used for the low-mass analysis corresponds to 24.3 fb^{-1} of 13 TeV collision data. A background estimation strategy similar to that of the dijet analysis is used in these analyses.

Dilepton The dilepton analysis [210] selects events with at least two same-flavour leptons. The pair of electrons (muons) with highest E_{T} (p_{T}) are chosen as the candidate decay products of the resonance. Only the muon channel candidates are required to have opposite charge, due to higher charge misidentification for high-E_{T} electrons and the p_{T} misreconstruction associated with wrongly measured charge in muons. Background processes with two prompt leptons are modelled using MC samples. The $Z/\gamma^* \to \ell\ell$ background is smoothed for 120 GeV $< m_{\ell\ell} <$ 1 TeV. This is done by fitting the MC spectrum and the resulting fitted function is used to set the expected event yields in that mass range. A data-driven method is employed to estimate backgrounds with at least one misidentified lepton. The $m_{\ell\ell}$ distribution is explored between 80 GeV and 6 TeV.

Same-sign tt Events in the same-sign tt analysis [107] are selected with exactly two leptons with positive charge and at least one b-jet. Events are required to satisfy $H_{\mathrm{T}} > 750$ GeV, where H_{T} is defined as the scalar sum of the p_{T} of all selected objects, including jets. Additionally, requirements on $E_{\mathrm{T}}^{\mathrm{miss}}$ and the azimuthal separation between the two leptons are imposed. Signal regions for the different lepton flavours (ee, $e\mu$ and $\mu\mu$) are treated separately. Irreducible SM backgrounds are determined using MC simulation samples. Backgrounds from fake leptons are estimated using data-driven techniques.

$t\bar{t}$ resonance The $t\bar{t}$ resonance analysis [176] selects events with two top-quark candidates. Events are required to have a leptonic top-quark decay, selected by requiring a charged lepton and $E_{\mathrm{T}}^{\mathrm{miss}}$ consistent with a leptonic decay of a W boson, and a small-R jet close by. Events are classified as boosted or resolved depending on their hadronic activity. In the boosted selection, events contain one large-R jet passing top-tagging requirements. In the resolved selection, events have at least four small-R jets and fail the

Table 6: Summary of searches for visible final states used to constrain the different DM models defined in Section 2. The (∗) indicates models which were presented in the original publication, all others are either new or updated.

Analysis	Models targeted	Final-state signature	Key Characteristics	Results
Dijet [201]	V/AV	2 jets, m_{jj}, y^*.	Sliding-window fit of the m_{jj} distribution.	Section 6.1.1
Dijet angular [201]	V/AV	2 jets, m_{jj}, y^*.	Binned likelihood fit of χ_{jj}.	Section 6.1.1
TLA dijet [205]	V/AV	2 trigger-level jets, m_{jj}, y^*.	Sliding-window fit of the m_{jj} distribution.	Section 6.1.1
Resolved dijet+ISR [206]	V/AV	3 jets (or 2 jets and 1 photon), m_{jj}, y^*.	Parametric function fit of the m_{jj} distribution.	Section 6.1.1
Boosted dijet+ISR [207]	V/AV(∗)	1 large-R jet, 1 jet or photon, m_J.	Data-driven extrapolation from control region via transfer factor.	Section 6.1.1
Dibjet [209]	V/AV	2 jets (1 and 2 b-jets), m_{jj}, y^*.	Sliding-window parametric fit of the m_{jj} distribution.	Section 6.1.1
Dilepton [210]	V/AV	2 e or 2 μ.	$Z/\gamma^* \to \ell\ell$ from fitted MC spectrum.	Section 6.1.1
Same-sign tt [107]	VFC	2 same-sign ℓ, 2 b-jets, H_T, E_T^{miss}.	Background with real leptons from MC.	Section 6.1.3
$t\bar{t}$ resonance [176]	V/AV	1 ℓ, hadronic t candidate (resolved and boosted topologies), E_T^{miss}.	$t\bar{t}$ bkg from MC, binned likelihood fit of $m_{t\bar{t}}$.	Section 6.1.1
$t\bar{t}t\bar{t}$ [211]	2HDM+a	1 ℓ, high jet multiplicity.	Parameterised extrapolation from low to high jet multiplicity. Binned likelihood fit of jet and b-jet multiplicities.	Section 6.3.2

boosted selection. The $t\bar{t}$ invariant mass, $m_{t\bar{t}}$, is reconstructed from the decay products of the two top-quark candidates in the event. The b-jet multiplicity is used for further categorisation. The SM $t\bar{t}$ production is estimated using MC samples and fixed-order theory calculations. The multi-jet and W+jets background contribution is estimated using data-driven techniques.

$t\bar{t}t\bar{t}$ The $t\bar{t}t\bar{t}$ analysis [211] searches for events characterised by a single lepton and high jet multiplicity. Events are categorised by their jet multiplicity, which is defined using three p_T thresholds: 40 GeV, 60 GeV, and 80 GeV. Events are further separated into five bins corresponding to the b-jet multiplicity. The $t\bar{t}$+jets and W/Z+jets background production is estimated using a combined fit to these jet and b-jet multiplicity bins. The normalisation of these backgrounds is extrapolated from lower to higher jet multiplicity, while the b-jet multiplicity shape is taken from a parameterised extrapolation from data (simulation) for the $t\bar{t}$ (W/Z+jets) background.

Table 6 summarises the searches for visible final states. As in the case of the searches for invisible final states, these analyses found no significant deviation from the expected SM backgrounds. Therefore, exclusion limits are placed on the allowed phase space of the corresponding signal models, as discussed in Section 6.

4.3 Complementarity and combination of signatures

It can be seen from Tables 5 and 6 that several analyses are often sensitive to the same model. In cases like the $X + E_T^{miss}$ final-states searches, X originating from initial-state radiation or associated production, a variety of final states are considered: X = jet, γ, W, Z, h, $t(\bar{t})$, $b(\bar{b})$. Since the mediator couples DM to SM

particles, it is also possible to reinterpret results from resonance searches targeting the mediator directly. The complementarity depends on the choice of model as well as coupling values. For the V/AV model, this paper considers jet/$\gamma/V + E_{\mathrm{T}}^{\mathrm{miss}}$, dijet, dibjet and $t\bar{t}$ resonance final states. All results for this model are new or have been updated from previous publications, except for the jet/$\gamma + E_{\mathrm{T}}^{\mathrm{miss}}$ interpretations. For the VBC and 2HDM+Z'_{V} models, this paper considers only $h + E_{\mathrm{T}}^{\mathrm{miss}}$, which dominates the sensitivity for the chosen parameter values. All possible final states (same-sign tt and the $t + E_{\mathrm{T}}^{\mathrm{miss}}$) are considered for the VFC model. Only invisible final states, $t\bar{t}/b\bar{b}$/jet + $E_{\mathrm{T}}^{\mathrm{miss}}$, are considered for the S/PS model. The SCC$_q$, SCC$_b$ and SCC$_t$ models are each addressed with a specific signature: jet + $E_{\mathrm{T}}^{\mathrm{miss}}$, $b + E_{\mathrm{T}}^{\mathrm{miss}}$, $t + E_{\mathrm{T}}^{\mathrm{miss}}$, respectively, and all results were presented in each specific analysis paper. Various final states are considered in order to place the first constraints on the 2HDM+a model by ATLAS searches: $Z/h + E_{\mathrm{T}}^{\mathrm{miss}}$, $t\bar{t}/b\bar{b} + E_{\mathrm{T}}^{\mathrm{miss}}$, h(inv) and $t\bar{t}t\bar{t}$. Finally, the constraints on DE models are set using jet+$E_{\mathrm{T}}^{\mathrm{miss}}$ and $t\bar{t}$ +$E_{\mathrm{T}}^{\mathrm{miss}}$ final states.

Complementarity can also be found when studying different SM decay channels of a given signature. Two natural candidates from the analyses discussed here are the $h + E_{\mathrm{T}}^{\mathrm{miss}}$ ($b\bar{b}, \gamma\gamma$) searches and the $t\bar{t} + E_{\mathrm{T}}^{\mathrm{miss}}$ (fully hadronic, semileptonic and fully leptonic) searches.

The results from the $h + E_{\mathrm{T}}^{\mathrm{miss}}$ searches presented in Section 6.3.1 correspond to a statistical combination of the $h(b\bar{b}) + E_{\mathrm{T}}^{\mathrm{miss}}$ and $h(\gamma\gamma) + E_{\mathrm{T}}^{\mathrm{miss}}$ searches. The $h(b\bar{b}) + E_{\mathrm{T}}^{\mathrm{miss}}$ analysis has a larger reach in mediator masses, however its sensitivity is limited at lower masses by the threshold requirement of the $E_{\mathrm{T}}^{\mathrm{miss}}$ trigger used to record the events for this analysis. The $h(\gamma\gamma) + E_{\mathrm{T}}^{\mathrm{miss}}$ analysis covers a lower mass region owing to its selection based on a photon trigger. For the combination, the luminosity, experimental, and signal modelling uncertainties were taken to be correlated between the two channels. In the $h(\gamma\gamma) + E_{\mathrm{T}}^{\mathrm{miss}}$ analysis the systematics uncertainties are not significantly constrained by the fit. This is mainly due to the use of a single signal region and no control regions. In the case of $h(b\bar{b}) + E_{\mathrm{T}}^{\mathrm{miss}}$ the systematics uncertainties are constrained due to the use of dedicated control regions. It is observed, however, that the results from the combination and the individual $h(b\bar{b}) + E_{\mathrm{T}}^{\mathrm{miss}}$ results are very similar. While the $h(b\bar{b}) + E_{\mathrm{T}}^{\mathrm{miss}}$ channel dominates the sensitivity, searches in different decay channels are of interest in probing different kinematic regions defined by different analyses strategies.

For this paper, the $t\bar{t} + E_{\mathrm{T}}^{\mathrm{miss}}$ exclusion limits discussed in Section 6 are combined based on the best expected exclusion for each signal model, unless separate contours are shown.

5 Systematic uncertainties

Systematic uncertainties for both the background and signal models are considered in each of the analyses presented in Section 4. These uncertainties, as well as statistical uncertainties, depend on the event selection, the phase space covered by a given analysis, and its background estimation strategy. The systematic uncertainties include experimental and theoretical uncertainties. Experimental uncertainties may include uncertainties in the absolute jet and $E_{\mathrm{T}}^{\mathrm{miss}}$ energy scales and resolutions, the jet quality requirements, pile-up corrections, b-tagging efficiencies, the soft contributions to $E_{\mathrm{T}}^{\mathrm{miss}}$ and the luminosity. Uncertainties in lepton identification and reconstruction efficiencies, energy/momentum scale and resolution are included for events with selected or vetoed leptons. Uncertainties due to the finite statistics of the background MC samples and others related to the modelling of the background processes are also included in the analyses.

The signal modelling is subject to experimental and theoretical uncertainties. The experimental uncertainties are the same as for the background processes. Theoretical uncertainties affecting the production cross-

section (normalisation) and the acceptance are considered separately. The strategy used to estimate systematic uncertainties for those signal models studied in this paper which are not discussed in previous publications is outlined below.

The results for the 2HDM+a and DE signal models include theoretical systematic uncertainties due to parton distribution functions (PDFs), evaluated following the PDF4LHC recommendations [212]. The choice of different PDFs results in up to 2% uncertainty in the acceptance and up to 10% uncertainty in the cross-section. Uncertainties related to the choice of renormalisation and factorisation scales are derived by varying such scales by a factor of 2.0 and 0.5 relative to the nominal values used for the MC generation. They account for an uncertainty in the acceptance below 5% for the different analyses. Uncertainties in initial- and final-state radiation due to the parton shower modelling are estimated by generating MC samples with alternative underlying event and multi-parton interaction parameter choices resulting in uncertainties between 5% and 15% in the signal acceptance, typically increasing at higher mediator masses. In the very large jet multiplicity phase space of the $t\bar{t}t\bar{t}$ analysis they reach values of 50%.

In some cases, additional uncertainties are included to account for non-closure effects of the rescaling procedure described in Section 3. These uncertainties include a contribution from the statistical uncertainty associated with the acceptance ratios determined from the baseline signal sample. For the $h(\gamma\gamma) + E_{\mathrm{T}}^{\mathrm{miss}}$ ($Z(\ell\ell) + E_{\mathrm{T}}^{\mathrm{miss}}$) analysis this translates in up to 7% (8%) uncertainty in the final 2HDM+a signal yields.

6 Interpretation of the results

This section summarises the exclusion limits set by ATLAS published searches briefly outlined in Section 4, on the various signal models described in Section 2 (following the notation in Table 1). The analyses and corresponding signal regions are referred to by their analysis labels defined in Tables 5 and 6. The observed and expected 95% confidence level (CL) exclusion limits are obtained from the signal region or combination of regions of each contributing analysis using the $\mathrm{CL_s}$ [213] method. In Section 6.3.1 a statistical combination of the $h + E_{\mathrm{T}}^{\mathrm{miss}}$ final states is used to derive the results.

6.1 Vector or axial-vector dark matter models

6.1.1 Neutral interaction

The V/AV simplified model is strongly constrained by searches for a high-mass resonance decaying into a pair of fermions and searches for associated production of DM particles with an ISR object.

As presented in Figure 10 for the case of an axial-vector mediator, each resonance search analysis is sensitive to complementary regions of the mass–coupling parameter space. Couplings above the exclusion line are excluded, as long as the width predicted by the model is smaller than the maximal ratio of width to mediator mass ($\Gamma/m_{Z'}$) to which the analysis is sensitive. This limitation arises where the background model is estimated via a sliding-window fit of the m_{jj} distribution. Specifically, the TLA dijet analysis assuming $|y^*| < 0.6$ is sensitive up to around $\Gamma/m_{Z'} = 7\%$, the TLA dijet analysis requiring $|y^*| < 0.3$ and the boosted dijet+ISR analysis are sensitive up to around $\Gamma/m_{Z'} = 10\%$, while the dijet and dibjet analyses are sensitive up to around $\Gamma/m_{Z'} = 15\%$. Finally, the dijet angular analysis is sensitive up to $\Gamma/m_{Z'} = 50\%$. No limitation in sensitivity arises from large width resonances in the $t\bar{t}$ resonance analysis, as the background is constrained in dedicated control regions. The different dijet analyses (see Section 4.2

for details) are sensitive to different mass regimes as well as coupling values. The boosted dijet+ISR analysis has the best reach for low masses, excluding Z'_{A} mediator masses between 100 GeV and 220 GeV. Two new interpretations, for the dibjet and $t\bar{t}$ resonance analyses, are presented for these models. The dibjet ($t\bar{t}$ resonance) analysis places constraints on Z'_{A} mediators with masses between 500 GeV and 2.5 (2) TeV, in the same region of sensitivity of the dijet, TLA dijet, and boosted dijet+ISR analyses.

To illustrate the complementarity of the searches [60, 62], three different coupling scenarios are also considered in the interpretation of the results:

Scenario 1 $g_q = 0.25$, $g_\ell = 0$, $g_\chi = 1$ (leptophobic $Z'_{\mathrm{V}}/Z'_{\mathrm{A}}$);

Scenario 2 $g_q = 0.1$, $g_\ell = 0.01$, $g_\chi = 1$ (leptophilic Z'_{V});

Scenario 3 $g_q = 0.1$, $g_\ell = 0.1$, $g_\chi = 1$ (leptophilic Z'_{A}).

In particular, the lower lepton coupling value is set to highlight the dilepton search sensitivity even for very small values of this parameter.

The exclusions from the resonance searches (dijet, dibjet, dilepton) in the $(m_{Z'_{\mathrm{V/A}}}, m_\chi)$ plane are derived from the limits placed on resonances reconstructed with a Gaussian shape, while the limits from the

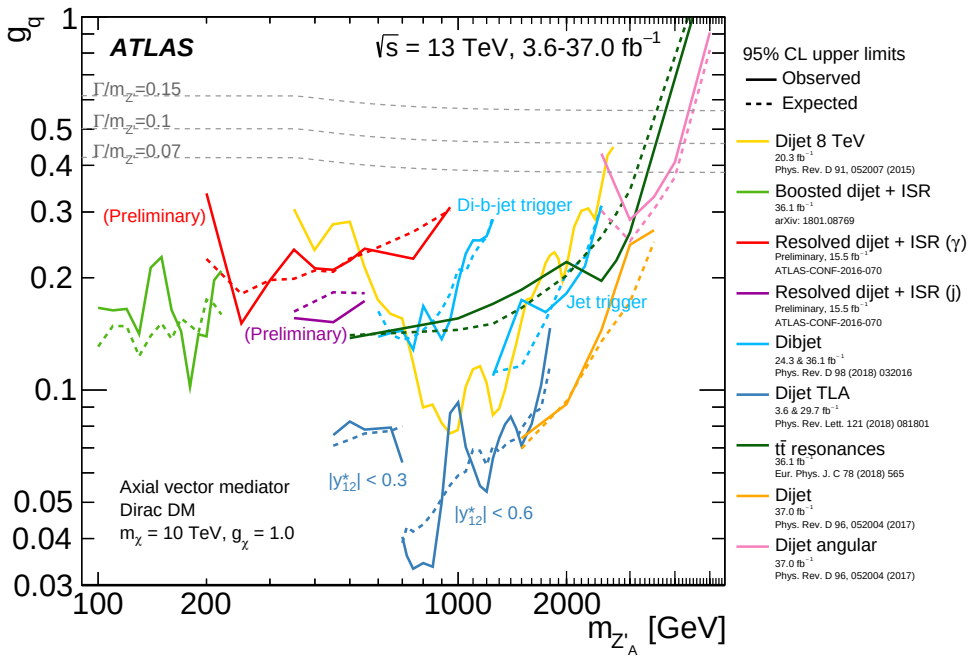

Figure 10: Dijet search contours for 95% CL upper limits on the coupling g_q as a function of the resonance mass $m_{Z'_{\mathrm{A}}}$ for the leptophobic axial-vector Z'_{A} model. The expected limits from each search are indicated by dotted lines. The TLA dijet analysis has two parts, employing different datasets with different selections in the rapidity difference y^* as indicated. The yellow contour shows the results of the dijet search using 20.3 fb^{-1} of 8 TeV data. Coupling values above the solid lines are excluded, as long as the signals are narrow enough to be detected using these searches. The TLA dijet search with $|y^*| < 0.6$ is sensitive up to $\Gamma/m_{Z'} = 7\%$, the TLA dijet with $|y^*| < 0.3$ and dijet + ISR searches are sensitive up to $\Gamma/m_{Z'} = 10\%$, and the dijet and dibjet searches are sensitive up to $\Gamma/m_{Z'} = 15\%$. The dijet angular analysis is sensitive up to $\Gamma/m_{Z'} = 50\%$. No limitation in sensitivity arises from large width resonances in the $t\bar{t}$ resonance analysis. Benchmark width lines are indicated in the canvas. The $\Gamma/m_{Z'} = 50\%$ lies beyond the canvas borders.

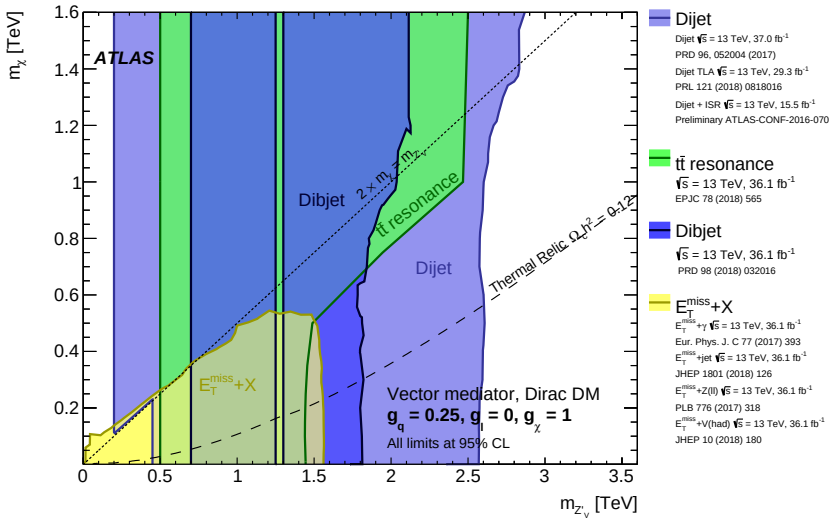

(a)

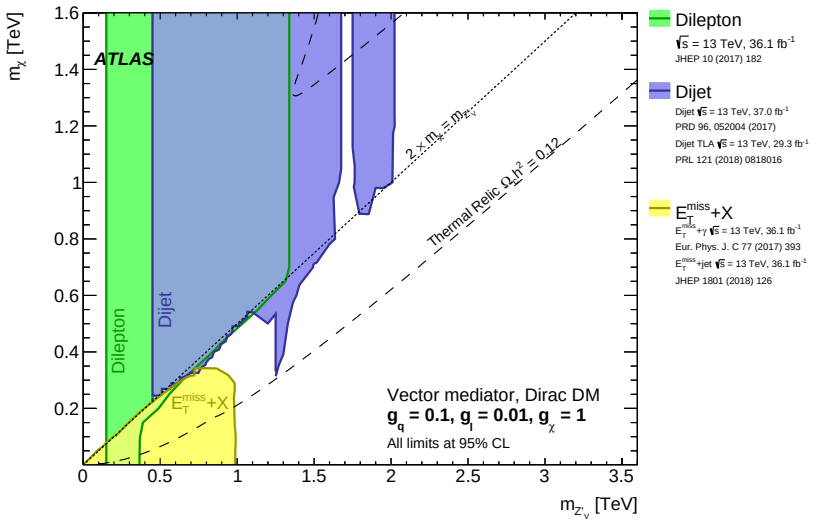

(b)

Figure 11: Regions in a (mediator-mass, DM-mass) plane excluded at 95% CL by dijet, dilepton and $E_{\mathrm{T}}^{\mathrm{miss}}+X$ searches, for leptophobic (a) or leptophilic (b) vector mediator simplified models described in Section 2.1.1. The exclusions are computed for a DM coupling g_χ, quark coupling g_q, universal to all flavours, and lepton coupling g_ℓ as indicated in each case. Dashed curves labelled "thermal relic" correspond to combinations of DM and mediator mass values that are consistent with a DM density of $\Omega h^2 = 0.12$ and a standard thermal history as computed in MadDM [62, 214]. Above the curve in (a) annihilation processes described by the simplified model deplete Ωh^2 to below 0.12. In (b), this occurs between the two dashed curves. The dotted line indicates the kinematic threshold where the mediator can decay on-shell into DM.

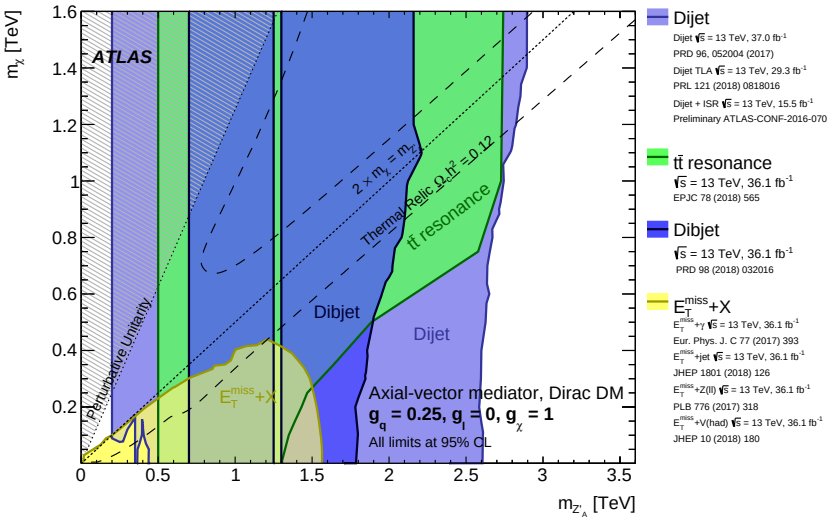

(a)

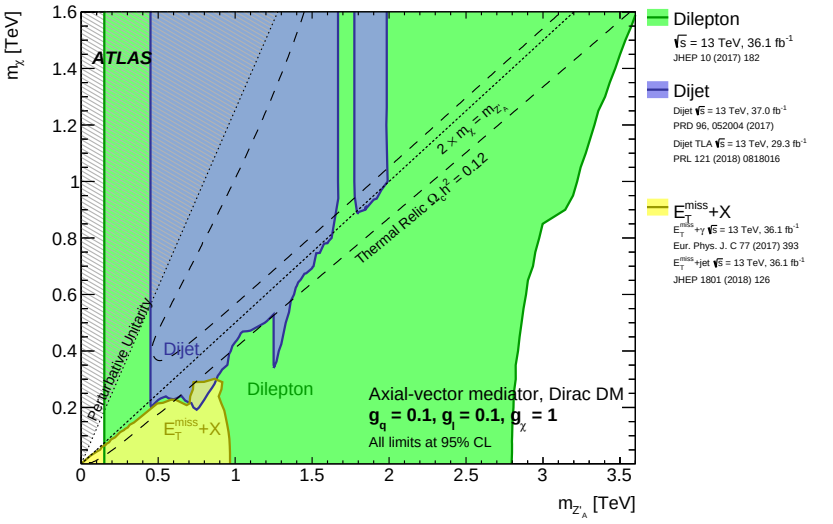

(b)

Figure 12: Regions in a (mediator-mass, DM-mass) plane excluded at 95% CL by visible and invisible searches, for leptophobic (a) or leptophilic (b) axial-vector mediator simplified models described in Section 2.1.1. The exclusions are computed for a DM coupling g_χ, quark coupling g_q, universal to all flavours, and lepton coupling g_ℓ as indicated in each case. Dashed curves labelled "thermal relic" correspond to combinations of DM and mediator mass values that are consistent with a DM density of $\Omega h^2 = 0.12$ and a standard thermal history, as computed in MadDM [62, 214]. Between the two curves, annihilation processes described by the simplified model deplete Ωh^2 to below 0.12. A dotted line indicates the kinematic threshold where the mediator can decay on-shell into DM. Excluded regions that are in tension with the perturbative unitary considerations of Ref. [215] are indicated by shading in the upper left corner.

$E_{\mathrm{T}}^{\mathrm{miss}}+X$ and $t\bar{t}$ resonance analyses are derived using a mixture of simulated signal samples and rescaling procedures as described in Section 3. For each scenario in Figures 11 and 12, dashed curves labelled "thermal relic" correspond to combinations of DM and mediator mass values that are consistent with a DM density of $\Omega h^2 = 0.12$ and a standard thermal history, as computed in MadDM [62, 214]. Between the two curves, annihilation processes described by the simplified model deplete the relic density to below the thermal value (except for Figure 11(a), where this occurs above the dashed curve). A dotted line indicates the kinematic threshold where the mediator can decay on-shell into DM particles. Excluded regions that are in tension with the perturbative unitary considerations of Ref. [215] are indicated by shading in Figure 12.

The sensitivity reach of the various experimental signatures for the leptophobic vector-mediator scenario as a function of the DM and mediator masses is summarised in Figure 11(a). Since the chosen universal quark coupling is relatively high in comparison with other benchmarks, the strongest limits are obtained from the resonance searches. These analyses are sensitive to mediator masses between 200 GeV and 2.5 TeV with little dependence on the DM mass. A reduction in the exclusion reach is observed at high mediator masses and for $200 < m_{Z'_{\mathrm{V}}} < 450$ GeV when $m_{Z'_{\mathrm{V}}} > 2m_{\chi}$, due to the opening of the $Z'_{\mathrm{V}} \to \chi\bar{\chi}$ decay channel. The boosted dijet + ISR search is not reinterpreted here but has sensitivity in this region. The lower limit on the mass is determined by the trigger requirements of the resolved dijet + ISR analysis. For $m_{Z'_{\mathrm{V}}} < 2m_{\chi}$, masses up to 2.9 TeV are excluded by the resolved dijet + ISR, dijet TLA and dijet searches. Compared to the dijet searches, the $t\bar{t}$ resonance analysis is particularly sensitive to the reduction in effective cross-section related to changes of the branching ratio, as can be inferred from the coupling reach of Figure 10. Conversely, the sensitivity of the $E_{\mathrm{T}}^{\mathrm{miss}}+X$ signatures is highest in the region $m_{Z'_{\mathrm{V}}} > 2m_{\chi}$, up to mediator masses of 1.5 TeV and provides unique coverage for masses below 500 GeV. The sensitivity of these analyses is strongly decreased for $m_{Z'_{\mathrm{V}}} < 2m_{\chi}$, where the DM particles are produced off-shell, with a consequent strong reduction of the production cross-section. For this reason, only the jet+$E_{\mathrm{T}}^{\mathrm{miss}}$ and $\gamma + E_{\mathrm{T}}^{\mathrm{miss}}$ analyses can probe the off-shell regime for this benchmark scenario, and only in the case of very low mediator and DM masses. It is important to highlight that if the value chosen for g_q were reduced, the relative interplay between the dijet and $E_{\mathrm{T}}^{\mathrm{miss}}+X$ searches would change, as exemplified by the change of the dijet limit in the different coupling scenarios described in the following.

The experimental limits for the leptophilic vector-mediator model are summarised in Figure 11(b). In this case, the mediator decay rates into quarks are reduced in favour of a higher branching ratio to DM particles, reducing the sensitivity of dijet searches to this scenario, whereas the leptonic branching ratio allows dilepton searches to impose constraints on a wide range of mediator masses. This benchmark highlights the complementarity among dijet, dilepton, and $E_{\mathrm{T}}^{\mathrm{miss}}+X$ final states. In this case, dibjet and $t\bar{t}$ resonance searches are not included in the final result. The resonance searches exclude mediator masses between 150 GeV and 2 TeV (except for a small gap around 1.7 TeV), if $m_{Z'_{\mathrm{V}}} < 2m_{\chi}$ and between 150 and 350 GeV for all DM masses. Complementarily, the $E_{\mathrm{T}}^{\mathrm{miss}}+X$ searches exclude mediator masses up to 1 TeV for $m_{Z'_{\mathrm{V}}} > 2m_{\chi}$.

Similar considerations can be made for the axial-vector mediator models, presented in Figure 12, with the exception that in the presence of non-vanishing coupling to leptons (leptophilic scenario), the dilepton resonance search becomes by far the most sensitive analysis for this model, excluding the mass range $150\ \mathrm{GeV} < m_{Z'_{\mathrm{A}}} < 2.8$ TeV for any DM mass. Also in this case, the sensitivity of this analysis increases when the $Z'_{\mathrm{A}} \to \chi\bar{\chi}$ is kinematically forbidden and becomes independent of the DM mass above threshold. For $m_{Z'_{\mathrm{A}}} < 2m_{\chi}$, masses up to 3.5 TeV are excluded.

Collider experiments provide an approach to DM searches which is complementary to direct and indirect

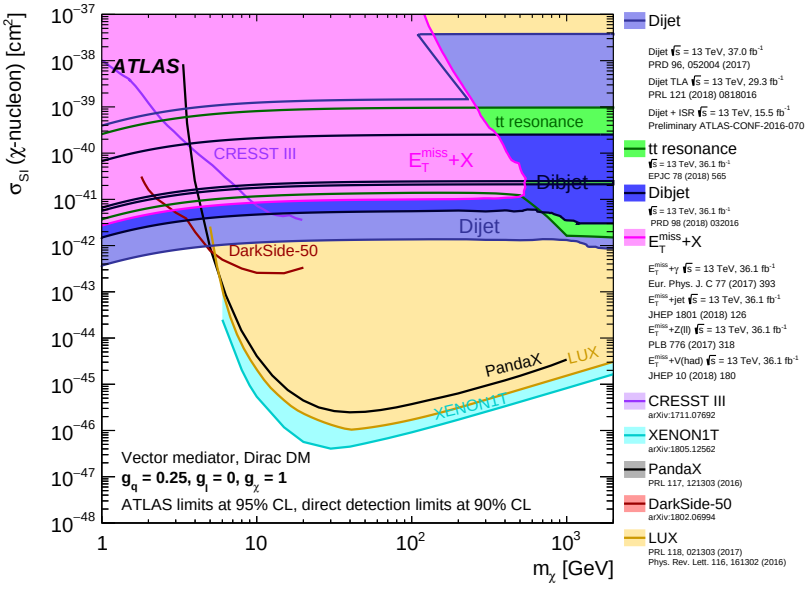

(a)

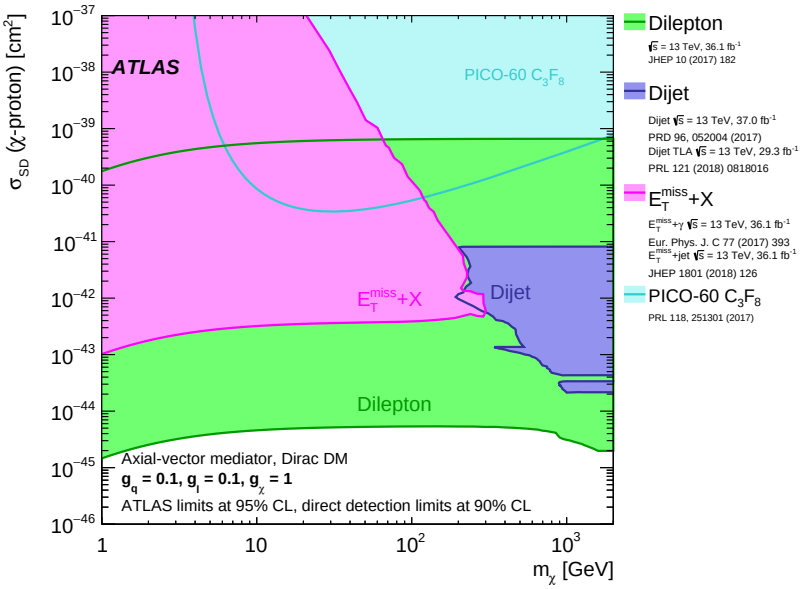

(b)

Figure 13: A comparison of the inferred limits with the constraints from direct detection experiments on (a) the spin-dependent WIMP–proton scattering cross-section in the context of the vector leptophobic model and (b) the spin-independent WIMP–nucleon scattering cross-section in the context of the axial-vector leptophilic model. The results from this analysis, excluding the region inside or to the left of the contour, are compared with limits from direct detection experiments. ATLAS limits are shown at 95% CL and direct detection limits at 90% CL. ATLAS searches and direct detection experiments exclude the shaded areas. Exclusions beyond the canvas are not implied for the ATLAS results. The dijet and $E_{\mathrm{T}}^{\mathrm{miss}}$ +X exclusion regions represent the union of exclusions from all analyses of that type.

detection experiments [61]. It is therefore interesting and informative, though model-dependent, to compare the V/AV limits with the results from other DM searches. Figure 13 shows the translation of the V/AV model limits into limits on the spin-dependent χ–proton and spin-independent χ–nucleon scattering cross-sections as a function of the DM mass. The direct detection experiments dominate the sensitivity by a few orders of magnitude for DM masses above 10 GeV, thanks to coherence effects, the spin-independent interaction cross-section with heavy nuclei is enhanced by A^2, where A is the number of nucleons in a nucleus. However, with the assumed coupling strengths, the analyses presented in this paper complement direct detection limits in the low DM mass range where the direct DM search experiments have less sensitivity due to the very low energy recoils that such low-mass DM particles would induce. The lower edge of the sensitivity contour for all analyses in Figure 13(a) (Figure 13(b)) is driven by the high-mass reach of each analysis in Figure 11(a) (12(b)), as the scattering cross-section limit is inversely proportional to the mediator mass reach (raised to the fourth power). Conversely, the upper edge of the scattering cross-section contour for the dijet and dilepton analyses is driven by their low-mass sensitivity limit due to the trigger requirements employed in these analyses. Further details of this comparison are discussed in Appendix B.

6.1.2 Baryon-charged interaction

In the context of the VBC model, the results from the $h(\gamma\gamma) + E_{\mathrm{T}}^{\mathrm{miss}}$ and $h(b\bar{b}) + E_{\mathrm{T}}^{\mathrm{miss}}$ analyses are interpreted in the plane formed by the Z'_{B} and DM masses, due to the characteristic signature of this model involving Higgs-strahlung from the Z'_{B} mediator. The $h(b\bar{b}) + E_{\mathrm{T}}^{\mathrm{miss}}$ interpretation was developed subsequently to the original publication [23]. The results are shown in Figure 14 in the $(m_{Z'_{\mathrm{B}}}, m_{\chi})$ plane for $g_q = 1/3$, $g_{\chi} = 1$ and $\sin\theta = 0.3$. The dashed lines indicate the expected exclusion contours from the two separate channels and their combination (based on best expected limits), while the black solid line shows the observed exclusion, presented only for the combined result. The band around the expected combined contour shows the effect of one-standard-deviation variation of the total systematic uncertainties. The $h(b\bar{b}) + E_{\mathrm{T}}^{\mathrm{miss}}$ analysis sets the strongest bounds in this model, excluding mediator masses up to 1.9 TeV for all DM mass hypotheses for which the mediator invisible decay is kinematically allowed. Due to the lower branching ratio, the $h(\gamma\gamma) + E_{\mathrm{T}}^{\mathrm{miss}}$ is less sensitive to this model for high mediator masses, but it is competitive for $m_{Z'_{\mathrm{B}}} < 50$ GeV.

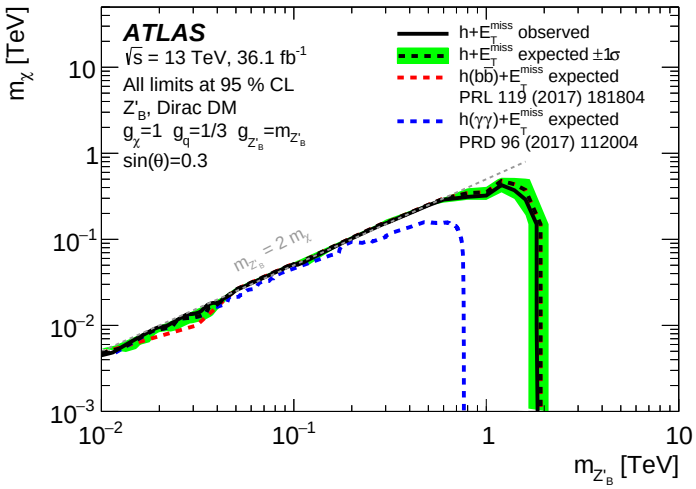

Figure 14: Exclusion contours for the VBC model in the $(m_{Z'_B}, m_\chi)$ plane for $g_q = 1/3$, $g_\chi = 1$ and $\sin\theta = 0.3$. The dashed lines indicate the expected exclusion contours from the two separate channels and their combination, while the solid line shows the observed exclusion, presented only for the combined result. The band around the expected combined contour shows the effect of a one-standard-deviation variation of the total systematic uncertainties. At high mediator masses, the combined exclusion fully overlaps with the exclusion from the $h(b\bar{b}) + E_{\mathrm{T}}^{\mathrm{miss}}$ analysis.

6.1.3 Neutral flavour-changing interaction

For the VFC models, expected and observed limits from the $t + E_{\mathrm{T}}^{\mathrm{miss}}$ and same-sign tt analyses are derived for each independent subprocess leading to the two signatures, as described in Section 2.1.3 and schematically summarised in Figures 2(b)–2(d). These individual results are converted into limits for the complete VFC model following the rescaling procedure described in Section A.2. These results were obtained subsequently to the original analyses publications.

The sensitivity of the experimental analyses to this model is explored in three scenarios that investigate different interpretation variables (where $\mathcal{B}$ is the invisible branching ratio of the mediator):

Scenario 1 $(m_{Z'_{\mathrm{VFC}}}, g_{ut})$ interpretation plane, assuming $g_\chi = 0.5$ or $g_\chi = 1.0$.

Scenario 2 $(\mathcal{B}(\chi\bar{\chi}), g_{ut})$ interpretation plane, assuming $m_{Z'_{\mathrm{VFC}}} = 1$ TeV.

Scenario 3 (g_χ, g_{ut}) interpretation plane, assuming $m_{Z'_{\mathrm{VFC}}} = 1$ TeV.

The first scenario, presented in Figure 15, directly identifies the constraints on the main parameters of the model. The two different g_χ coupling values highlight the different contributions of the invisible final state $(t + E_{\mathrm{T}}^{\mathrm{miss}})$, which probes g_{ut} values down to 0.7 for 1 TeV mediators and can exclude couplings down to 0.13 for 1.5 TeV mediators when the DM coupling is set to unity. In this scenario the visible final state (tt) is independent of g_χ and constrains couplings down to 0.3 for mediator masses up to 3 TeV. In this result, only mediator masses above 1 TeV are considered. However, mediator masses down to 100 GeV are excluded by previous publications [216] for a coupling assumption of $g_q \sim 3 \cdot 10^{-2}$.

The second and third scenarios, presented in Figure 16, further highlight the complementarity between the visible and invisible final states as a function of the couplings and the invisible branching ratio of the

mediator. Couplings of the Z'_{VFC} mediator to SM fermions can be excluded down to 0.14 for any value of g_χ or $\mathcal{B}(\chi\bar{\chi})$.

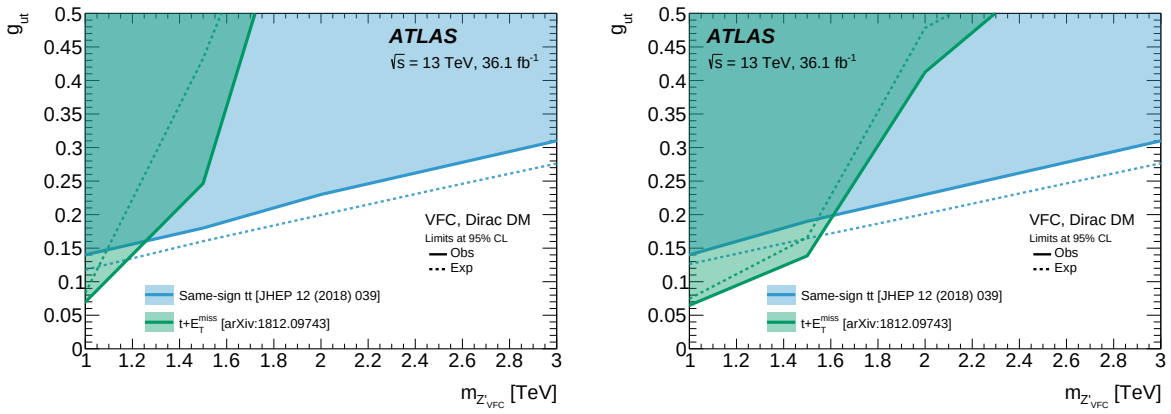

(a) (b)

Figure 15: Exclusion regions in the $(m_{Z'_{\mathrm{VFC}}}, g_{ut})$ plane from the $t + E_{\mathrm{T}}^{\mathrm{miss}}$ and same-sign tt analyses for the VFC model. The observed exclusion is indicated for each of the two analyses by the filled area. The mass of the DM particle is set to 1 GeV and the DM coupling, g_χ, is set to (a) 0.5 or (b) 1.

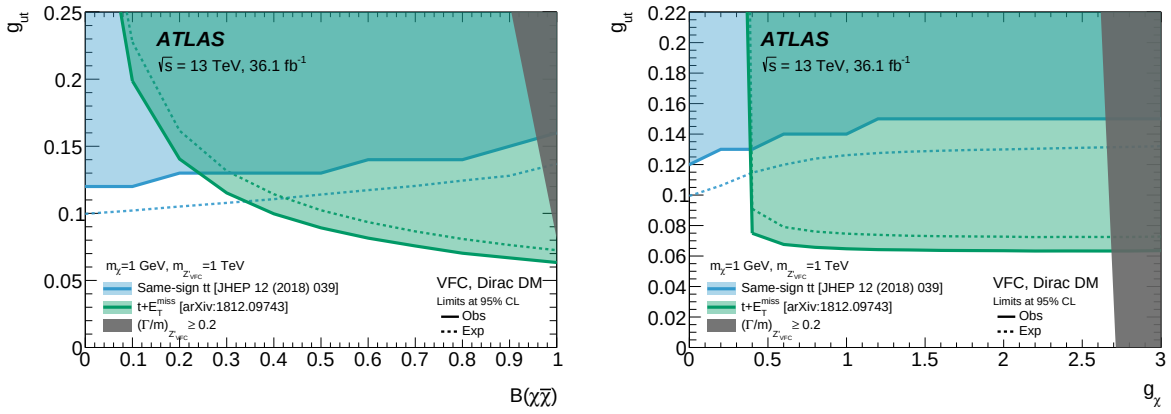

(a) (b)

Figure 16: Exclusion limits from the $t + E_{\mathrm{T}}^{\mathrm{miss}}$ and same-sign tt analyses for the VFC model as a function of the SM coupling g_{ut} and (a) the DM branching ratio or (b) the DM coupling g_χ. The observed exclusion is indicated for each of the two analyses by the filled area. The mass of the DM particle is set to 1 GeV and the mass of the Z'_{VFC} boson is set to 1 TeV. The dark shaded area corresponds to an invisible partial width of the mediator above 20%.

6.2 Scalar or pseudo-scalar dark matter models

6.2.1 Colour-neutral interaction

The most stringent limits on S/PS models are obtained from $t\bar{t} + E_{\mathrm{T}}^{\mathrm{miss}}$ final states, which are studied in three channels assuming fully-hadronic, semileptonic and fully-leptonic top pair decays, respectively. The

fully leptonic channel excludes scalar-mediator models with unitary couplings $g_\chi = g_q = g = 1$ up to mediator masses of 45 GeV, setting in this mass range the strongest upper limits on the ratio of the signal production cross-section to the nominal cross-section (signal strength or $\sigma/\sigma(g = 1.0)$), as shown in Figure 17(a). In the case of pseudo-scalar mediator models (Figure 17(b)), similar sensitivity is obtained by all channels and mediator masses in the range 15–25 GeV are excluded. In all cases, a DM mass of 1 GeV is assumed, but the results are valid for all DM mass choices for which the mediator's decay into a pair of DM particles is kinematically allowed ($m_{\phi/a} > 2m_\chi$). Pseudo-scalar mediator models can also be constrained by jet+$E_{\mathrm{T}}^{\mathrm{miss}}$ final states, where the mediator is produced through loop-induced gluon fusion. Although the limits obtained by this signature are not competitive with the $t\bar{t}$ +$E_{\mathrm{T}}^{\mathrm{miss}}$ final state, except in the mass range above 300 GeV, they provide a complementary constraint, which would become particularly important in the case of a discovery. For the scalar model, the jet+$E_{\mathrm{T}}^{\mathrm{miss}}$ final-states cross-section is instead too small to be probed. Ditop resonance searches in final states with two or four tops can also constrain this parameter space for $m_{\phi/a} > 2m_t$. However, $t\bar{t}$ production through a spin-0 resonance presents a strong interference pattern with SM top pair production [217], which needs to be treated with care. On the other hand, four-top final states are characterised by relatively low event yields with the currently available integrated luminosity. For these reasons the study of these final states is not considered here. Finally, $b\bar{b}$ +$E_{\mathrm{T}}^{\mathrm{miss}}$ final states are also used to set constraints on these simplified models, resulting in upper limits on the signal strength between 200 and 300 for mediator masses below 100 GeV. These results quantify the sensitivity to these models if up-type couplings are suppressed.

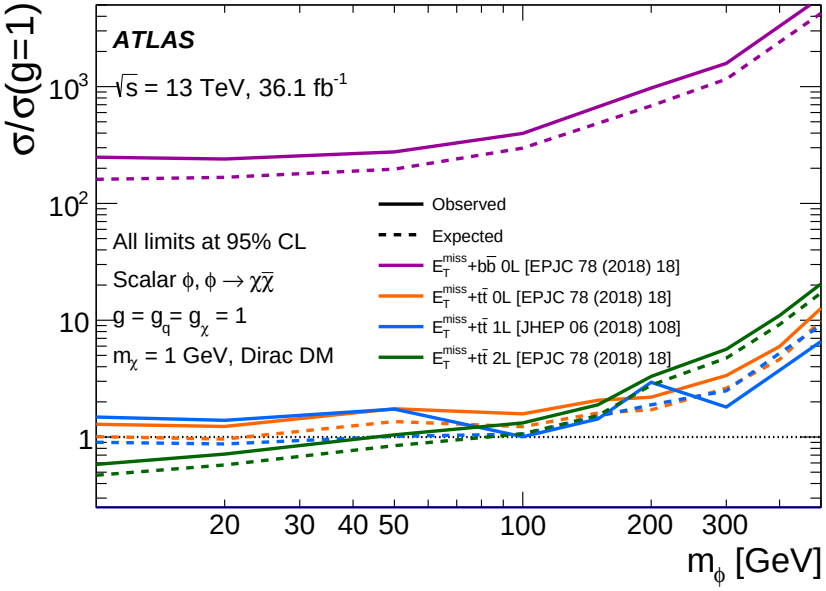

(a)

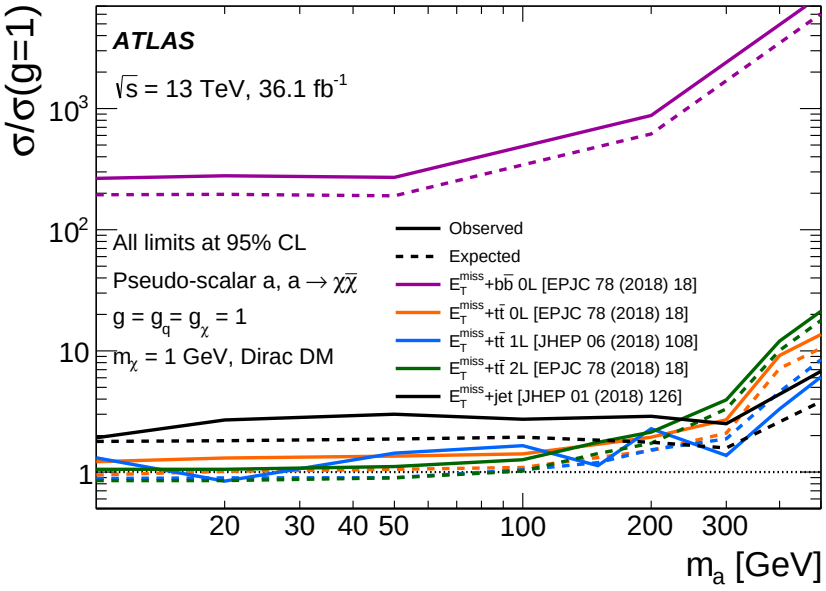

(b)

Figure 17: Exclusion limits for (a) colour-neutral scalar or (b) pseudo-scalar mediator models as a function of the mediator mass for a DM mass of 1 GeV. The limits are calculated at 95% CL and are expressed in terms of the ratio of the excluded cross-section to the nominal cross-section for a coupling assumption of $g = g_q = g_\chi = 1$. The solid (dashed) lines show the observed (expected) exclusion limits for each channel.

6.2.2 Colour-charged interaction

The strongest exclusion limits on colour-charged mediators η_q that couple to first- and second-generations left-handed quarks are set by the jet+$E_{\mathrm{T}}^{\mathrm{miss}}$ analysis. Assuming a unitary coupling, η_q mediator masses up to 1.7 TeV are excluded for $m_\chi = 50$ GeV. Furthermore, η_q mediator masses below 600 GeV are excluded for all DM masses such that the decay $\eta_q \to q\chi$ is kinematically allowed. The strongest exclusion limits on colour-charged mediators η_b that couple to third-generation right-handed b-quarks are set by the $b + E_{\mathrm{T}}^{\mathrm{miss}}$ analysis. Assuming a coupling set to the value that yields a relic density value consistent with astrophysical observations, masses up to 1.4 TeV are excluded for $m_\chi = 1$ GeV. Finally, $t + E_{\mathrm{T}}^{\mathrm{miss}}$ final states are used to constrain the colour-charged mediator's η_t coupling to right-handed top quarks. Mediator masses up to 3.4 TeV are excluded, assuming a 10 GeV DM particle mass and setting the coupling strengths of this model to: $\lambda_t = 0.4$ and $g_s = 0.2$.

6.3 Extended Higgs sector dark matter models

6.3.1 Two-Higgs-doublet models with a vector mediator

The 2HDM+Z'_{V} model is constrained by the $h(b\bar{b}) + E_{\mathrm{T}}^{\mathrm{miss}}$ and $h(\gamma\gamma) + E_{\mathrm{T}}^{\mathrm{miss}}$ analyses. The results are interpreted in terms of exclusion limits in the (m_A, $m_{Z'_{\mathrm{V}}}$) plane shown in Figure 18. The statistical combination of the two analyses is also presented. Masses of the pseudo-scalar A in the range 200–600 GeV are excluded for $m_{Z'_{\mathrm{V}}} = 1.5$ TeV. The limit in sensitivity is driven by the fact that the $A \to \chi\bar{\chi}$ branching ratio decreases with increasing m_A due to decay channels involving top quarks or other heavy bosons of the extended Higgs sector becoming accessible ($t\bar{t}$, HZ and $W^{\pm}H^{\mp}$). At higher $m_{Z'_{\mathrm{V}}}$ the loss in branching ratio is combined with the smaller production cross-section so that the reach of the analysis is limited to smaller pseudo-scalar masses. For $m_A < 2m_t$ and $m_A > 2m_\chi$, there are no more competing decay channels and the reach of the analysis does not depend on m_A any longer. This creates the turnover in the exclusion contour for $m_{Z'_{\mathrm{V}}} = 2.5$ TeV.

The two $h + E_{\mathrm{T}}^{\mathrm{miss}}$ decay signatures are highly complementary at low Z'_{V} masses, as can be observed in the enlarged inset in the figure, while the $h(b\bar{b}) + E_{\mathrm{T}}^{\mathrm{miss}}$ analysis dominates the sensitivity at high Z'_{V} masses. Due to this complementarity, the gain obtained by the statistical combination of the two signatures is limited to the low mass region for this model.

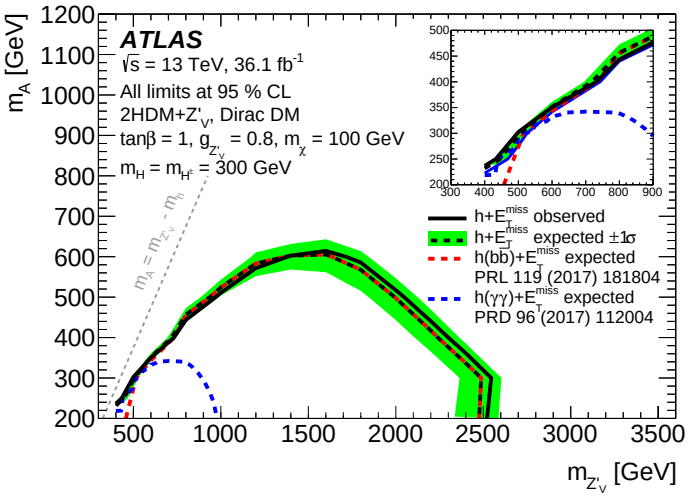

Figure 18: Exclusion contours for the 2HDM+Z'_{V} scenario in the $(m_{Z'_{\mathrm{V}}}, m_A)$ plane for $\tan\beta = 1$, $g_{Z'_{\mathrm{V}}} = 0.8$ and $m_\chi = 100$ GeV. The dashed lines indicate the expected exclusion contours from the two separate channels and their statistical combination, while the black solid line shows the observed exclusion, presented only for the combined result. The band around the expected combined contour shows the effect of a one-standard-deviation variation of the total systematic uncertainties. The sharp turn in the exclusion contour for $m_{Z'_{\mathrm{V}}} = 2.5$ GeV is given by the opening A decay channels competing with the considered final state for $m_A > 2m_t$. For this reason the exclusion sensitivity does not depend on m_A below threshold. The inset in the top-right side of the panel shows a zoomed-in version of the result for low $m_{Z'_{\mathrm{V}}}$ masses to highlight the complementarity between the $h(b\bar{b}) + E_{\mathrm{T}}^{\mathrm{miss}}$ and the $h(\gamma\gamma) + E_{\mathrm{T}}^{\mathrm{miss}}$ analyses in this parameter region.

6.3.2 Two-Higgs-doublet models with a pseudo-scalar mediator

As highlighted in Section 2.3.2, the 2HDM+a model is characterised by a rich phenomenology. Constraints on this model from ATLAS searches are presented in this paper. Four different benchmark scenarios are used to evaluate the sensitivity to this model achieved by the $Z/h + E_{\mathrm{T}}^{\mathrm{miss}}$, $t\bar{t}/b\bar{b}$+$E_{\mathrm{T}}^{\mathrm{miss}}$, h(inv), and $t\bar{t}t\bar{t}$ analyses. These four benchmark scenarios [63] are consistent with bounds from electroweak precision, flavour and Higgs observables and are chosen to highlight the complementarity of the various final states. These scenarios represent two-dimensional and one-dimensional scans of a five-dimensional parameter space, used to present the exclusion limits.

Scenario 1 (m_a, m_A) exclusion plane assuming $\tan\beta = 1$ and $\sin\theta = 0.35$;

Scenario 2 $(m_a, \tan\beta)$ exclusion plane assuming $m_A = 600$ GeV and $\sin\theta = 0.35$;

Scenario 3 $\sin\theta$ exclusion scan assuming

a) $m_A = 600$ GeV , $m_a = 200$ GeV and $\tan\beta = 0.5$, 1 or 50;

b) $m_A = 1000$ GeV , $m_a = 350$ GeV and $\tan\beta = 0.5$ or 1;

Scenario 4 m_χ exclusion scan assuming $m_A = 600$ GeV, $m_a = 250$ GeV, $\tan\beta = 1$, $\sin\theta = 0.35$.

In all cases, the masses of the heavy pseudo-scalar, heavy scalar, and charged bosons are kept equal ($m_A = m_H = m_{H^\pm}$). As visible in the results presented in Figure 19(a), the exclusion sensitivity is vastly dominated by the $h(b\bar{b}) + E_{\mathrm{T}}^{\mathrm{miss}}$ and $Z(\ell\ell) + E_{\mathrm{T}}^{\mathrm{miss}}$ analyses in the first scenario. These analyses are

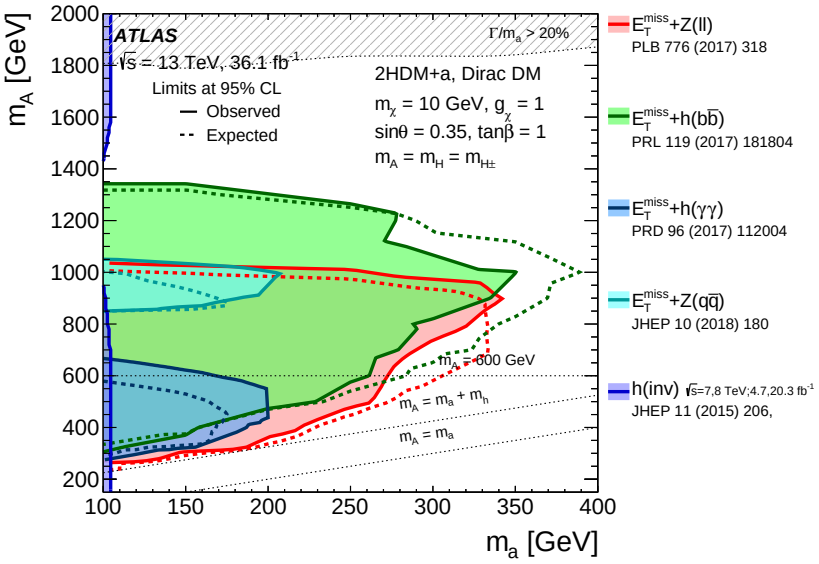

(a)

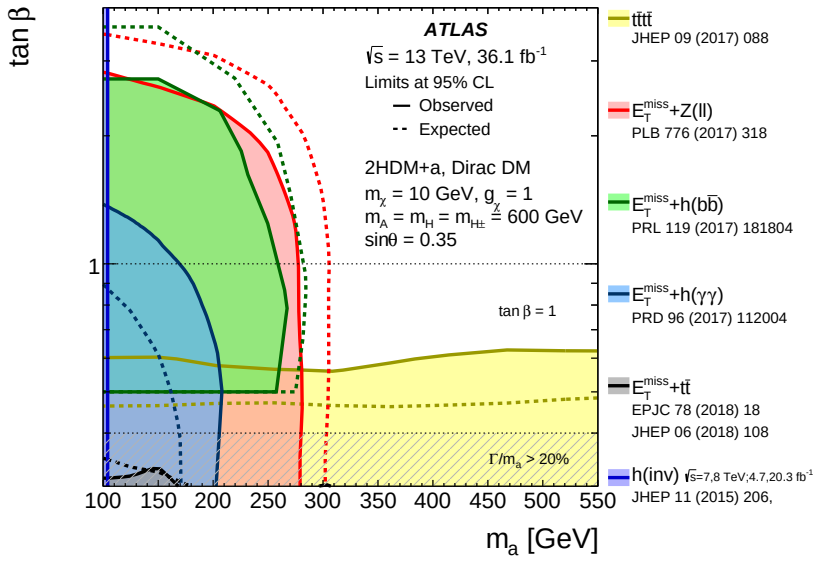

(b)

Figure 19: Regions in the (a) (m_a, m_A) and (b) $(m_a, \tan\beta)$ planes excluded by data at 95% CL by $X + E_{\mathrm{T}}^{\mathrm{miss}}$ and $t\bar{t}t\bar{t}$ analyses, following the parameter choices of scenarios 1 and 2 of the 2HDM+a model. The dashed grey regions at the top of (a) and the bottom of (b) indicate the region where the width of any of the Higgs bosons exceeds 20% of its mass. The exclusion limits presented above conservatively neglect the contribution from $b\bar{b}$-initiated production, which might be sizeable for $\tan\beta \geq 3$ for the $Z + E_{\mathrm{T}}^{\mathrm{miss}}$ channel and, to a lesser extent, for the $h + E_{\mathrm{T}}^{\mathrm{miss}}$ one.

mostly sensitive to the production diagrams of Figures 6(d) and 6(e) and their sensitivity depends on both pseudo-scalar mediator masses. The maximum reach is obtained for light pseudo-scalar m_a up to 340 GeV, if the A boson mass is set to 1 TeV, while for $m_a = 150$ GeV A boson masses between 280 GeV and 1.35 TeV are excluded. The combined contours of the $h(b\bar{b}) + E_{\mathrm{T}}^{\mathrm{miss}}$ and $Z(\ell\ell) + E_{\mathrm{T}}^{\mathrm{miss}}$ analyses include the $h(\gamma\gamma) + E_{\mathrm{T}}^{\mathrm{miss}}$ and $Z(q\bar{q}) + E_{\mathrm{T}}^{\mathrm{miss}}$ exclusion areas, although the $h(\gamma\gamma) + E_{\mathrm{T}}^{\mathrm{miss}}$ analysis still complements $h(b\bar{b}) + E_{\mathrm{T}}^{\mathrm{miss}}$ at low (m_a, m_A) values. Finally, the h(inv) branching ratio limit constrains very low values of m_a for m_A mass below 900 GeV and above 1.4 TeV, being sensitive only to the a boson production cross-section.

In the context of 2HDM models, it is customary to investigate the sensitivity in terms of the $\tan\beta$ parameter. This is achieved in the second scenario presented in Figure 19(b). Although the exclusion reach is dominated also in this case by the $h(b\bar{b}) + E_{\mathrm{T}}^{\mathrm{miss}}$ and $Z(\ell\ell) + E_{\mathrm{T}}^{\mathrm{miss}}$ analyses, two additional signatures contribute at $\tan\beta \sim 0.5$: the $t\bar{t} + E_{\mathrm{T}}^{\mathrm{miss}}$ and the $t\bar{t}t\bar{t}$ analyses. The sensitivity of the former analysis is driven by the production cross-section of the a mediator in association with a top-quark pair and it decreases when the decay of the light pseudo-scalar into a top-quark pair is kinematically allowed and competes with $a \to \chi\bar{\chi}$. On the other hand, the sensitivity of the latter analysis is fairly independent of m_a due to the contribution to the total four-top production cross-section from the heavy bosons $H/A \to t\bar{t}$, both of which have masses fixed to 600 GeV in this scenario. In the case of the $h(b\bar{b}) + E_{\mathrm{T}}^{\mathrm{miss}}$ analysis, the exclusion was not investigated below $\tan\beta = 0.5$. Given the non-trivial dependency of the width on $\tan\beta$ in this channel, it is not possible to extrapolate beyond the area explored.

Figures 20(a) and 20(b) present the exclusion limits dependence on the mixing angle, $\sin\theta$, for a low-mass and high-mass a hypothesis, as considered in the third scenario. The limits are expressed in terms of the ratio of the excluded cross-section to the nominal cross-section of the model. For scenario 3a (Figure 20(a)), the lowest cross-section values are excluded by the $Z(\ell\ell) + E_{\mathrm{T}}^{\mathrm{miss}}$ and $h(b\bar{b}) + E_{\mathrm{T}}^{\mathrm{miss}}$ analyses. The sensitivity of both $Z + E_{\mathrm{T}}^{\mathrm{miss}}$ analyses monotonically improves as a function of $\sin\theta$, as the cross-section of the non-resonant and resonant production diagrams, in Figures 6(d) and 6(e) respectively, increases with $\sin\theta$. Conversely, the same production diagrams for the $h + E_{\mathrm{T}}^{\mathrm{miss}}$ signatures have very different dependence on the mixing angle [149] in the two m_a regimes explored here. The contribution of each diagram is also affected by the different $h(b\bar{b}) + E_{\mathrm{T}}^{\mathrm{miss}}$ and $h(\gamma\gamma) + E_{\mathrm{T}}^{\mathrm{miss}}$ analysis selections. For this scenario, both analyses have maximum of sensitivity around $\sin\theta \sim 0.5$. The three heavy-flavour signatures, $b\bar{b} + E_{\mathrm{T}}^{\mathrm{miss}}$, $t\bar{t} + E_{\mathrm{T}}^{\mathrm{miss}}$ and $t\bar{t}t\bar{t}$, are presented for different $\tan\beta$ assumptions. A value of $\tan\beta = 50$ is considered for $b\bar{b} + E_{\mathrm{T}}^{\mathrm{miss}}$, with the aim of probing the parameter space where the coupling of the a mediator to down-type quarks is enhanced. However, the $t\bar{t} + E_{\mathrm{T}}^{\mathrm{miss}}$ and $t\bar{t}t\bar{t}$ signatures are presented for $\tan\beta = 0.5$ as they are not yet able to probe $\tan\beta$ values near unity. The $t\bar{t}t\bar{t}$ signature, in particular, shows a $\sin\theta$ dependence complementary to the other signatures due to the combined contribution of all neutral bosons decaying into top-quark pairs and is particularly sensitive at very small mixing angles. Scenario 3b, presented in Figure 20(b), sets the mass of the light pseudo-scalar so that the $a \to t\bar{t}$ decay is kinematically allowed, which introduces an additional $\sin\theta$ dependence to the $X + E_{\mathrm{T}}^{\mathrm{miss}}$ analyses interpreted in this scenario. For this reason, the highest sensitivity for each analysis is found to be broadly around (or slightly below) the maximal mixing condition ($\theta = \pi/4$), except for the $t\bar{t}t\bar{t}$ and $h + E_{\mathrm{T}}^{\mathrm{miss}}$ signatures. The $t\bar{t}t\bar{t}$ signature shows a constant sensitivity as a function of $\sin\theta$ (with an increase for very high values) due to the mass assumptions of this scenario ($m_a = 350$ GeV and $m_{A/H} = 1$ TeV) which cause the $t\bar{t}t\bar{t}$ production cross-section to be completely dominated by the $t\bar{t} + a(tt)$ process. The $h + E_{\mathrm{T}}^{\mathrm{miss}}$ signatures have a complex dependence on the mixing angle. This is due to the different contributions of resonant and non-resonant processes to the final selection in the two analyses. In this case it is possible to observe that the $h(b\bar{b}) + E_{\mathrm{T}}^{\mathrm{miss}}$ analysis presents a maximum in sensitivity around the maximal mixing condition. The $h(\gamma\gamma) + E_{\mathrm{T}}^{\mathrm{miss}}$ analysis instead shows a local sensitivity minimum around $\sin\theta \sim 0.55$.

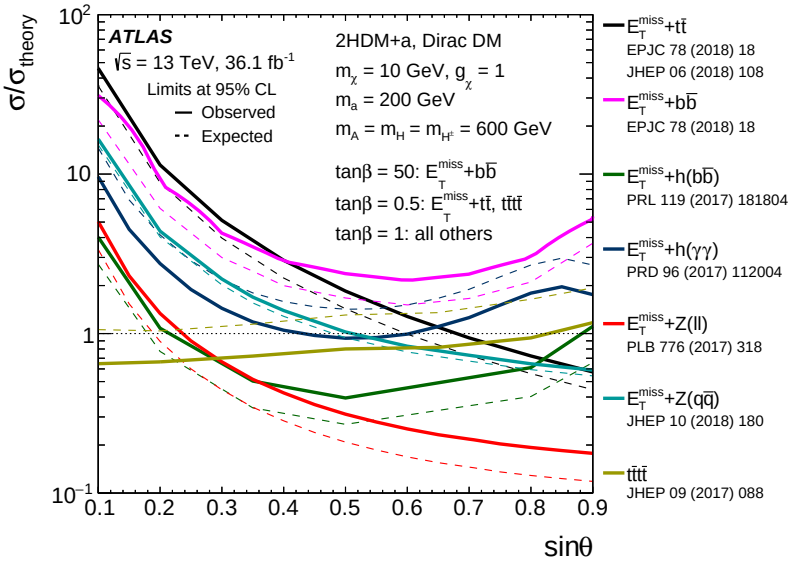

(a)

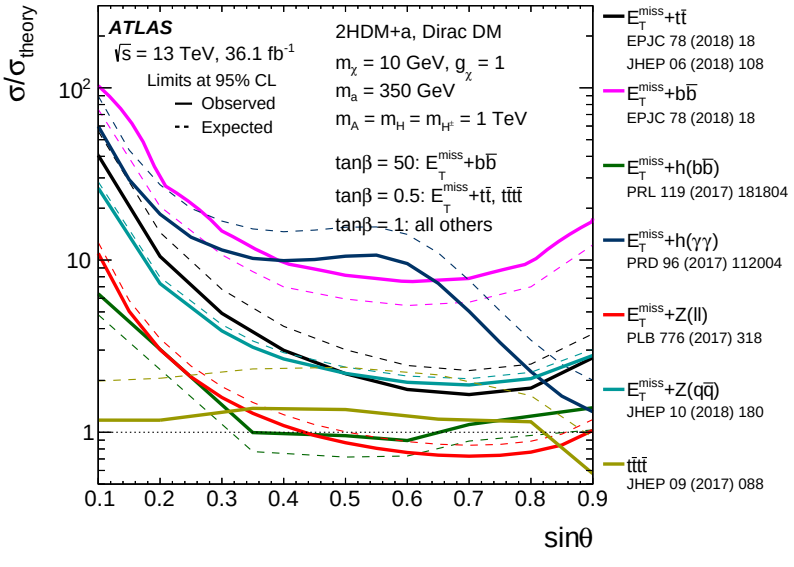

(b)

Figure 20: Observed exclusion limits for the 2HDM+a model as a function of $\sin\theta$, following the two parameter choices of scenario 3, (a) low-mass and (b) high-mass a hypotheses. The limits are calculated at 95% CL and are expressed in terms of the ratio of the excluded cross-section to the nominal cross-section of the model.

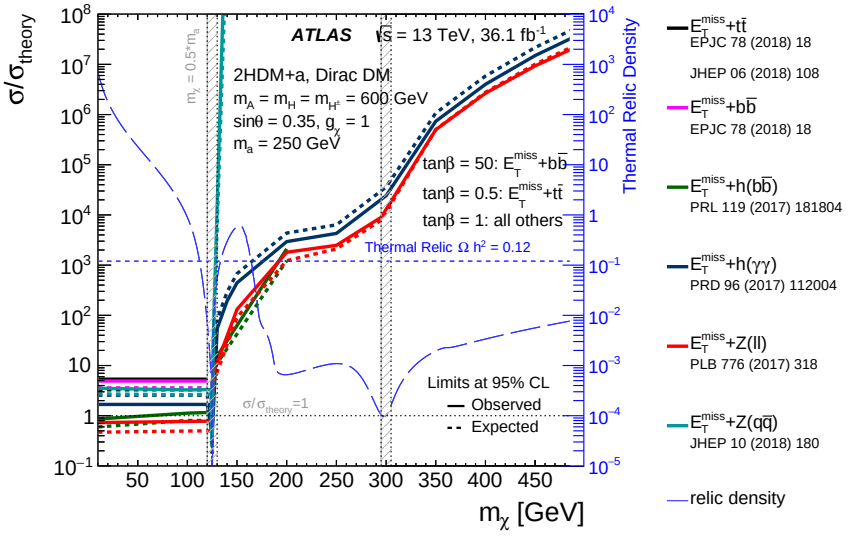

Figure 21: Observed exclusion limits for the 2HDM+a model as a function of m_χ, following the parameter choices of scenario 4. The limits are calculated at 95% CL and are expressed in terms of the ratio of the excluded cross-section to the nominal cross-section of the model. The relic density for each m_χ assumption is superimposed in the plot (long-dashed line) and described by the right vertical axis. For DM mass values where the relic density line is below $\Omega h^2 = 0.12$, the model depletes the relic density to below the thermal value. The two valleys at $m_\chi = 125$ GeV and $m_\chi = 300$ GeV determine the two a-funnel and A-funnel regions [63, 218, 219] where the predicted relic density is depleted by the resonant enhancement of the processes $\chi\bar{\chi} \to A/a \to$ SM.

Finally, Figure 21 presents the reach of the various experimental searches in a cosmological perspective, following the prescription of the fourth benchmark scenario. In this case, the observed exclusion limits in terms of the ratio of the excluded cross-section to the nominal cross-section of the model are investigated as a function of the DM mass, which is the parameter with the strongest impact on the relic density predicted by the 2HDM+a model. The region beyond $m_\chi = 200$ GeV was not explored by the $h(b\bar{b}) + E_{\mathrm{T}}^{\mathrm{miss}}$ analysis, thus the exclusion is not shown. For the same reason, the $b\bar{b} + E_{\mathrm{T}}^{\mathrm{miss}}$ exclusion is not shown beyond $m_\chi = 125$ GeV. The long-dashed line indicates the computed relic density for the 2HDM+a model as a function of the DM mass. The two valleys at $m_\chi = 125$ GeV and $m_\chi = 300$ GeV determine the two a-funnel and A-funnel regions [63, 218, 219] where the predicted relic density is depleted by the resonant enhancement of the processes $\chi\bar{\chi} \to A/a \to$ SM. The plateau around and above $m_\chi \sim 200$ GeV is determined by the increase in annihilation cross-section of the DM particles close to threshold for $\chi\bar{\chi} \to ha \to$ SM and $\chi\bar{\chi} \to t\bar{t}$. For DM masses around $m_a/2$ or $m_\chi > 170$ GeV the model predicts a relic density which is equal to or below the thermal value, $\Omega h^2 = 0.12$. As the DM mass increases further, annihilation via single s-channel diagrams is more and more suppressed and the observed DM relic density can again be reproduced. At low values of m_a this happens around $m_\chi \sim 10$ TeV and is outside the range considered in Figure 21. For all $X + E_{\mathrm{T}}^{\mathrm{miss}}$ signatures considered, the sensitivity is independent of the DM mass as long as the lightest pseudo-scalar mediator, whose mass is fixed at 250 GeV in this scenario, is allowed to decay into a $\chi\bar{\chi}$ pair. The $Z(\ell\ell) + E_{\mathrm{T}}^{\mathrm{miss}}$ analysis excludes this parameter space. For higher DM masses, the sensitivity of all analyses quickly decreases and no exclusion is observed. For $m_\chi > m_a/2$ all parameter choices that fulfil or deplete the relic density value are still unconstrained.

6.4 Scalar dark energy model

The results of the jet+$E_{\mathrm{T}}^{\mathrm{miss}}$ and $t\bar{t}$ +$E_{\mathrm{T}}^{\mathrm{miss}}$ analyses are interpreted in terms of limits on the two Lagrangian effective operators $\mathcal{L}_1$ and $\mathcal{L}_2$ for a scalar DE model, introduced in Section 2.4. The results are derived as a function of the suppression scale, M_1 and M_2, for each operator and the effective coupling associated with the UV completion of the EFT, g_*, and are shown in Figure 22. The EFT operators are only valid in the regime where the momentum transfer is $Q_{\mathrm{tr}} \ll M$. For the limits shown in Figure 22, it is assumed that the EFT approximation is valid for events where $Q_{\mathrm{tr}} < g_* M$. For events failing this requirement, the iterative rescaling procedure detailed in Ref. [60] is applied. The $t\bar{t}$ +$E_{\mathrm{T}}^{\mathrm{miss}}$ analysis yields the most stringent constraints on the $\mathcal{L}_1$ operator (Figure 22(a)), as expected from the fact that the interaction described by $\mathcal{L}_1$ is proportional to the masses of the SM fermions to which the DE scalar couples. The limits are obtained from the search channel (fully hadronic, semileptonic or fully leptonic top pair decays) that provides the smallest expected $\mathrm{CL_s}$ value. The fully-hadronic and semileptonic channels contribute the most and similarly to the final sensitivity of the analysis, which excludes a suppression scale of about 200 GeV for $g_* \gtrsim \pi^2$. The $t\bar{t}$ +$E_{\mathrm{T}}^{\mathrm{miss}}$ search is not yet sensitive to weakly coupled models, due to the high momentum transfers involved in the production of the top quarks, which are close to the exclusion limit.

The jet+$E_{\mathrm{T}}^{\mathrm{miss}}$ analysis yields the most stringent constraints on the $\mathcal{L}_2$ operator (Figure 22(b)), due to the fact that this interaction is proportional to the momenta of the particles involved, excluding up to $M \simeq 1.2$ TeV for $g_* \gtrsim \pi$. Due to the absence of heavy particles in the final state, the region of EFT validity for the jet+$E_{\mathrm{T}}^{\mathrm{miss}}$ search is larger, with the constraints extending to lower values of the effective coupling.

These results improve upon the constraints on the disformal operator from astrophysical probes and non-collider experiments by several orders of magnitude [220] and also represent a significant improvement on the limits obtained by a similar reinterpretation of ATLAS and CMS results that made use of a smaller dataset at $\sqrt{s} = 8$ TeV [79].

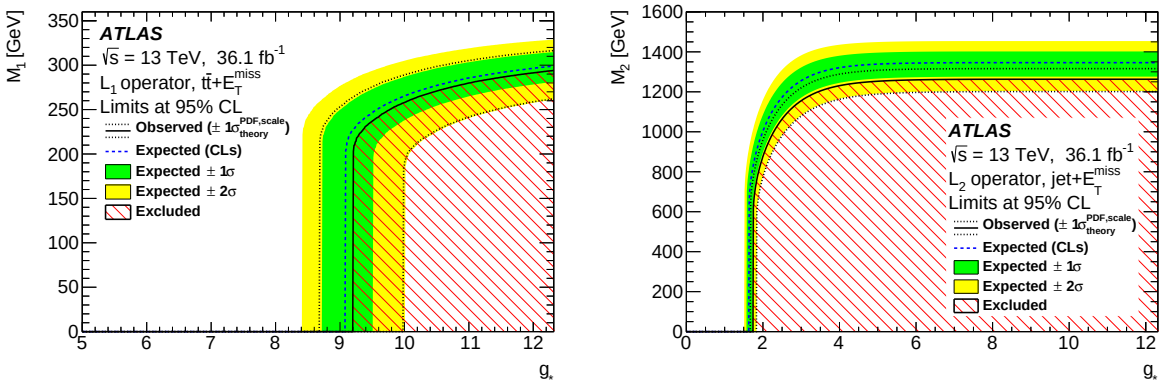

(a) (b)

Figure 22: Exclusion plots for (a) $\mathcal{L}_1$ and (b) $\mathcal{L}_2$ on the (g_*, M) plane, after rescaling to take into account the EFT validity criterion [60].

7 Conclusions

This paper summarises the lively experimental programme of searches for mediator-based particle dark matter and scalar dark energy performed by the ATLAS Collaboration. The analyses presented are based on up to 37 fb^{-1} of proton–proton collisions data at a centre-of-mass energy of $\sqrt{s}$ = 13 TeV collected by the ATLAS detector at the LHC in 2015 and 2016. The h(inv) analysis considers up to 4.7 fb^{-1} at centre-of-mass energy of $\sqrt{s}$ = 7 TeV and 20.3 fb^{-1} at centre-of-mass energy of $\sqrt{s}$ = 8 TeV. The results from the searches presented are in agreement with the Standard Model predictions, thus results are translated into exclusion limits on mediator-based dark matter and dark energy models.

Simplified models with the exchange of a vector or axial-vector mediator in the s-channel with Dirac fermions as dark matter candidates are studied. Masses of leptophobic (leptophilic) vector and axial-vector mediators between 200 GeV and 2.5 TeV (3.5 TeV), for coupling values $g_q = 0.25$ and $g_\chi = 1$, and $m_\chi = 1$ TeV, are excluded at 95% CL. In the context of a baryon-charged interaction, masses of the Z'_B boson are excluded up to 1.9 TeV for $m_\chi = 1$ GeV and coupling values of $g_\chi = 1$ and $g_q = 1/3$. Limits on a flavour-changing mediator model are set by two complementary searches targeting visible and invisible decays of the mediator, Z'_{VFC}. Masses up to 1.85 TeV for coupling values of $g_q = 0.35$ and $g_\chi = 1.0$ are excluded for invisible decays, while g_q coupling values between 0.14 and 0.35 for mediator masses between 1 TeV and 3 TeV are excluded for visible decays.

A simplified model of dark matter production including a colour-neutral scalar (pseudo-scalar) mediator is considered, and mediator masses below 45 GeV (in the range 15–25 GeV) are excluded for dark matter particles with $m_\chi = 1$ GeV and $g_\chi = 1$. Masses for colour-charged mediators, coupling to first- and second-generation left-handed quarks, are excluded up to 1.7 TeV, for $m_\chi = 50$ GeV for $g_\chi = 1$. Colour-charged mediators that couple to right-handed b-quarks (t-quarks) are excluded for masses up to 1.4 TeV (3.4 TeV) for low dark matter masses.

An extended two-Higgs-doublet model with an additional pseudo-scalar, a, which couples the dark matter particles to the Standard Model is used to exploit the broad phenomenology with diverse final-state signatures predicted by this type of model. Masses of the pseudo-scalar mediator, a, are excluded up to 350 GeV for $m_A = m_H = m_{H^\pm} = 1$ TeV, $\sin\theta = 0.35$ and $\tan\beta = 1.0$. The $Z(\ell\ell) + E_{\mathrm{T}}^{\mathrm{miss}}$ and $h(b\bar{b}) + E_{\mathrm{T}}^{\mathrm{miss}}$ searches are the most sensitive analyses in this high mediator-mass region. Previously published limits on a two-Higgs-doublet model with an additional vector mediator are improved upon by the statistical combination of the two decay channels studied: $h(b\bar{b}) + E_{\mathrm{T}}^{\mathrm{miss}}$ and $h(\gamma\gamma) + E_{\mathrm{T}}^{\mathrm{miss}}$. Mediator masses between 400 GeV and 2.5 TeV are excluded for dark matter masses of 100 GeV.

Finally, a Horndeski model for dark energy is studied in the context of ATLAS searches. This model introduces a dark energy scalar which couples to gravity. Limits on the two Lagrangian effective operators, $\mathcal{L}_1$ and $\mathcal{L}_2$, are set by the $t\bar{t} + E_{\mathrm{T}}^{\mathrm{miss}}$ and jet+$E_{\mathrm{T}}^{\mathrm{miss}}$ analyses, respectively. The suppression scale is excluded up to 200 GeV for $g_* = \pi^2$ for the $\mathcal{L}_1$ operator. For the $\mathcal{L}_2$ operator, suppression scales up to 1.2 TeV for $g_* = \pi$ are excluded. These results are the first interpretation of a dark energy model by a collider experiment.

Appendix

A Rescaling details for signal models

A.1 V/AV models

For all V/AV models, reconstructed samples were produced only for a specific reference scenario (either a vector or an axial-vector leptophobic mediator model). Rescaling factors for the acceptance ($w_{\mathcal{A}}$) and the cross-section (w_{σ}) were calculated to match the acceptance and cross-section of each of the other scenarios to the reference. The acceptance weights were calculated for each $(m_{Z'}, m_{\chi})$ mass hypothesis as the ratio of the particle-level acceptance for each of the NLO benchmark models considered ($\mathcal{A}^{\text{NLO}}_{\text{truth}}$) to the particle-level acceptance of the analysis for the reference NLO scenario in a fiducial region ($\mathcal{A}^{\text{ref}}_{\text{truth}}$):

$$w_{\mathcal{A}}(m_{Z'}, m_{\chi}) = \frac{\mathcal{A}^{\text{NLO}}_{\text{truth}}(m_{Z'}, m_{\chi})}{\mathcal{A}^{\text{ref}}_{\text{truth}}(m_{Z'}, m_{\chi})}.$$

The cross-section weights were calculated for each $(m_{Z'}, m_{\chi})$ mass hypothesis in a similar way, as the ratio of the reference cross-section at NLO to each cross-section of the four NLO benchmark models. The acceptance rescaling weights were found to be consistent with unity for the $Z'(\chi\bar{\chi}) + j$ and $Z'(\chi\bar{\chi}) + \gamma$ signatures.

A few specific exceptions apply to this treatment. In case of the $Z'(\chi\bar{\chi}) + j$ signature, the cross-section rescaling factors were calculated from LO samples (DMSimp [113, 182] generated with MG5_aMC@NLO 2.4.3 (LO) [174]) and applied to the samples described in Table 2. In the specific case of the $Z'(\chi\bar{\chi}) + V$ signature, the baseline samples were generated at LO and rescaled at particle level to match the NLO samples described in the table. Finally, the exclusions from the resonance searches (dijet, dilepton, dibjet) as a function of the $(m_{Z'}, m_{\chi})$ interpretations are derived from the limits calculated for Gaussian-shape resonances [175], and the samples in Table 2 are only used to derive the cross-section normalisation for the final results and the limits for the leptophobic Z'_{A} mediator models as a function of the universal coupling strength. The $Z'(t\bar{t})$ samples were obtained from the topcolour-assisted technicolour samples of [176] rescaled at particle level to match the DMSimp models described in Table 2. The correction weights between the two samples were calculated from the bin-by-bin ratio of the invariant mass distributions of the $t\bar{t}$ system for the two samples at particle level. An additional uncertainty is assigned to account for this procedure as described in Section 5.

A.2 VFC model

The VFC model is studied in two final states: $pp \to tZ'_{\text{VFC}} \to t\chi\bar{\chi}$ and $pp \to tt(j)$ (via Z'_{VFC}).

A complete set of models with the full ATLAS detector simulation was generated as a function of $m(Z'_{\text{VFC}})$ and assuming minimal width and unitary couplings, following the generation settings summarised in Table 2. In order to assess the experimental constraints on all the the model parameters, g_{ut}, g_{χ} and subsequently $\Gamma(Z'_{\text{VFC}})$, a rescaling procedure is applied.

In the case of the $t\chi\bar{\chi}$ final state, for each point in the parameter space, rescaling factors were calculated at particle level to match the acceptance and cross-section to those of the simulated reference model.

Three different matrix-element amplitudes contribute to the same-sign top-quark signature ($tt(j)$) relevant for this model: (i) prompt tt production in Figure 2(c), (ii) on-shell mediator in Figure 2(b), (iii) off-shell mediator in Figure 2(d). The relative contributions of the three amplitudes depend on the model parameters, but not the kinematic properties of each process. The three subprocesses, which were generated separately with full detector simulation, are combined according to the following formula to model the signal kinematics for any choice of parameter values (ξ):

$$\mathrm{d}\sigma(\boldsymbol{\xi}) \;=\; \alpha(\boldsymbol{\xi})\,\mathrm{d}\sigma^{\mathrm{ref}}_{tt} \;+\; \beta(\boldsymbol{\xi})\,\mathrm{d}\sigma^{\mathrm{ref}}_{\mathrm{OnShell}} \;+\; \gamma(\boldsymbol{\xi})\,\mathrm{d}\sigma^{\mathrm{ref}}_{\mathrm{OffShell}}.$$

The functions α, β, γ can be computed with MadGraph as the ratio of the desired cross-section to the baseline cross-section:

$$\alpha(\boldsymbol{\xi}) \;\equiv\; \frac{\sigma_{tt}(\boldsymbol{\xi})}{\sigma_{tt}(\boldsymbol{\xi}_{\mathrm{ref}})} \quad,\quad \beta(\boldsymbol{\xi}) \;\equiv\; \frac{\sigma_{\mathrm{OnShell}}(\boldsymbol{\xi})}{\sigma_{\mathrm{OnShell}}(\boldsymbol{\xi}_{\mathrm{ref}})} \quad,\text{ and }\quad \gamma(\boldsymbol{\xi}) \;\equiv\; \frac{\sigma_{\mathrm{OffShell}}(\boldsymbol{\xi})}{\sigma_{\mathrm{OffShell}}(\boldsymbol{\xi}_{\mathrm{ref}})}.$$

A.3 2HDM+a models with heavy-flavour final states

The $\chi\bar{\chi} + t\bar{t}/b\bar{b}$ signature of the 2HDM+a model can be successfully described [63] as the superposition of the associated production of two heavy-flavour quarks with either the light or the heavy pseudo-scalar mediator, which subsequently decays into a $\chi\bar{\chi}$ pair. When the masses of the two pseudo-scalar mediators are sufficiently different, the contributions of the two processes can be factorised, and the 2HDM+a model can be described in terms of two sets of colour-neutral pseudo-scalar simplified models, each corresponding to the desired choice for m_a and m_A.

The acceptance $\mathcal{A}$ of the analysis for each point of interest in the 2HDM+a parameter space is therefore derived as:

$$\mathcal{A}_{\mathrm{2HDM}}(m_A, m_a) = \frac{\sigma_a \times \mathcal{A}_{\mathrm{simp}}(m_a) + \sigma_A \times \mathcal{A}_{\mathrm{simp}}(m_A)}{\sigma_a + \sigma_A},$$

where $\mathcal{A}_{\mathrm{simp}}$ is the acceptance of the analysis for the colour-neutral pseudo-scalar simplified model for a certain mass choice of the $A(a)$-boson, and σ_a computed in fully reconstructed samples and σ_A are the production cross-sections for $pp \to t\bar{t}a(\to \chi\bar{\chi})$ and $pp \to t\bar{t}A(\to \chi\bar{\chi})$, respectively. [5] This rescaling is valid in the on-shell region, $m_a(m_A) > 2m_\chi$ [63].

B Comparison with direct and indirect searches

Searches for weakly-interactive massive particles (WIMPs) [57] represent the current paradigm for searches for particle dark matter (DM). Within this paradigm, understanding the nature of DM requires a measurement of its interaction cross-section with Standard Model particles. This can be achieved using three complementary methods [221], schematically depicted in Figure 23 and briefly outlined in the following.

[5] The procedure is also valid for $pp \to b\bar{b}a/A$ production. However the impact of the correction was found to be minimal [63] and is neglected in this paper.

Direct Searches These searches aim to measure the elastic scattering of DM with nuclei in low background underground detectors such as CRESST-II [6], LUX [7], PICO [8], DEAP [9], PandaX [10], XENON [11, 12] and SuperCDMS [13, 14]. These direct detection experiments ultimately measure the strength of the interactions between WIMPs and the partons composing protons and neutrons and are sensitive to the properties of the DM halo around Earth.

Indirect Searches These searches aim to measure the annihilations or decays of DM particles in astrophysical systems, by means of neutrino detectors such as SuperKamiokande [15] or IceCube [16] or by means of either ground or space telescopes, for example the H.E.S.S. Cherenkov telescope [17, 18] and Fermi-LAT [19]. This measurement closely relates to the processes that determine the abundance of DM in the early universe and the interpretation of the results depends on the DM distribution in the universe as well as the SM particles into which the DM preferentially annihilates or decays.

Collider Searches These searches aim to discover DM particles and to measure the DM production cross-section through collisions of high-energy particles. The most stringent results to date on WIMPs are provided by the ATLAS [20–30], CMS [31, 32, 34, 35, 222] and LHCb [223, 224] experiments at the LHC. Sub-GeV DM candidates are also constrained by the MiniBooNE experiment at Fermilab [225]. The interpretation of these results closely depends on the underlying mechanisms that couple DM to SM particles. In the simplified model framework considered in this paper this underlying mechanism is assumed to be the production of new mediator(s) state(s) which subsequently decay into DM.

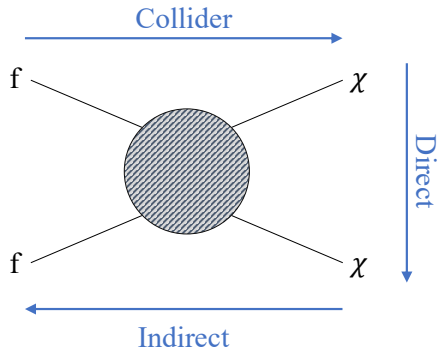

Figure 23: Schematic summary of the complementary approaches used in searches for WIMP DM.

The present understanding of the DM puzzle is encompassed in the summary and comparison of the experimental results of these three approaches. Likewise, the discovery of DM as an elementary particle will require determination of its interaction cross-section with SM particles via each of these methods. It is convenient and customary to compare these different approaches in terms of spin-dependent (spin-independent) χ–nucleon scattering cross-sections as a function of the DM mass. In this paper, the ATLAS exclusion limits are converted into bounds on the χ–nucleon scattering cross-sections for the following models:

- Vector and axial-vector neutral (V/AV) mediator models (two of the benchmark coupling scenarios, see Section 6.1.1 for details).
- Vector baryon-charged (VBC) mediator model.

- Scalar colour-neutral mediator model.

For each model, the translation procedure to convert and compare these limits is well defined and described in Ref. [61]. The interpretation in the spin-dependent (SD) and spin-independent (SI) DM–nucleon cross-sections, σ_{SD} and σ_{SI}, respectively, depends on the mediator mass and the couplings assumptions. Each comparison is valid solely in the context of the specific model and coupling assumptions. The ATLAS limits are always shown at 95% confidence level (CL) and the direct detection limits at 90% CL.

ATLAS exclusion limits for pseudo-scalar colour-neutral mediator models should be compared with indirect search experiments in terms of the DM annihilation cross-section $\langle\sigma v_{\text{rel}}\rangle$, as the rate in direct searches experiments is suppressed by additional velocity-dependent terms entering the cross-section. However, the observed exclusion limits for pseudo-scalar mediator models with a unitary coupling assumption are limited to a very narrow mass range, due to a small data excess in the analysis (Figure 17(b)). Therefore, this comparison is deferred to the results with the full Run-2 dataset.

The observed limits for the V/AV, VBC and scalar mediator models are compared with limits from direct search experiments in Figures 24–26. The excluded regions are indicated by shaded areas inside the contours. Each combined contour summarises the ATLAS results for each considered model, obtained by using the best expected limit for each parameter point in the figure. When the contour does not close inside the plotted area, the exclusion of smaller scattering cross-sections does not imply that larger scattering cross-sections (beyond the vertical axis range) are also excluded.

The spin-dependent WIMP–neutron (WIMP–proton) scattering cross-section in the context of the leptophobic Z'_{A} mediator model is shown in the upper (lower) panel of Figure 24. The difference between the WIMP–proton and WIMP–neutron cross-sections is negligible. The ATLAS exclusion curves are therefore identical in the two panels. The collider searches for this specific leptophobic axial-vector model complement the reach of the direct searches and extend beyond it, being particularly sensitive in the low-DM-mass parameter space, where the LUX and PICO experiments have less sensitivity due to the very low-energy recoils that such low-mass dark matter particles would induce. As in the case of the interpretation of the results in terms of mediator and DM masses (Section 6.1.1), if the values chosen for the couplings are reduced, the relative interplay between direct and collider searches changes. This is exemplified by the change of lepton and quark couplings in the leptophilic Z'_{A} mediator model shown in Figure 25, where the reach of resonant dijet final states is greatly reduced in favour of dilepton searches (differently for the two scenarios) and limited to mediator masses above 200 GeV. The sensitivity of the $E_{\text{T}}^{\text{miss}} + X$ searches is the same for the two models in Figures 24 and 25(b). This is a coincidental result of two opposite effects [61]: the fact that the scattering cross-section limit is inversely proportional to the mediator mass reach (raised to the fourth power), which is higher in the leptophobic mediator model (Figure 12(a)), and the fact that the σ_{SD} limit is proportional to g_q^2, which is lower in the leptophilic mediator model.

The spin-independent WIMP–nucleon scattering cross-section results for leptophobic, leptophilic, or baryon-charged vector mediator Z' and scalar colour-neutral mediator ϕ are compared with the most stringent direct detection limits to date from the LUX, CRESST-II, XENON1T, SuperCDMS and PandaX experiments in Figure 26. One contour for each model is presented in the figure and it includes the combination, based on the best expected limit for each parameter point, of every analysis considered for each model and presented in Section 6. The excluded regions are indicated by shaded areas inside the contour. As before, when the contour does not close inside the plotted area, the exclusion of smaller scattering cross-sections does not imply that larger scattering cross-sections (beyond the vertical axis range) are also excluded. The collider searches in this case complement the reach of the direct searches

for $m_\chi \lesssim 5$ GeV. By comparing the exclusion reach of the ATLAS searches for each of the four models considered in Figure 26, it is possible to gauge the importance of the production mechanism assumptions for the collider limits, which represent a complementary and not exclusive approach to DM searches with respect to direct and indirect searches.

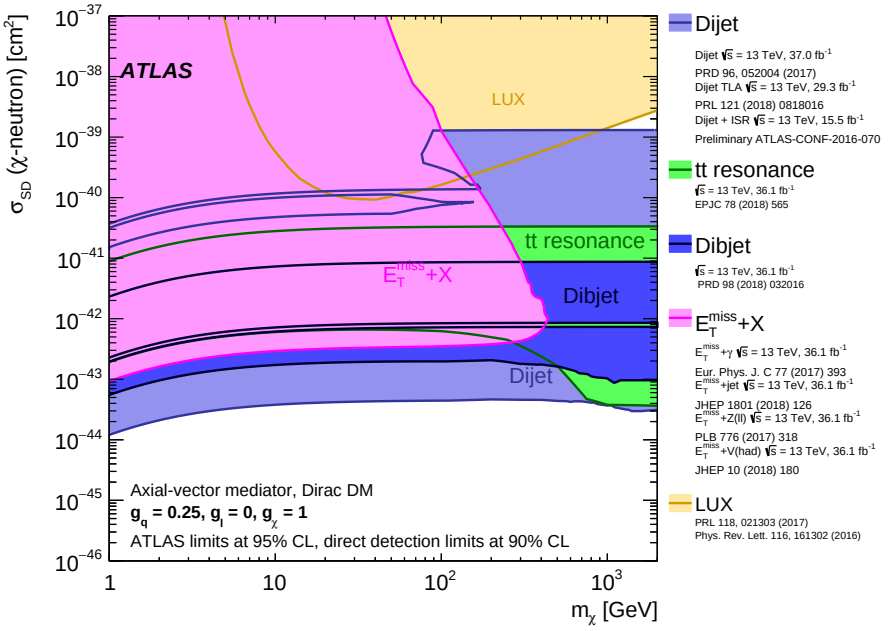

(a)

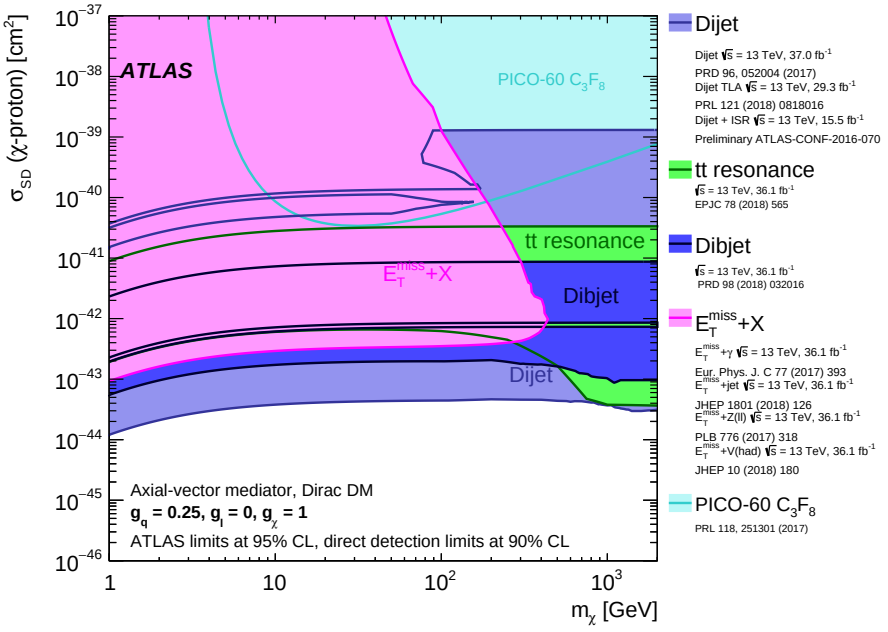

(b)

Figure 24: A comparison of the inferred limits with the constraints from direct detection experiments on (a) the spin-dependent WIMP–neutron or (b) WIMP–proton scattering cross-section in the context of the Z'-like simplified model with axial-vector couplings. The results from this analysis, excluding the region to the left of the contour, are compared with limits from direct detection experiments. LHC limits are shown at 95% CL and direct detection limits at 90% CL. The comparison is valid solely in the context of this model, assuming a mediator width fixed by the dark matter mass and coupling values $g_q = 0.1, g_\ell = 0.1$, and $g_\chi = 1$. LHC searches and direct detection experiments exclude the shaded areas. Exclusions of smaller scattering cross-sections do not imply that larger scattering cross-sections are also excluded. The resonance and $E_{\mathrm{T}}^{\mathrm{miss}}$+X exclusion region represents the union of exclusions from all analyses of that type.

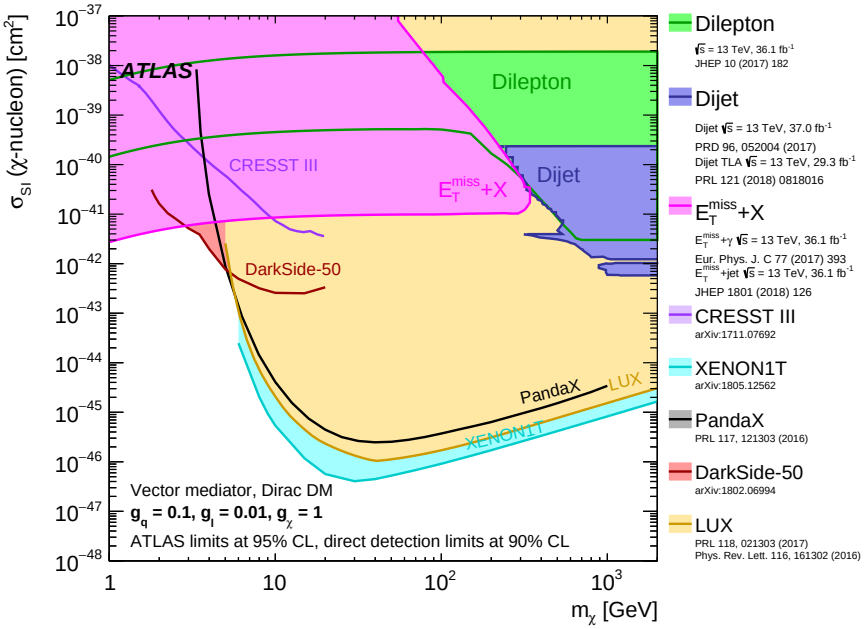

(a)

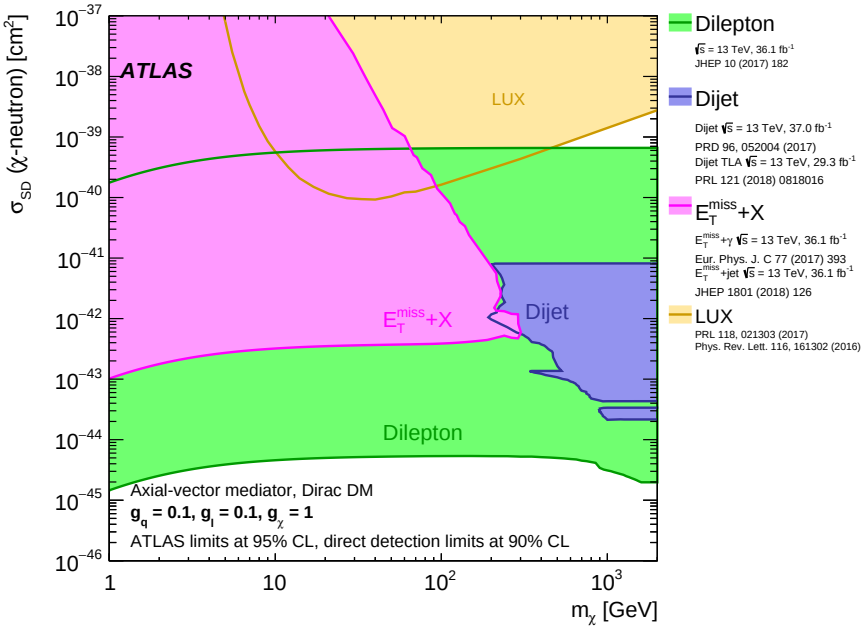

(b)

Figure 25: A comparison of the inferred limits with the constraints from direct detection experiments on the spin-independent WIMP–nucleon (spin-dependent WIMP–neutron) scattering cross-section in the context of (a) the Z'-like simplified model with leptophilic vector or (b) axial-vector couplings. The results from this analysis, excluding the region to the left of the contour, are compared with limits from the direct detection experiments. LHC limits are shown at 95% CL and direct detection limits at 90% CL. The comparison is valid solely in the context of this model, assuming a mediator width fixed by the dark matter mass and the coupling values highlighted in each figure. LHC searches and direct detection experiments exclude the shaded areas. Exclusions of smaller scattering cross-sections do not imply that larger scattering cross-sections are also excluded. The resonance and $E_{\mathrm{T}}^{\mathrm{miss}}$+X exclusion region represents the union of exclusions from all analyses of that type.

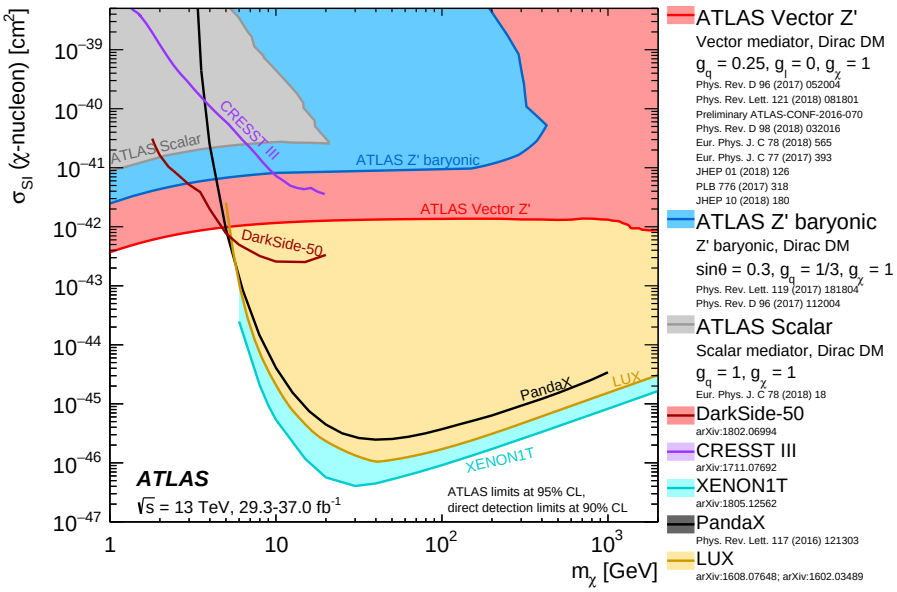

Figure 26: A comparison of the inferred limits with the constraints from direct detection experiments on the spin-independent WIMP–nucleon scattering cross-section. The results from ATLAS analyses, excluding the shaded regions, are compared with limits from direct detection experiments. LHC limits are shown at 95% CL and direct detection limits at 90% CL. The comparison is valid solely in the context of this model, assuming a mediator width fixed by the dark matter mass and coupling values $g_q = 0.25$, $g_\ell = 0$ or $g_q = 0.1$, $g_\ell = 0.01$ for the neutral-mediator model and coupling $g_q = 0.33$ for the baryon-charged mediator. The coupling to the DM particle g_χ, is set to unity in all cases. LHC searches and direct detection experiments exclude the shaded areas. Exclusions of smaller scattering cross-sections do not imply that larger scattering cross-sections are also excluded. The single dijet and $E_{\mathrm{T}}^{\mathrm{miss}}+X$ exclusion region represents the union of exclusions from all analyses of that type.

Acknowledgements

We thank CERN for the very successful operation of the LHC, as well as the support staff from our institutions without whom ATLAS could not be operated efficiently.

We acknowledge the support of ANPCyT, Argentina; YerPhI, Armenia; ARC, Australia; BMWFW and FWF, Austria; ANAS, Azerbaijan; SSTC, Belarus; CNPq and FAPESP, Brazil; NSERC, NRC and CFI, Canada; CERN; CONICYT, Chile; CAS, MOST and NSFC, China; COLCIENCIAS, Colombia; MSMT CR, MPO CR and VSC CR, Czech Republic; DNRF and DNSRC, Denmark; IN2P3-CNRS, CEA-DRF/IRFU, France; SRNSFG, Georgia; BMBF, HGF, and MPG, Germany; GSRT, Greece; RGC, Hong Kong SAR, China; ISF and Benoziyo Center, Israel; INFN, Italy; MEXT and JSPS, Japan; CNRST, Morocco; NWO, Netherlands; RCN, Norway; MNiSW and NCN, Poland; FCT, Portugal; MNE/IFA, Romania; MES of Russia and NRC KI, Russian Federation; JINR; MESTD, Serbia; MSSR, Slovakia; ARRS and MIZŠ, Slovenia; DST/NRF, South Africa; MINECO, Spain; SRC and Wallenberg Foundation, Sweden; SERI, SNSF and Cantons of Bern and Geneva, Switzerland; MOST, Taiwan; TAEK, Turkey; STFC, United Kingdom; DOE and NSF, United States of America. In addition, individual groups and members have received support from BCKDF, CANARIE, CRC and Compute Canada, Canada; COST, ERC, ERDF, Horizon 2020, and Marie Skłodowska-Curie Actions, European Union; Investissements d'

Avenir Labex and Idex, ANR, France; DFG and AvH Foundation, Germany; Herakleitos, Thales and Aristeia programmes co-financed by EU-ESF and the Greek NSRF, Greece; BSF-NSF and GIF, Israel; CERCA Programme Generalitat de Catalunya, Spain; The Royal Society and Leverhulme Trust, United Kingdom.

The crucial computing support from all WLCG partners is acknowledged gratefully, in particular from CERN, the ATLAS Tier-1 facilities at TRIUMF (Canada), NDGF (Denmark, Norway, Sweden), CC-IN2P3 (France), KIT/GridKA (Germany), INFN-CNAF (Italy), NL-T1 (Netherlands), PIC (Spain), ASGC (Taiwan), RAL (UK) and BNL (USA), the Tier-2 facilities worldwide and large non-WLCG resource providers. Major contributors of computing resources are listed in Ref. [226].

References

[1] G. Hinshaw et al., *Nine-Year Wilkinson Microwave Anisotropy Probe (WMAP) Observations: Cosmological Parameter Results*, Astrophys. J. Suppl. **208** (2013) 19, arXiv: 1212.5226 [astro-ph.CO] (cit. on p. 3).

[2] Y. Akrami et al., *Planck 2018 results. I. Overview and the cosmological legacy of Planck*, (2018), arXiv: 1807.06205 [astro-ph.CO] (cit. on p. 3).

[3] V. Trimble, *Existence and Nature of Dark Matter in the Universe*, Ann. Rev. Astron. Astrophys. **25** (1987) 425 (cit. on p. 3).

[4] G. Bertone, D. Hooper, and J. Silk, *Particle dark matter: Evidence, candidates and constraints*, Phys. Rept. **405** (2005) 279, arXiv: hep-ph/0404175 [hep-ph] (cit. on p. 3).

[5] J. L. Feng, *Dark Matter Candidates from Particle Physics and Methods of Detection*, Ann. Rev. Astron. Astrophys. **48** (2010) 495, arXiv: 1003.0904 [astro-ph.CO] (cit. on p. 3).

[6] G. Angloher et al., *Results on light dark matter particles with a low-threshold CRESST-II detector*, Eur. Phys. J. C **76** (2016) 25, arXiv: 1509.01515 [astro-ph.CO] (cit. on pp. 3, 47).

[7] D. S. Akerib et al., *Results from a Search for Dark Matter in the Complete LUX Exposure*, Phys. Rev. Lett. **118** (2017) 021303, arXiv: 1608.07648 [astro-ph.CO] (cit. on pp. 3, 47).

[8] C. Amole et al., *Dark Matter Search Results from the PICO-60 C_3F_8 Bubble Chamber*, Phys. Rev. Lett. **118** (2017) 251301, arXiv: 1702.07666 [astro-ph.CO] (cit. on pp. 3, 47).

[9] P. A. Amaudruz et al., *First Results from the DEAP-3600 Dark Matter Search with Argon at SNOLAB*, Phys. Rev. Lett. **121** (2018) 071801, arXiv: 1707.08042 [astro-ph.CO] (cit. on pp. 3, 47).

[10] X. Cui et al., *Dark Matter Results From 54-Ton-Day Exposure of PandaX-II Experiment*, Phys. Rev. Lett. **119** (2017) 181302, arXiv: 1708.06917 [astro-ph.CO] (cit. on pp. 3, 47).

[11] E. Aprile et al., *Dark Matter Search Results from a One Ton-Year Exposure of XENON1T*, Phys. Rev. Lett. **121** (2018) 111302, arXiv: 1805.12562 [astro-ph.CO] (cit. on pp. 3, 47).

[12] E. Aprile et al., *First Dark Matter Search Results from the XENON1T Experiment*, Phys. Rev. Lett. **119** (2017) 181301, arXiv: 1705.06655 [astro-ph.CO] (cit. on pp. 3, 47).

[13] R. Agnese et al., *Low-mass dark matter search with CDMSlite*, Phys. Rev. D **97** (2018) no.2 022002, arXiv: 1707.01632 [astro-ph.CO] (cit. on pp. 3, 47).

[14] R. Agnese et al., *Results from the Super Cryogenic Dark Matter Search Experiment at Soudan*, Phys. Rev. Lett. **120** (2018) 061802, arXiv: 1708.08869 [hep-ex] (cit. on pp. 3, 47).

[15] K. Choi et al., *Search for Neutrinos from Annihilation of Captured Low-Mass Dark Matter Particles in the Sun by Super-Kamiokande*, Phys. Rev. Lett. **114** (2015) 141301, arXiv: 1503.04858 [hep-ex] (cit. on pp. 3, 47).

[16] M. G. Aartsen et al., *Search for neutrinos from decaying dark matter with IceCube*, Eur. Phys. J. C **78** (2018) 831, arXiv: 1804.03848 [astro-ph.HE] (cit. on pp. 3, 47).

[17] F. Acero et al., *Spectrum and variability of the Galactic Center VHE gamma-ray source HESS J1745-290*, Astron. & Astrophys. **503** (2009) 817, arXiv: 0906.1247 (cit. on pp. 3, 47).

[18] F. Acero et al., *Localising the VHE gamma-ray source at the Galactic Centre*, Mon. Not. R. Astron. Soc **402** (2010) 1877, arXiv: 0911.1912 (cit. on pp. 3, 47).

[19] M. Ackermann et al., *The Fermi Galactic Center GeV Excess and Implications for Dark Matter*, Astrophys. J. **840** (2017) 43, arXiv: 1704.03910 [astro-ph.HE] (cit. on pp. 3, 47).

[20] ATLAS Collaboration, *Search for dark matter in events with a hadronically decaying vector boson and missing transverse momentum in pp collisions at* $\sqrt{s} = 13$ *TeV with the ATLAS detector*, JHEP **10** (2018) 180, arXiv: 1807.11471 [hep-ex] (cit. on pp. 3, 14, 16, 17, 21, 47).

[21] ATLAS Collaboration, *Search for dark matter at* $\sqrt{s} = 13$ *TeV in final states containing an energetic photon and large missing transverse momentum with the ATLAS detector*, Eur. Phys. J. C **77** (2017) 393, arXiv: 1704.03848 [hep-ex] (cit. on pp. 3, 17, 21, 47).

[22] ATLAS Collaboration, *Search for dark matter in association with a Higgs boson decaying to two photons at* $\sqrt{s} = 13$ *TeV with the ATLAS detector*, Phys. Rev. D **96** (2017) 112004, arXiv: 1706.03948 [hep-ex] (cit. on pp. 3, 14, 18, 21, 47).

[23] ATLAS Collaboration, *Search for Dark Matter Produced in Association with a Higgs Boson Decaying to* $b\bar{b}$ *using* $36\,fb^{-1}$ *of pp collisions at* $\sqrt{s} = 13$ *TeV with the ATLAS Detector*, Phys. Rev. Lett. **119** (2017) 181804, arXiv: 1707.01302 [hep-ex] (cit. on pp. 3, 14, 17, 21, 32, 47).

[24] ATLAS Collaboration, *Search for an invisibly decaying Higgs boson or dark matter candidates produced in association with a Z boson in pp collisions at* $\sqrt{s} = 13$ *TeV with the ATLAS detector*, Phys. Lett. B **776** (2018) 318, arXiv: 1708.09624 [hep-ex] (cit. on pp. 3, 16, 17, 21, 47).

[25] ATLAS Collaboration, *Search for dark matter produced in association with bottom or top quarks in* $\sqrt{s} = 13$ *TeV pp collisions with the ATLAS detector*, Eur. Phys. J. C **78** (2018) 18, arXiv: 1710.11412 [hep-ex] (cit. on pp. 3, 7, 9, 15, 18, 19, 21, 47).

[26] ATLAS Collaboration, *Search for dark matter and other new phenomena in events with an energetic jet and large missing transverse momentum using the ATLAS detector*, JHEP **01** (2018) 126, arXiv: 1711.03301 [hep-ex] (cit. on pp. 3, 9, 14–16, 21, 47).

[27] ATLAS Collaboration, *Search for top-squark pair production in final states with one lepton, jets, and missing transverse momentum using* $36\,fb^{-1}$ *of* $\sqrt{s} = 13$ *TeV pp collision data with the ATLAS detector*, JHEP **06** (2018) 108, arXiv: 1711.11520 [hep-ex] (cit. on pp. 3, 18, 19, 21, 47).

[28] ATLAS Collaboration, *Search for a scalar partner of the top quark in the jets plus missing transverse momentum final state at* $\sqrt{s} = 13$ *TeV with the ATLAS detector*, JHEP **12** (2017) 085, arXiv: 1709.04183 [hep-ex] (cit. on pp. 3, 18, 47).

[29] ATLAS Collaboration, *Constraints on new phenomena via Higgs boson couplings and invisible decays with the ATLAS detector*, JHEP **11** (2015) 206, arXiv: 1509.00672 [hep-ex] (cit. on pp. 3, 16, 21, 47).

[30] ATLAS Collaboration, *Search for large missing transverse momentum in association with one top-quark in proton–proton collisions at* $\sqrt{s} = 13$ *TeV with the ATLAS detector*, JHEP (2018), arXiv: 1812.09743 [hep-ex] (cit. on pp. 3, 14, 15, 18, 21, 47).

[31] CMS Collaboration, *Search for dark matter produced with an energetic jet or a hadronically decaying W or Z boson at* $\sqrt{s} = 13$ *TeV*, JHEP **07** (2017) 014, arXiv: 1703.01651 [hep-ex] (cit. on pp. 3, 47).

[32] CMS Collaboration, *Search for associated production of dark matter with a Higgs boson decaying to* $b\bar{b}$ *or* $\gamma\gamma$ *at* $\sqrt{s} = 13$ *TeV*, JHEP **10** (2017) 180, arXiv: 1703.05236 [hep-ex] (cit. on pp. 3, 10, 47).

[33] CMS Collaboration, *Search for dark matter produced in association with a Higgs boson decaying to* $\gamma\gamma$ *or* $\tau^+\tau^-$ *at* $\sqrt{s} = 13$ *TeV*, JHEP **09** (2018) 046, arXiv: 1806.04771 [hep-ex] (cit. on p. 3).

[34] CMS Collaboration, *Search for dark matter produced in association with heavy-flavor quark pairs in proton–proton collisions at* $\sqrt{s}$ = 13 *TeV*, Eur. Phys. J. C **77** (2017) 845, arXiv: 1706.02581 [hep-ex] (cit. on pp. 3, 47).

[35] CMS Collaboration, *Search for new physics in the monophoton final state in proton–proton collisions at* $\sqrt{s}$ = 13 *TeV*, JHEP **10** (2017) 073, arXiv: 1706.03794 [hep-ex] (cit. on pp. 3, 47).

[36] CMS Collaboration, *Search for top squarks and dark matter particles in opposite-charge dilepton final states at* $\sqrt{s}$ = 13 *TeV*, Phys. Rev. D **97** (2018) 032009, arXiv: 1711.00752 [hep-ex] (cit. on p. 3).

[37] CMS Collaboration, *Search for new physics in events with a leptonically decaying Z boson and a large transverse momentum imbalance in proton–proton collisions at* $\sqrt{s}$ = 13 *TeV*, Eur. Phys. J. C **78** (2018) 291, arXiv: 1711.00431 [hep-ex] (cit. on p. 3).

[38] CMS Collaboration, *Combined measurements of Higgs boson couplings in proton–proton collisions at* $\sqrt{s}$ = 13 *TeV*, Eur. Phys. J. (2018), arXiv: 1809.10733 [hep-ex] (cit. on p. 3).

[39] M. Roos, *Astrophysical and cosmological probes of dark matter*, J. of Modern Physics **3** (2012) 1152, arXiv: 1208.3662 (cit. on p. 3).

[40] S. Arrenberg et al., *Working Group Report: Dark Matter Complementarity*, 2013, arXiv: 1310.8621 [hep-ph] (cit. on p. 3).

[41] A. G. Riess et al., *Observational Evidence from Supernovae for an Accelerating Universe and a Cosmological Constant*, Astron. J. **116** (1998) 1009, arXiv: astro-ph/9805201 [astro-ph] (cit. on p. 3).

[42] S. Perlmutter et al., *Measurements of Omega and Lambda from 42 high redshift supernovae*, Astrophys. J. **517** (1999) 565, arXiv: astro-ph/9812133 [astro-ph] (cit. on p. 3).

[43] A. Einstein, *Kosmologische Betrachtungen zur allgemeinen Relativitätstheorie*, Sitzungsberichte der Königlich Preußischen Akademie der Wissenschaften (Berlin), Seite 142-152. (1917) (cit. on p. 3).

[44] D. Weinberg et al., *Facilities for Dark Energy Investigations*, (2013), arXiv: 1309.5380 [astro-ph.CO] (cit. on p. 3).

[45] D. J. Kapner et al., *Tests of the Gravitational Inverse-Square Law below the Dark-Energy Length Scale*, Phys. Rev. Lett. **98** (2007) 021101, arXiv: hep-ph/0611184 [hep-ph] (cit. on p. 3).

[46] P. Hamilton et al., *Atom-interferometry constraints on dark energy*, Science **349** (2015) 849, arXiv: 1502.03888 [physics.atom-ph] (cit. on p. 3).

[47] V. Anastassopoulos et al., *Search for chameleons with CAST*, Phys. Lett. B **749** (2015) 172, arXiv: 1503.04561 [astro-ph.SR] (cit. on p. 3).

[48] J. H. Steffen et al., *Laboratory Constraints on Chameleon Dark Energy and Power-Law Fields*, Phys. Rev. Lett. **105** (2010) 261803, arXiv: 1010.0988 [astro-ph.CO] (cit. on p. 3).

[49] P. Brax and A.-C. Davis, *Atomic interferometry test of dark energy*, Phys. Rev. D **94** (2016) 104069, arXiv: 1609.09242 [astro-ph.CO] (cit. on p. 3).

[50] C. Burrage, A. Kuribayashi-Coleman, J. Stevenson, and B. Thrussell, *Constraining symmetron fields with atom interferometry*, JCAP **12** (2016) 041, arXiv: 1609.09275 [astro-ph.CO] (cit. on p. 3).

[51] H. Lemmel et al., *Neutron interferometry constrains dark energy chameleon fields*, Phys. Lett. B **743** (2015) 310, arXiv: 1502.06023 [hep-ph] (cit. on p. 3).

[52] B. Elder et al., *Chameleon dark energy and atom interferometry*, Phys. Rev. D **94** (2016) 044051, arXiv: 1603.06587 [astro-ph.CO] (cit. on p. 3).

[53] P. Brax, G. Pignol, and D. Roulier, *Probing strongly coupled chameleons with slow neutrons*, Phys. Rev. D **88** (2013) 083004, arXiv: 1306.6536 [quant-ph] (cit. on p. 3).

[54] B. P. Abbott et al., *Tests of General Relativity with GW150914*, Phys. Rev. Lett. **116** (2016) 221101, arXiv: 1602.03841 [gr-qc] (cit. on p. 3).

[55] B. Abbott et al., *GW170817: Observation of Gravitational Waves from a Binary Neutron Star Inspiral*, Phys. Rev. Lett. **119** (2017) 161101, arXiv: 1710.05832 [gr-qc] (cit. on p. 3).

[56] B. P. Abbott et al., *Multi-messenger Observations of a Binary Neutron Star Merger*, Astrophys. J. **848** (2017) L12, arXiv: 1710.05833 [astro-ph.HE] (cit. on p. 3).

[57] G. Steigman and M. S. Turner, *Cosmological constraints on the properties of Weakly Interacting Massive Particles*, Nucl. Phys. B **253** (1985) 375 (cit. on pp. 3, 46).

[58] E. W. Kolb and M. S. Turner, *The Early Universe*, Front. Phys. **69** (1990) 1 (cit. on p. 3).

[59] L. Evans and P. Bryant, *LHC Machine*, JINST **3** (2008) S08001 (cit. on p. 3).

[60] D. Abercrombie et al., *Dark Matter Benchmark Models for Early LHC Run-2 Searches: Report of the ATLAS/CMS Dark Matter Forum*, (2015), arXiv: 1507.00966 [hep-ex] (cit. on pp. 3–7, 12, 14, 27, 43).

[61] A. Boveia et al., *Recommendations on presenting LHC searches for missing transverse energy signals using simplified s-channel models of dark matter*, (2016), arXiv: 1603.04156 [hep-ex] (cit. on pp. 3, 14, 32, 48).

[62] A. Albert et al., *Recommendations of the LHC Dark Matter Working Group: Comparing LHC searches for heavy mediators of dark matter production in visible and invisible decay channels*, (2017), arXiv: 1703.05703 [hep-ex] (cit. on pp. 3, 6, 14, 27–30).

[63] T. Abe et al., *LHC Dark Matter Working Group: Next-generation spin-0 dark matter models*, (2018), arXiv: 1810.09420 [hep-ex] (cit. on pp. 3, 4, 11, 14, 38, 42, 46).

[64] S. P. Martin, *A Supersymmetry primer*, Adv. Ser. Direct. High Energy Phys. **18** (1998) 1, arXiv: hep-ph/9709356 (cit. on p. 3).

[65] G. R. Farrar and P. Fayet, *Phenomenology of the production, decay, and detection of new hadronic states associated with supersymmetry*, Phys. Lett. B **76** (1978) 575 (cit. on p. 3).

[66] H. Goldberg, *Constraint on the Photino Mass from Cosmology*, Phys. Rev. Lett. **50** (1983) 1419, Erratum: Phys. Rev. Lett. **103** (2009) 099905 (cit. on p. 3).

[67] J. R. Ellis, J. S. Hagelin, D. V. Nanopoulos, K. A. Olive, and M. Srednicki, *Supersymmetric relics from the big bang*, Nucl. Phys. B **238** (1984) 453 (cit. on p. 3).

[68] ATLAS Collaboration, *Search for the electroweak production of supersymmetric particles in $\sqrt{s} = 8$ TeV pp collisions with the ATLAS detector*, Phys. Rev. D **93** (2016) 052002, arXiv: 1509.07152 [hep-ex] (cit. on p. 3).

[69] ATLAS Collaboration, *Summary of the searches for squarks and gluinos using $\sqrt{s} = 8$ TeV pp collisions with the ATLAS experiment at the LHC*, JHEP **10** (2015) 054, arXiv: 1507.05525 [hep-ex] (cit. on p. 3).

[70] ATLAS Collaboration, *ATLAS Run 1 searches for direct pair production of third-generation squarks at the Large Hadron Collider*, Eur. Phys. J. C **75** (2015) 510, arXiv: 1506.08616 [hep-ex] (cit. on p. 3).

[71] ATLAS Collaboration, *Summary of the ATLAS experiment's sensitivity to supersymmetry after LHC Run 1 — interpreted in the phenomenological MSSM*, JHEP **10** (2015) 134, arXiv: 1508.06608 [hep-ex] (cit. on p. 3).

[72] ATLAS Collaboration, *Dark matter interpretations of ATLAS searches for the electroweak production of supersymmetric particles in $\sqrt{s}$ = 8 TeV proton–proton collisions*, JHEP **09** (2016) 175, arXiv: 1608.00872 [hep-ex] (cit. on p. 3).

[73] ATLAS Collaboration, *Search for the direct production of charginos and neutralinos in final states with tau leptons in $\sqrt{s}$ = 13 TeV pp collisions with the ATLAS detector*, Eur. Phys. J. C **78** (2018) 154, arXiv: 1708.07875 [hep-ex] (cit. on p. 3).

[74] ATLAS Collaboration, *Search for electroweak production of supersymmetric particles in final states with two or three leptons at $\sqrt{s}$ = 13 TeV with the ATLAS detector*, Eur. Phys. J. C **78** (2018) 995, arXiv: 1803.02762 [hep-ex] (cit. on p. 3).

[75] ATLAS Collaboration, *Search for electroweak production of supersymmetric states in scenarios with compressed mass spectra at $\sqrt{s}$ = 13 TeV with the ATLAS detector*, Phys. Rev. D **97** (2018) 052010, arXiv: 1712.08119 [hep-ex] (cit. on p. 3).

[76] L. Lee, C. Ohm, A. Soffer, and T.-T. Yu, *Collider Searches for Long-Lived Particles Beyond the Standard Model*, (2018), arXiv: 1810.12602 [hep-ph] (cit. on p. 4).

[77] M. Kunz and D. Sapone, *Dark Energy versus Modified Gravity*, Phys. Rev. Lett. **98** (2007) 121301, arXiv: astro-ph/0612452 [astro-ph] (cit. on p. 4).

[78] M. Kunz, *Degeneracy between the dark components resulting from the fact that gravity only measures the total energy-momentum tensor*, Phys. Rev. D **80** (2009) 123001, arXiv: astro-ph/0702615 [astro-ph] (cit. on p. 4).

[79] P. Brax, C. Burrage, C. Englert, and M. Spannowsky, *LHC signatures of scalar dark energy*, Phys. Rev. D **94** (2016) 084054, arXiv: 1604.04299 [hep-ph] (cit. on pp. 4, 11, 15, 43).

[80] H. Georgi, *Effective field theory*, Ann. Rev. Nucl. Part. Sci. **43** (1993) 209 (cit. on p. 4).

[81] ATLAS Collaboration, *The ATLAS Experiment at the CERN Large Hadron Collider*, JINST **3** (2008) S08003 (cit. on p. 4).

[82] P. J. Fox and E. Poppitz, *Leptophilic dark matter*, Phys. Rev. D **79** (2009) 083528, arXiv: 0811.0399 [hep-ph] (cit. on p. 4).

[83] S. Cassel, D. M. Ghilencea, and G. G. Ross, *Electroweak and dark matter constraints on a Z' in models with a hidden valley*, Nucl. Phys. B **827** (2010) 256, arXiv: 0903.1118 [hep-ph] (cit. on p. 4).

[84] Y. Bai, P. J. Fox, and R. Harnik, *The Tevatron at the frontier of dark matter direct detection*, JHEP **12** (2010) 048, arXiv: 1005.3797 [hep-ph] (cit. on p. 4).

[85] J. Abdallah et al., *Simplified models for dark matter searches at the LHC*, Phys. Dark Univ. **9-10** (2015) 8, arXiv: 1506.03116 [hep-ph] (cit. on p. 4).

[86] M. Beltran, D. Hooper, E. W. Kolb, Z. A. C. Krusberg, and T. M. P. Tait, *Maverick dark matter at colliders*, JHEP **09** (2010) 037, arXiv: 1002.4137 [hep-ph] (cit. on p. 4).

[87] J. Goodman et al., *Constraints on light Majorana dark matter from colliders*, Phys. Lett. B **695** (2011) 185, arXiv: 1005.1286 [hep-ph] (cit. on p. 4).

[88] J. Goodman et al., *Constraints on dark matter from colliders*, Phys. Rev. D **82** (2010) 116010, arXiv: 1008.1783 [hep-ph] (cit. on p. 4).

[89] A. Rajaraman, W. Shepherd, T. M. P. Tait, and A. M. Wijangco, *LHC bounds on interactions of dark matter*, Phys. Rev. D **84** (2011) 095013, arXiv: 1108.1196 [hep-ph] (cit. on p. 4).

[90] P. J. Fox, R. Harnik, J. Kopp, and Y. Tsai, *Missing energy signatures of dark matter at the LHC*, Phys. Rev. D **85** (2012) 056011, arXiv: 1109.4398 [hep-ph] (cit. on pp. 4, 5).

[91] G. W. Horndeski, *Second-order scalar-tensor field equations in a four-dimensional space*, Int. J. Theor. Phys. **10** (1974) 363 (cit. on pp. 4, 11).

[92] A. Alves, A. Berlin, S. Profumo, and F. S. Queiroz, *Dark matter complementarity and the Z' portal*, Phys. Rev. D **92** (2015) 083004, arXiv: 1501.03490 [hep-ph] (cit. on p. 5).

[93] P. Gondolo, P. Ko, and Y. Omura, *Light dark matter in leptophobic Z' models*, Phys. Rev. D **85** (2012) 035022, arXiv: 1106.0885 [hep-ph] (cit. on p. 5).

[94] M. T. Frandsen, F. Kahlhoefer, S. Sarkar, and K. Schmidt-Hoberg, *Direct detection of dark matter in models with a light Z'*, JHEP **09** (2011) 128, arXiv: 1107.2118 [hep-ph] (cit. on p. 5).

[95] H. An, X. Ji, and L.-T. Wang, *Light dark matter and Z' dark force at colliders*, JHEP **07** (2012) 182, arXiv: 1202.2894 [hep-ph] (cit. on p. 5).

[96] A. Alves, S. Profumo, and F. S. Queiroz, *The dark $Z^{'}$ portal: direct, indirect and collider searches*, JHEP **04** (2014) 063, arXiv: 1312.5281 [hep-ph] (cit. on p. 5).

[97] O. Lebedev and Y. Mambrini, *Axial dark matter: The case for an invisible Z'*, Phys. Lett. B **734** (2014) 350, arXiv: 1403.4837 [hep-ph] (cit. on p. 5).

[98] M. Papucci, A. Vichi, and K. M. Zurek, *Monojet versus the rest of the world I: t-channel models*, JHEP **11** (2014) 024, arXiv: 1402.2285 [hep-ph] (cit. on pp. 5, 9, 15).

[99] O. Buchmueller, M. J. Dolan, S. A. Malik, and C. McCabe, *Characterising dark matter searches at colliders and direct detection experiments: Vector mediators*, JHEP **01** (2015) 037, arXiv: 1407.8257 [hep-ph] (cit. on p. 5).

[100] C. D. Carone and H. Murayama, *Possible Light U(1) Gauge Boson Coupled to Baryon Number*, Phys. Rev. Lett. **74** (1995) 3122, arXiv: hep-ph/9411256 [hep-ph] (cit. on p. 5).

[101] K. Agashe and G. Servant, *Warped Unification, Proton Stability, and Dark Matter*, Phys. Rev. Lett. **93** (2004) 231805, arXiv: hep-ph/0403143 [hep-ph] (cit. on p. 5).

[102] P. Fileviez Perez and M. B. Wise, *Baryon and lepton number as local gauge symmetries*, Phys. Rev. D **82** (2010) 011901, Erratum: Phys. Rev. D **82** (2010) 079901, arXiv: 1002.1754 [hep-ph] (cit. on p. 5).

[103] L. Carpenter et al., *Mono-Higgs-boson: A new collider probe of dark matter*, Phys. Rev. D **89** (2014) 075017, arXiv: 1312.2592 [hep-ph] (cit. on pp. 5, 6, 14).

[104] J. Andrea, B. Fuks, and F. Maltoni, *Monotops at the LHC*, Phys. Rev. D **84** (2011) 074025, arXiv: 1106.6199 [hep-ph] (cit. on pp. 5, 7).

[105] J.-L. Agram, J. Andrea, M. Buttignol, E. Conte, and B. Fuks, *Monotop phenomenology at the Large Hadron Collider*, Phys. Rev. D **89** (2014) 014028, arXiv: 1311.6478 [hep-ph] (cit. on pp. 5, 7).

[106] I. Boucheneb, G. Cacciapaglia, A. Deandrea, and B. Fuks, *Revisiting monotop production at the LHC*, JHEP **01** (2015) 017, arXiv: 1407.7529 [hep-ph] (cit. on pp. 5, 7, 9).

[107] ATLAS Collaboration, *Search for new phenomena in events with same-charge leptons and b-jets in pp collisions at $\sqrt{s} = 13$ TeV with the ATLAS detector*, JHEP **12** (2018) 039, arXiv: 1807.11883 [hep-ex] (cit. on pp. 7, 23, 24).

[108] K. Cheung, K. Mawatari, E. Senaha, P.-Y. Tseng, and T.-C. Yuan, *The top window for dark matter*, JHEP **10** (2010) 081, arXiv: 1009.0618 [hep-ph] (cit. on p. 7).

[109] U. Haisch, A. Hibbs, and E. Re, *Determining the structure of dark-matter couplings at the LHC*, Phys. Rev. D **89** (2014) 034009, arXiv: 1311.7131 [hep-ph] (cit. on p. 7).

[110] M. R. Buckley, D. Feld, and D. Goncalves, *Scalar simplified models for dark matter*, Phys. Rev. D **91** (2015) 015017, arXiv: 1410.6497 [hep-ph] (cit. on pp. 7, 15).

[111] M. R. Buckley and D. Goncalves, *Constraining the Strength and CP Structure of Dark Production at the LHC: the Associated Top-Pair Channel*, Phys. Rev. D **93** (2016) 034003, [Phys. Rev.D93,034003(2016)], arXiv: 1511.06451 [hep-ph] (cit. on p. 7).

[112] U. Haisch and E. Re, *Simplified dark matter top-quark interactions at the LHC*, JHEP **06** (2015) 078, arXiv: 1503.00691 [hep-ph] (cit. on p. 7).

[113] M. Backovic et al., *Higher-order QCD predictions for dark matter production at the LHC in simplified models with s-channel mediators*, Eur. Phys. J. C **75** (2015) 482, arXiv: 1508.05327 [hep-ph] (cit. on pp. 7, 14, 15, 45).

[114] C. Arina et al., *A comprehensive approach to dark matter studies: exploration of simplified top-philic models*, JHEP **11** (2016) 111, arXiv: 1605.09242 [hep-ph] (cit. on p. 7).

[115] U. Haisch, P. Pani, and G. Polesello, *Determining the CP nature of spin-0 mediators in associated production of dark matter and $t\bar{t}$ pairs*, JHEP **02** (2017) 131, arXiv: 1611.09841 [hep-ph] (cit. on p. 7).

[116] S. Banerjee et al., *Cornering pseudoscalar-mediated dark matter with the LHC and cosmology*, JHEP **07** (2017) 080, arXiv: 1705.02327 [hep-ph] (cit. on p. 7).

[117] U. Haisch and G. Polesello, *Searching for dark matter in final states with two jets and missing transverse energy*, (2018), arXiv: 1812.08129 [hep-ph] (cit. on p. 7).

[118] B. Batell, J. Pradler, and M. Spannowsky, *Dark matter from minimal flavor violation*, JHEP **08** (2011) 038, arXiv: 1105.1781 [hep-ph] (cit. on p. 7).

[119] P. Agrawal, S. Blanchet, Z. Chacko, and C. Kilic, *Flavored dark matter, and its implications for direct detection and colliders*, Phys. Rev. D **86** (2012) 055002, arXiv: 1109.3516 [hep-ph] (cit. on p. 7).

[120] K. Cheung, K. Mawatari, E. Senaha, P. Y. Tseng, and T. C. Yuan, *Top window for dark matter*, Int. J. Mod. Phys. D **20** (2011) 1413 (cit. on p. 7).

[121] J. Kile, *Flavored Dark Matter: A Review*, Mod. Phys. Lett. A **28** (2013) 1330031, arXiv: 1308.0584 [hep-ph] (cit. on p. 7).

[122] H. An, L.-T. Wang, and H. Zhang, *Dark matter with t-channel mediator: a simple step beyond contact interaction*, Phys. Rev. D **89** (2014) 115014, arXiv: 1308.0592 [hep-ph] (cit. on p. 7).

[123] Y. Bai and J. Berger, *Fermion portal dark matter*, JHEP **11** (2013) 171, arXiv: 1308.0612 [hep-ph] (cit. on p. 7).

[124] A. DiFranzo, K. I. Nagao, A. Rajaraman, and T. M. P. Tait, *Simplified Models for Dark Matter Interacting with Quarks*, JHEP **11** (2013) 014, Erratum: JHEP **01** (2014) 162, arXiv: 1308.2679 [hep-ph] (cit. on p. 7).

[125] B. Batell, T. Lin, and L.-T. Wang, *Flavored dark matter and R-parity violation*, JHEP **01** (2014) 075, arXiv: 1309.4462 [hep-ph] (cit. on p. 7).

[126] S. Chang, R. Edezhath, J. Hutchinson, and M. Luty, *Effective WIMPs*, Phys. Rev. D **89** (2014) 015011, arXiv: 1307.8120 [hep-ph] (cit. on p. 7).

[127] P. Agrawal, M. Blanke, and K. Gemmler, *Flavored dark matter beyond Minimal Flavor Violation*, JHEP **10** (2014) 072, arXiv: 1405.6709 [hep-ph] (cit. on p. 7).

[128] P. Agrawal, B. Batell, D. Hooper, and T. Lin, *Flavored dark matter and the Galactic Center gamma-ray excess*, Phys. Rev. D **90** (2014) 063512, arXiv: 1404.1373 [hep-ph] (cit. on pp. 7, 9, 15).

[129] M. A. Gomez, C. B. Jackson, and G. Shaughnessy, *Dark matter on top*, JCAP **12** (2014) 025, arXiv: 1404.1918 [hep-ph] (cit. on p. 7).

[130] C. Kilic, M. D. Klimek, and J.-H. Yu, *Signatures of top flavored dark matter*, Phys. Rev. D **91** (2015) 054036, arXiv: 1501.02202 [hep-ph] (cit. on p. 7).

[131] M. Blanke and S. Kast, *Top-flavoured dark matter in Dark Minimal Flavour Violation*, JHEP **05** (2017) 162, arXiv: 1702.08457 [hep-ph] (cit. on p. 7).

[132] M. Blanke, S. Das, and S. Kast, *Flavoured Dark Matter Moving Left*, JHEP **02** (2018) 105, arXiv: 1711.10493 [hep-ph] (cit. on p. 7).

[133] G. D'Ambrosio, G. F. Giudice, G. Isidori, and A. Strumia, *Minimal flavor violation: An Effective field theory approach*, Nucl. Phys. B **645** (2002) 155, arXiv: hep-ph/0207036 [hep-ph] (cit. on pp. 7, 9).

[134] J. Charles et al., *CP violation and the CKM matrix: Assessing the impact of the asymmetric B factories*, Eur. Phys. J. C **41** (2005) 1, arXiv: hep-ph/0406184 [hep-ph] (cit. on p. 7).

[135] M. Tanabashi et al., *Review of Particle Physics*, Phys. Rev. D **98** (2018) 030001 (cit. on p. 7).

[136] D. Pinna, A. Zucchetta, M. R. Buckley, and F. Canelli, *Single top quarks and dark matter*, Phys. Rev. D **96** (2017) 035031, arXiv: 1701.05195 [hep-ph] (cit. on p. 8).

[137] P. Pani and G. Polesello, *Dark matter production in association with a single top-quark at the LHC in a two-Higgs-doublet model with a pseudoscalar mediator*, Phys. Dark Univ. **21** (2018) 8, arXiv: 1712.03874 [hep-ph] (cit. on p. 8).

[138] T. Plehn, J. Thompson, and S. Westhoff, *Dark matter from electroweak single top production*, Phys. Rev. D **98** (2018) 015012, arXiv: 1712.08065 [hep-ph] (cit. on p. 8).

[139] G. Brooijmans et al., *Les Houches 2017: Physics at TeV Colliders New Physics Working Group Report*, 2018, arXiv: 1803.10379 [hep-ph] (cit. on p. 8).

[140] ATLAS Collaboration, *ATLAS sensitivity to dark matter produced in association with heavy quarks at the HL-LHC*, ATL-PHYS-PUB-2018-036, 2018, URL: https://cds.cern.ch/record/2649243 (cit. on p. 8).

[141] U. Haisch and G. Polesello, *Searching for production of dark matter in association with top quarks at the LHC*, (2018), arXiv: 1812.00694 [hep-ph] (cit. on p. 8).

[142] P. Fayet, *Supersymmetry and weak, electromagnetic and strong interactions*, Phys. Lett. B **64** (1976) 159 (cit. on p. 8).

[143] P. Fayet, *Spontaneously broken supersymmetric theories of weak, electromagnetic and strong interactions*, Phys. Lett. B **69** (1977) 489 (cit. on p. 8).

[144] ATLAS Collaboration, *Search for dark matter in events with heavy quarks and missing transverse momentum in pp collisions with the ATLAS detector*, Eur. Phys. J. C **75** (2015) 92, arXiv: 1410.4031 [hep-ex] (cit. on p. 9).

[145] S. Ipek, D. McKeen, and A. E. Nelson, *Renormalizable model for the Galactic Center gamma-ray excess from dark matter annihilation*, Phys. Rev. D **90** (2014) 055021, arXiv: 1404.3716 [hep-ph] (cit. on p. 9).

[146] J. M. No, *Looking through the pseudoscalar portal into dark matter: Novel mono-Higgs and mono-Z signatures at the LHC*, Phys. Rev. D **93** (2016) 031701, arXiv: 1509.01110 [hep-ph] (cit. on p. 9).

[147] D. Goncalves, P. A. N. Machado, and J. M. No, *Simplified models for dark matter face their consistent completions*, Phys. Rev. D **95** (2017) 055027, arXiv: 1611.04593 [hep-ph] (cit. on p. 9).

[148] N. F. Bell, G. Busoni, and I. W. Sanderson, *Self-consistent Dark Matter Simplified Models with an s-channel scalar mediator*, JCAP **03** (2017) 015, arXiv: 1612.03475 [hep-ph] (cit. on p. 9).

[149] M. Bauer, U. Haisch, and F. Kahlhoefer, *Simplified dark matter models with two Higgs doublets: I. Pseudoscalar mediators*, JHEP **05** (2017) 138, arXiv: 1701.07427 [hep-ph] (cit. on pp. 9–11, 15, 40).

[150] M. Bauer, M. Klassen, and V. Tenorth, *Universal Properties of Pseudoscalar Mediators*, (2017), arXiv: 1712.06597 [hep-ph] (cit. on p. 9).

[151] U. Haisch and A. Malinauskas, *Let there be light from a second light Higgs doublet*, JHEP **03** (2018) 135, arXiv: 1712.06599 [hep-ph] (cit. on p. 9).

[152] G. Arcadi, M. Lindner, F. S. Queiroz, W. Rodejohann, and S. Vogl, *Pseudoscalar mediators: a WIMP model at the neutrino floor*, JCAP **03** (2018) 042, arXiv: 1711.02110 [hep-ph] (cit. on p. 9).

[153] N. F. Bell, G. Busoni, and I. W. Sanderson, *Two Higgs doublet dark matter portal*, JCAP **01** (2018) 015, arXiv: 1710.10764 [hep-ph] (cit. on p. 9).

[154] J. F. Gunion and H. E. Haber, *The CP conserving two Higgs doublet model: The Approach to the decoupling limit*, Phys. Rev. D **67** (2003) 075019, arXiv: hep-ph/0207010 [hep-ph] (cit. on pp. 9, 10).

[155] A. Berlin, T. Lin, and L.-T. Wang, *Mono-Higgs detection of dark matter at the LHC*, JHEP **06** (2014) 078, arXiv: 1402.7074 [hep-ph] (cit. on pp. 10, 14).

[156] G. C. Branco et al., *Theory and phenomenology of two-Higgs-doublet models*, Phys. Rept. **516** (2012) 1, arXiv: 1106.0034 [hep-ph] (cit. on p. 10).

[157] ATLAS Collaboration, *Search for dark matter produced in association with a Higgs boson decaying to two bottom quarks in pp collisions at $\sqrt{s} = 8$ TeV with the ATLAS detector*, Phys. Rev. D **93** (2016) 072007, arXiv: 1510.06218 [hep-ex] (cit. on p. 10).

[158] ATLAS Collaboration, *ATLAS sensitivity to Two-Higgs-Doublet models with an additional pseudoscalar exploiting four top quark signatures with $3ab^{-1}$ of $\sqrt{s} = 14$ TeV proton–proton collisions*, ATL-PHYS-PUB-2018-027, 2018, URL: https://cds.cern.ch/record/2645845 (cit. on p. 11).

[159] A. Joyce, B. Jain, J. Khoury, and M. Trodden, *Beyond the cosmological standard model*, Phys. Rept. **568** (2015) 1, arXiv: 1407.0059 [astro-ph.CO] (cit. on p. 12).

[160] P. Brax and P. Valageas, *Goldstone models of modified gravity*, Phys. Rev. D **95** (2017) 043515, arXiv: 1611.08279 [astro-ph.CO] (cit. on p. 12).

[161] A. Nicolis, R. Rattazzi, and E. Trincherini, *Galileon as a local modification of gravity*, Phys. Rev. D **79** (2009) 064036, arXiv: 0811.2197 [hep-th] (cit. on p. 12).

[162] G. Busoni, A. De Simone, E. Morgante, and A. Riotto, *On the validity of the effective field theory for dark matter searches at the LHC*, Phys. Lett. B **728** (2014) 412, arXiv: 1307.2253 [hep-ph] (cit. on p. 12).

[163] G. Busoni, A. De Simone, J. Gramling, E. Morgante, and A. Riotto, *On the Validity of the effective field theory for dark matter searches at the LHC, Part II: Complete analysis for the s-channel*, JCAP **06** (2014) 060, arXiv: 1402.1275 [hep-ph] (cit. on p. 12).

[164] G. Busoni, A. De Simone, T. Jacques, E. Morgante, and A. Riotto, *On the validity of the effective field theory for dark matter searches at the LHC Part III: analysis for the t-channel*, JCAP **09** (2014) 022, arXiv: 1405.3101 [hep-ph] (cit. on p. 12).

[165] ATLAS Collaboration, *The ATLAS Simulation Infrastructure*, Eur. Phys. J. C **70** (2010) 823, arXiv: 1005.4568 [physics.ins-det] (cit. on p. 13).

[166] S. Agostinelli et al., *GEANT4: A simulation toolkit*, Nucl. Instrum. Meth. A **506** (2003) 250 (cit. on p. 13).

[167] ATLAS Collaboration, *The simulation principle and performance of the ATLAS fast calorimeter simulation FastCaloSim*, ATL-PHYS-PUB-2010-013, 2010, URL: https://cds.cern.ch/record/1300517 (cit. on p. 13).

[168] ATLAS Collaboration, *Proposal for particle-level object and observable definitions for use in physics measurements at the LHC*, ATL-PHYS-PUB-2015-013, 2015, URL: https://cds.cern.ch/record/2022743 (cit. on p. 13).

[169] C. Degrande et al., *UFO - The Universal FeynRules Output*, Comput. Phys. Commun. **183** (2012) 1201, arXiv: 1108.2040 [hep-ph] (cit. on p. 13).

[170] DM Forum repository, *DMV UFO model*, URL: https://svnweb.cern.ch/cern/wsvn/LHCDMF/trunk/models/Monojet_DMV/?#ae98247b340ee12c1e7b0139c2062d807 (cit. on p. 14).

[171] S. Alioli, P. Nason, C. Oleari, and E. Re, *A general framework for implementing NLO calculations in shower Monte Carlo programs: the POWHEG BOX*, JHEP **06** (2010) 043, arXiv: 1002.2581 [hep-ph] (cit. on p. 14).

[172] T. Sjöstrand, S. Mrenna, and P. Z. Skands, *A brief introduction to PYTHIA 8.1*, Comput. Phys. Commun. **178** (2008) 852, arXiv: 0710.3820 [hep-ph] (cit. on p. 14).

[173] DMSimp Repository, *DMSimp UFO model*, URL: http://feynrules.irmp.ucl.ac.be/wiki/DMsimp (cit. on p. 14).

[174] J. Alwall et al., *The automated computation of tree-level and next-to-leading order differential cross sections, and their matching to parton shower simulations*, JHEP **07** (2014) 079, arXiv: 1405.0301 [hep-ph] (cit. on pp. 14, 45).

[175] ATLAS Collaboration, *Search for New Phenomena in Dijet Angular Distributions in Proton–Proton Collisions at* $\sqrt{s} = 8$ *TeV Measured with the ATLAS Detector*, Phys. Rev. Lett. **114** (2015) 221802, arXiv: 1504.00357 [hep-ex] (cit. on pp. 14, 45).

[176] ATLAS Collaboration, *Search for heavy particles decaying into top-quark pairs using lepton-plus-jets events in proton–proton collisions at* $\sqrt{s} = 13$ *TeV with the ATLAS detector*, Eur. Phys. J. C **78** (2018) 565, arXiv: 1804.10823 [hep-ex] (cit. on pp. 14, 23, 24, 45).

[177] DM Forum repository, *MonotopDMF UFO model*, URL: https://svnweb.cern.ch/cern/wsvn/LHCDMF/trunk/models/Monojet_tChannel/HF_SingleTop/ (cit. on pp. 14, 15).

[178] DM Forum repository, *Higgs_scalar UFO model*, URL: https://svnweb.cern.ch/cern/wsvn/LHCDMF/trunk/models/Higgs_scalar_UFO/ (cit. on p. 14).

[179] DM Forum repository, *Zp2HDM_UFO UFO model*, URL: https://svnweb.cern.ch/cern/wsvn/LHCDMF/trunk/models/EW_Higgs_2HDM/ (cit. on p. 14).

[180] DM Forum repository, *DMS_tloop UFO model*, URL: https://svnweb.cern.ch/cern/wsvn/LHCDMF/trunk/models/Monojet_DMS_tloop/ (cit. on p. 15).

[181] DM Forum repository, *DMScalarMed_loop UFO model*, URL: https://svnweb.cern.ch/cern/wsvn/LHCDMF/trunk/models/HF_S%2BPS/ (cit. on p. 15).

[182] Y. Afik et al., *DM+$b\bar{b}$ simulations with DMSimp: an update*, 2018, arXiv: 1811.08002 [hep-ex] (cit. on pp. 15, 45).

[183] DM Forum repository, *dmS_T UFO model*, URL: https://svnweb.cern.ch/cern/wsvn/LHCDMF/trunk/models/Monojet_tChannel/contributed_by_Amelia_Brennan/ (cit. on p. 15).

[184] DM Forum repository, *DM_Bflavored UFO model*, URL: https://svnweb.cern.ch/cern/wsvn/LHCDMF/trunk/models/HF_singleb/ (cit. on p. 15).

[185] DM Forum repository, *Pseudoscalar_2HDM UFO model*, URL: https://svnweb.cern.ch/cern/wsvn/LHCDMF/trunk/models/Pseudoscalar_2HDM/ (cit. on p. 15).

[186] ATLAS Collaboration, *Electron efficiency measurements with the ATLAS detector using 2012 LHC proton–proton collision data*, Eur. Phys. J. C **77** (2017) 195, arXiv: 1612.01456 [hep-ex] (cit. on p. 15).

[187] ATLAS Collaboration, *Electron efficiency measurements with the ATLAS detector using the 2015 LHC proton–proton collision data*, ATLAS-CONF-2016-024, 2016, URL: https://cds.cern.ch/record/2157687 (cit. on p. 15).

[188] ATLAS Collaboration, *Muon reconstruction performance of the ATLAS detector in proton–proton collision data at $\sqrt{s}$ = 13 TeV*, Eur. Phys. J. C **76** (2016) 292, arXiv: 1603.05598 [hep-ex] (cit. on p. 15).

[189] ATLAS Collaboration, *Measurement of the photon identification efficiencies with the ATLAS detector using LHC Run 2 data collected in 2015 and 2016*, Eur. Phys. J. (2018), arXiv: 1810.05087 [hep-ex] (cit. on p. 15).

[190] ATLAS Collaboration, *Properties of jets and inputs to jet reconstruction and calibration with the ATLAS detector using proton–proton collisions at $\sqrt{s}$ = 13 TeV*, ATL-PHYS-PUB-2015-036, 2015, URL: https://cds.cern.ch/record/2044564 (cit. on p. 15).

[191] ATLAS Collaboration, *Electron identification measurements in ATLAS using $\sqrt{s}$ = 13 TeV data with 50 ns bunch spacing*, ATL-PHYS-PUB-2015-041, 2015, URL: https://cds.cern.ch/record/2048202 (cit. on p. 15).

[192] ATLAS Collaboration, *Electron and photon energy calibration with the ATLAS detector using 2015–2016 LHC proton–proton collision data*, JINST (2018), arXiv: 1812.03848 [hep-ex] (cit. on p. 15).

[193] M. Cacciari, G. P. Salam, and G. Soyez, *The anti-k_t jet clustering algorithm*, JHEP **04** (2008) 063, arXiv: 0802.1189 [hep-ph] (cit. on p. 15).

[194] M. Cacciari, G. P. Salam, and G. Soyez, *FastJet user manual*, Eur. Phys. J. C **72** (2012) 1896, arXiv: 1111.6097 [hep-ph] (cit. on p. 15).

[195] ATLAS Collaboration, *Performance of b-jet identification in the ATLAS experiment*, JINST **11** (2016) P04008, arXiv: 1512.01094 [hep-ex] (cit. on p. 15).

[196] ATLAS Collaboration, *Optimisation of the ATLAS b-tagging performance for the 2016 LHC Run*, ATL-PHYS-PUB-2016-012, 2016, URL: https://cds.cern.ch/record/2160731 (cit. on p. 15).

[197] ATLAS Collaboration, *Performance of missing transverse momentum reconstruction with the ATLAS detector using proton–proton collisions at* $\sqrt{s}$ = 13 *TeV*, Eur. Phys. J. C **78** (2018) 903, arXiv: 1802.08168 [hep-ex] (cit. on p. 15).

[198] J. M. Lindert et al., *Precise predictions for V+ jets dark matter backgrounds*, Eur. Phys. J. C **77** (2017) 829, arXiv: 1705.04664 [hep-ph] (cit. on p. 16).

[199] ATLAS Collaboration, *Search for invisible decays of a Higgs boson using vector-boson fusion in pp collisions at* $\sqrt{s}$ = 8 *TeV with the ATLAS detector*, JHEP **01** (2016) 172, arXiv: 1508.07869 [hep-ex] (cit. on pp. 16, 21).

[200] ATLAS Collaboration, *Search for invisible Higgs boson decays in vector boson fusion at* $\sqrt{s}$ = 13 *TeV with the ATLAS detector*, Phys. Lett. (2018), arXiv: 1809.06682 [hep-ex] (cit. on p. 16).

[201] ATLAS Collaboration, *Search for new phenomena in dijet events using* 37 fb^{-1} *of pp collision data collected at* $\sqrt{s}$ = 13 *TeV with the ATLAS detector*, Phys. Rev. D **96** (2017) 052004, arXiv: 1703.09127 [hep-ex] (cit. on pp. 19, 22, 24).

[202] ATLAS Collaboration, *Search for new phenomena in the dijet mass distribution using pp collision data at* $\sqrt{s}$ = 8 *TeV with the ATLAS detector*, Phys. Rev. D **91** (2015) 052007, arXiv: 1407.1376 [hep-ex] (cit. on p. 22).

[203] Z. Nagy, *Three-Jet Cross Sections in Hadron-Hadron Collisions at Next-To-Leading Order*, Phys. Rev. Lett. **88** (2002) 122003, arXiv: hep-ph/0110315 [hep-ph] (cit. on p. 22).

[204] Z. Nagy, *Next-to-leading order calculation of three jet observables in hadron hadron collision*, Phys. Rev. D **68** (2003) 094002, arXiv: hep-ph/0307268 [hep-ph] (cit. on p. 22).

[205] ATLAS Collaboration, *Search for Low-Mass Dijet Resonances Using Trigger-Level Jets with the ATLAS Detector in pp Collisions at* $\sqrt{s}$ = 13 *TeV*, Phys. Rev. Lett. **121** (2018) 081801, arXiv: 1804.03496 [hep-ex] (cit. on pp. 22, 24).

[206] ATLAS Collaboration, *Search for new light resonances decaying to jet pairs and produced in association with a photon or a jet in proton–proton collisions at* $\sqrt{s}$ = 13 *TeV with the ATLAS detector*, ATLAS-CONF-2016-070, 2016, URL: https://cds.cern.ch/record/2206221 (cit. on pp. 22, 24).

[207] ATLAS Collaboration, *Search for light resonances decaying to boosted quark pairs and produced in association with a photon or a jet in proton–proton collisions at* $\sqrt{s}$ = 13 *TeV with the ATLAS detector*, Phys. Lett. B **788** (2019) 316, arXiv: 1801.08769 [hep-ex] (cit. on pp. 23, 24).

[208] J. Thaler and K. Van Tilburg, *Identifying boosted objects with N-subjettiness*, JHEP **03** (2011) 015, arXiv: 1011.2268 [hep-ph] (cit. on p. 23).

[209] ATLAS Collaboration, *Search for resonances in the mass distribution of jet pairs with one or two jets identified as b-jets in proton–proton collisions at* $\sqrt{s}$ = 13 *TeV with the ATLAS detector*, Phys. Rev. D **98** (2018) 032016, arXiv: 1805.09299 [hep-ex] (cit. on pp. 23, 24).

[210] ATLAS Collaboration, *Search for new high-mass phenomena in the dilepton final state using 36 fb^{-1} of proton–proton collision data at $\sqrt{s}$ = 13 TeV with the ATLAS detector*, JHEP **10** (2017) 182, arXiv: 1707.02424 [hep-ex] (cit. on pp. 23, 24).

[211] ATLAS Collaboration, *Search for new phenomena in a lepton plus high jet multiplicity final state with the ATLAS experiment using $\sqrt{s}$ = 13 TeV proton–proton collision data*, JHEP **09** (2017) 088, arXiv: 1704.08493 [hep-ex] (cit. on p. 24).

[212] J. Butterworth et al., *PDF4LHC recommendations for LHC Run II*, J. Phys. G **43** (2016) 023001, arXiv: 1510.03865 [hep-ph] (cit. on p. 26).

[213] A. L. Read, *Presentation of search results: the CL_S technique*, J. Phys. G **28** (2002) 2693 (cit. on p. 26).

[214] M. Backovic, A. Martini, K. Kong, O. Mattelaer, and G. Mohlabeng, *MadDM: New dark matter tool in the LHC era*, AIP Conf. Proc. **1743** (2016) 060001, arXiv: 1509.03683 [hep-ph] (cit. on pp. 28–30).

[215] F. Kahlhoefer, K. Schmidt-Hoberg, T. Schwetz, and S. Vogl, *Implications of unitarity and gauge invariance for simplified dark matter models*, JHEP **02** (2016) 016, arXiv: 1510.02110 [hep-ph] (cit. on pp. 29, 30).

[216] ATLAS Collaboration, *Search for invisible particles produced in association with single-top-quarks in proton–proton collisions at $\sqrt{s}$ = 8 TeV with the ATLAS detector*, Eur. Phys. J. C **75** (2015) 79, arXiv: 1410.5404 [hep-ex] (cit. on p. 33).

[217] ATLAS Collaboration, *Search for heavy Higgs bosons A/H decaying to a top quark pair in pp collisions at $\sqrt{s}$ = 8 TeV with the ATLAS detector*, Phys. Rev. Lett. **119** (2017) 191803, arXiv: 1707.06025 [hep-ex] (cit. on p. 35).

[218] A. Djouadi, M. Drees, and J.-L. Kneur, *Neutralino dark matter in mSUGRA: Reopening the light Higgs pole window*, Phys. Lett. B **624** (2005) 60, arXiv: hep-ph/0504090 [hep-ph] (cit. on p. 42).

[219] E. A. Bagnaschi et al., *Supersymmetric dark matter after LHC Run 1*, Eur. Phys. J. C **75** (2015) 500, arXiv: 1508.01173 [hep-ph] (cit. on p. 42).

[220] P. Brax and C. Burrage, *Constraining disformally coupled scalar fields*, Phys. Rev. D **90** (2014) 104009, arXiv: 1407.1861 [astro-ph.CO] (cit. on p. 43).

[221] L. E. Strigari, *Galactic searches for dark matter*, Phys. Rept. **531** (2013) 1, arXiv: 1211.7090 [astro-ph.CO] (cit. on p. 46).

[222] CMS Collaboration, *Search for top squarks and dark matter particles in opposite-charge dilepton final states at $\sqrt{s}$ = 13 TeV*, Phys. Rev. D **97** (2018) 032009, arXiv: 1711.00752 [hep-ex] (cit. on p. 47).

[223] LHCb Collaboration, *Search for Higgs-like bosons decaying into long-lived exotic particles*, Eur. Phys. J. C **76** (2016) 664, arXiv: 1609.03124 [hep-ex] (cit. on p. 47).

[224] LHCb Collaboration, *Search for Dark Photons Produced in 13 TeV pp Collisions*, Phys. Rev. Lett. **120** (2018) 061801, arXiv: 1710.02867 [hep-ex] (cit. on p. 47).

[225] A. A. Aguilar-Arevalo et al., *Dark matter search in nucleon, pion, and electron channels from a proton beam dump with MiniBooNE*, Phys. Rev. D **98** (2018) 112004, arXiv: 1807.06137 [hep-ex] (cit. on p. 47).

[226] ATLAS Collaboration, *ATLAS Computing Acknowledgements*, ATL-GEN-PUB-2016-002, URL: https://cds.cern.ch/record/2202407 (cit. on p. 53).

The ATLAS Collaboration

M. Aaboud[34d], G. Aad[100], B. Abbott[126], D.C. Abbott[101], O. Abdinov[13,*], D.K. Abhayasinghe[92], S.H. Abidi[165], O.S. AbouZeid[39], N.L. Abraham[154], H. Abramowicz[159], H. Abreu[158], Y. Abulaiti[6], B.S. Acharya[65a,65b,o], S. Adachi[161], L. Adam[98], L. Adamczyk[82a], L. Adamek[165], J. Adelman[120], M. Adersberger[113], A. Adiguzel[12c,ah], T. Adye[142], A.A. Affolder[144], Y. Afik[158], C. Agapopoulou[130], M.N. Agaras[37], A. Aggarwal[118], C. Agheorghiesei[27c], J.A. Aguilar-Saavedra[138f,138a,ag], F. Ahmadov[78], G. Aielli[72a,72b], S. Akatsuka[84], T.P.A. Åkesson[95], E. Akilli[53], A.V. Akimov[109], K. Al Khoury[130], G.L. Alberghi[23b,23a], J. Albert[174], M.J. Alconada Verzini[87], S. Alderweireldt[118], M. Aleksa[35], I.N. Aleksandrov[78], C. Alexa[27b], D. Alexandre[19], T. Alexopoulos[10], M. Alhroob[126], B. Ali[140], G. Alimonti[67a], J. Alison[36], S.P. Alkire[146], C. Allaire[130], B.M.M. Allbrooke[154], B.W. Allen[129], P.P. Allport[21], A. Aloisio[68a,68b], A. Alonso[39], F. Alonso[87], C. Alpigiani[146], A.A. Alshehri[56], M.I. Alstaty[100], M. Alvarez Estevez[97], B. Alvarez Gonzalez[35], D. Álvarez Piqueras[172], M.G. Alviggi[68a,68b], Y. Amaral Coutinho[79b], A. Ambler[102], L. Ambroz[133], C. Amelung[26], D. Amidei[104], S.P. Amor Dos Santos[138a,138c], S. Amoroso[45], C.S. Amrouche[53], F. An[77], C. Anastopoulos[147], N. Andari[143], T. Andeen[11], C.F. Anders[60b], J.K. Anders[20], A. Andreazza[67a,67b], V. Andrei[60a], C.R. Anelli[174], S. Angelidakis[37], I. Angelozzi[119], A. Angerami[38], A.V. Anisenkov[121b,121a], A. Annovi[70a], C. Antel[60a], M.T. Anthony[147], M. Antonelli[50], D.J.A. Antrim[169], F. Anulli[71a], M. Aoki[80], J.A. Aparisi Pozo[172], L. Aperio Bella[35], G. Arabidze[105], J.P. Araque[138a], V. Araujo Ferraz[79b], R. Araujo Pereira[79b], A.T.H. Arce[48], F.A. Arduh[87], J-F. Arguin[108], S. Argyropoulos[76], J.-H. Arling[45], A.J. Armbruster[35], L.J. Armitage[91], A. Armstrong[169], O. Arnaez[165], H. Arnold[119], A. Artamonov[110,*], G. Artoni[133], S. Artz[98], S. Asai[161], N. Asbah[58], E.M. Asimakopoulou[170], L. Asquith[154], K. Assamagan[29], R. Astalos[28a], R.J. Atkin[32a], M. Atkinson[171], N.B. Atlay[149], K. Augsten[140], G. Avolio[35], R. Avramidou[59a], M.K. Ayoub[15a], A.M. Azoulay[166b], G. Azuelos[108,av], A.E. Baas[60a], M.J. Baca[21], H. Bachacou[143], K. Bachas[66a,66b], M. Backes[133], F. Backman[44a,44b], P. Bagnaia[71a,71b], M. Bahmani[83], H. Bahrasemani[150], A.J. Bailey[172], V.R. Bailey[171], J.T. Baines[142], M. Bajic[39], C. Bakalis[10], O.K. Baker[181], P.J. Bakker[119], D. Bakshi Gupta[8], S. Balaji[155], E.M. Baldin[121b,121a], P. Balek[178], F. Balli[143], W.K. Balunas[133], J. Balz[98], E. Banas[83], A. Bandyopadhyay[24], S. Banerjee[179,k], A.A.E. Bannoura[180], L. Barak[159], W.M. Barbe[37], E.L. Barberio[103], D. Barberis[54b,54a], M. Barbero[100], T. Barillari[114], M-S. Barisits[35], J. Barkeloo[129], T. Barklow[151], R. Barnea[158], S.L. Barnes[59c], B.M. Barnett[142], R.M. Barnett[18], Z. Barnovska-Blenessy[59a], A. Baroncelli[59a], G. Barone[29], A.J. Barr[133], L. Barranco Navarro[172], F. Barreiro[97], J. Barreiro Guimarães da Costa[15a], R. Bartoldus[151], G. Bartolini[100], A.E. Barton[88], P. Bartos[28a], A. Basalaev[45], A. Bassalat[130], R.L. Bates[56], S.J. Batista[165], S. Batlamous[34e], J.R. Batley[31], M. Battaglia[144], M. Bauce[71a,71b], F. Bauer[143], K.T. Bauer[169], H.S. Bawa[151], J.B. Beacham[124], T. Beau[134], P.H. Beauchemin[168], P. Bechtle[24], H.C. Beck[52], H.P. Beck[20,r], K. Becker[51], M. Becker[98], C. Becot[45], A. Beddall[12d], A.J. Beddall[12a], V.A. Bednyakov[78], M. Bedognetti[119], C.P. Bee[153], T.A. Beermann[75], M. Begalli[79b], M. Begel[29], A. Behera[153], J.K. Behr[45], F. Beisiegel[24], A.S. Bell[93], G. Bella[159], L. Bellagamba[23b], A. Bellerive[33], P. Bellos[9], K. Beloborodov[121b,121a], K. Belotskiy[111], N.L. Belyaev[111], O. Benary[159,*], D. Benchekroun[34a], N. Benekos[10], Y. Benhammou[159], D.P. Benjamin[6], M. Benoit[53], J.R. Bensinger[26], S. Bentvelsen[119], L. Beresford[133], M. Beretta[50], D. Berge[45], E. Bergeaas Kuutmann[170], N. Berger[5], B. Bergmann[140], L.J. Bergsten[26], J. Beringer[18], S. Berlendis[7], N.R. Bernard[101], G. Bernardi[134], C. Bernius[151], F.U. Bernlochner[24], T. Berry[92], P. Berta[98], C. Bertella[15a], G. Bertoli[44a,44b], I.A. Bertram[88], G.J. Besjes[39], O. Bessidskaia Bylund[180], N. Besson[143], A. Bethani[99], S. Bethke[114], A. Betti[24], A.J. Bevan[91], J. Beyer[114], R. Bi[137], R.M. Bianchi[137], O. Biebel[113], D. Biedermann[19], R. Bielski[35], K. Bierwagen[98], N.V. Biesuz[70a,70b], M. Biglietti[73a], T.R.V. Billoud[108], M. Bindi[52], A. Bingul[12d], C. Bini[71a,71b], S. Biondi[23b,23a], M. Birman[178], T. Bisanz[52], J.P. Biswal[159], A. Bitadze[99],

C. Bittrich[47], D.M. Bjergaard[48], J.E. Black[151], K.M. Black[25], T. Blazek[28a], I. Bloch[45], C. Blocker[26], A. Blue[56], U. Blumenschein[91], Dr. Blunier[145a], G.J. Bobbink[119], V.S. Bobrovnikov[121b,121a], S.S. Bocchetta[95], A. Bocci[48], D. Boerner[45], D. Bogavac[113], A.G. Bogdanchikov[121b,121a], C. Bohm[44a], V. Boisvert[92], P. Bokan[52,170], T. Bold[82a], A.S. Boldyrev[112], A.E. Bolz[60b], M. Bomben[134], M. Bona[91], J.S. Bonilla[129], M. Boonekamp[143], H.M. Borecka-Bielska[89], A. Borisov[122], G. Borissov[88], J. Bortfeldt[35], D. Bortoletto[133], V. Bortolotto[72a,72b], D. Boscherini[23b], M. Bosman[14], J.D. Bossio Sola[30], K. Bouaouda[34a], J. Boudreau[137], E.V. Bouhova-Thacker[88], D. Boumediene[37], C. Bourdarios[130], S.K. Boutle[56], A. Boveia[124], J. Boyd[35], D. Boye[32b,ap], I.R. Boyko[78], A.J. Bozson[92], J. Bracinik[21], N. Brahimi[100], G. Brandt[180], O. Brandt[60a], F. Braren[45], U. Bratzler[162], B. Brau[101], J.E. Brau[129], W.D. Breaden Madden[56], K. Brendlinger[45], L. Brenner[45], R. Brenner[170], S. Bressler[178], B. Brickwedde[98], D.L. Briglin[21], D. Britton[56], D. Britzger[114], I. Brock[24], R. Brock[105], G. Brooijmans[38], T. Brooks[92], W.K. Brooks[145b], E. Brost[120], J.H Broughton[21], P.A. Bruckman de Renstrom[83], D. Bruncko[28b], A. Bruni[23b], G. Bruni[23b], L.S. Bruni[119], S. Bruno[72a,72b], B.H. Brunt[31], M. Bruschi[23b], N. Bruscino[137], P. Bryant[36], L. Bryngemark[95], T. Buanes[17], Q. Buat[35], P. Buchholz[149], A.G. Buckley[56], I.A. Budagov[78], M.K. Bugge[132], F. Bührer[51], O. Bulekov[111], T.J. Burch[120], S. Burdin[89], C.D. Burgard[119], A.M. Burger[127], B. Burghgrave[8], K. Burka[83], I. Burmeister[46], J.T.P. Burr[45], V. Büscher[98], E. Buschmann[52], P. Bussey[56], J.M. Butler[25], C.M. Buttar[56], J.M. Butterworth[93], P. Butti[35], W. Buttinger[35], A. Buzatu[156], A.R. Buzykaev[121b,121a], G. Cabras[23b,23a], S. Cabrera Urbán[172], D. Caforio[140], H. Cai[171], V.M.M. Cairo[2], O. Cakir[4a], N. Calace[35], P. Calafiura[18], A. Calandri[100], G. Calderini[134], P. Calfayan[64], G. Callea[56], L.P. Caloba[79b], S. Calvente Lopez[97], D. Calvet[37], S. Calvet[37], T.P. Calvet[153], M. Calvetti[70a,70b], R. Camacho Toro[134], S. Camarda[35], D. Camarero Munoz[97], P. Camarri[72a,72b], D. Cameron[132], R. Caminal Armadans[101], C. Camincher[35], S. Campana[35], M. Campanelli[93], A. Camplani[39], A. Campoverde[149], V. Canale[68a,68b], M. Cano Bret[59c], J. Cantero[127], T. Cao[159], Y. Cao[171], M.D.M. Capeans Garrido[35], M. Capua[40b,40a], R. Cardarelli[72a], F.C. Cardillo[147], I. Carli[141], T. Carli[35], G. Carlino[68a], B.T. Carlson[137], L. Carminati[67a,67b], R.M.D. Carney[44a,44b], S. Caron[118], E. Carquin[145b], S. Carrá[67a,67b], J.W.S. Carter[165], M.P. Casado[14,g], A.F. Casha[165], D.W. Casper[169], R. Castelijn[119], F.L. Castillo[172], V. Castillo Gimenez[172], N.F. Castro[138a,138e], A. Catinaccio[35], J.R. Catmore[132], A. Cattai[35], J. Caudron[24], V. Cavaliere[29], E. Cavallaro[14], D. Cavalli[67a], M. Cavalli-Sforza[14], V. Cavasinni[70a,70b], E. Celebi[12b], L. Cerda Alberich[172], A.S. Cerqueira[79a], A. Cerri[154], L. Cerrito[72a,72b], F. Cerutti[18], A. Cervelli[23b,23a], S.A. Cetin[12b], A. Chafaq[34a], D. Chakraborty[120], S.K. Chan[58], W.S. Chan[119], W.Y. Chan[89], J.D. Chapman[31], B. Chargeishvili[157b], D.G. Charlton[21], C.C. Chau[33], C.A. Chavez Barajas[154], S. Che[124], A. Chegwidden[105], S. Chekanov[6], S.V. Chekulaev[166a], G.A. Chelkov[78,au], M.A. Chelstowska[35], B. Chen[77], C. Chen[59a], C.H. Chen[77], H. Chen[29], J. Chen[59a], J. Chen[38], S. Chen[135], S.J. Chen[15c], X. Chen[15b,at], Y. Chen[81], Y-H. Chen[45], H.C. Cheng[62a], H.J. Cheng[15d], A. Cheplakov[78], E. Cheremushkina[122], R. Cherkaoui El Moursli[34e], E. Cheu[7], K. Cheung[63], T.J.A. Chevalérias[143], L. Chevalier[143], V. Chiarella[50], G. Chiarelli[70a], G. Chiodini[66a], A.S. Chisholm[35,21], A. Chitan[27b], I. Chiu[161], Y.H. Chiu[174], M.V. Chizhov[78], K. Choi[64], A.R. Chomont[130], S. Chouridou[160], Y.S. Chow[119], M.C. Chu[62a], J. Chudoba[139], A.J. Chuinard[102], J.J. Chwastowski[83], L. Chytka[128], D. Cinca[46], V. Cindro[90], I.A. Cioară[27b], A. Ciocio[18], F. Cirotto[68a,68b], Z.H. Citron[178], M. Citterio[67a], B.M. Ciungu[165], A. Clark[53], M.R. Clark[38], P.J. Clark[49], C. Clement[44a,44b], Y. Coadou[100], M. Cobal[65a,65c], A. Coccaro[54b], J. Cochran[77], H. Cohen[159], A.E.C. Coimbra[178], L. Colasurdo[118], B. Cole[38], A.P. Colijn[119], J. Collot[57], P. Conde Muiño[138a,h], E. Coniavitis[51], S.H. Connell[32b], I.A. Connelly[99], S. Constantinescu[27b], F. Conventi[68a,aw], A.M. Cooper-Sarkar[133], F. Cormier[173], K.J.R. Cormier[165], L.D. Corpe[93], M. Corradi[71a,71b], E.E. Corrigan[95], F. Corriveau[102,ac], A. Cortes-Gonzalez[35], M.J. Costa[172], F. Costanza[5], D. Costanzo[147], G. Cowan[92], J.W. Cowley[31], J. Crane[99], K. Cranmer[123], S.J. Crawley[56], R.A. Creager[135], S. Crépé-Renaudin[57], F. Crescioli[134], M. Cristinziani[24], V. Croft[123], G. Crosetti[40b,40a], A. Cueto[97], T. Cuhadar Donszelmann[147], A.R. Cukierman[151], S. Czekierda[83], P. Czodrowski[35],

M.J. Da Cunha Sargedas De Sousa[59b], J.V. Da Fonseca Pinto[79b], C. Da Via[99], W. Dabrowski[82a], T. Dado[28a], S. Dahbi[34e], T. Dai[104], C. Dallapiccola[101], M. Dam[39], G. D'amen[23b,23a], J. Damp[98], J.R. Dandoy[135], M.F. Daneri[30], N.P. Dang[179,k], N.D Dann[99], M. Danninger[173], V. Dao[35], G. Darbo[54b], O. Dartsi[5], A. Dattagupta[129], T. Daubney[45], S. D'Auria[67a,67b], W. Davey[24], C. David[45], T. Davidek[141], D.R. Davis[48], E. Dawe[103], I. Dawson[147], K. De[8], R. De Asmundis[68a], A. De Benedetti[126], M. De Beurs[119], S. De Castro[23b,23a], S. De Cecco[71a,71b], N. De Groot[118], P. de Jong[119], H. De la Torre[105], A. De Maria[70a,70b], D. De Pedis[71a], A. De Salvo[71a], U. De Sanctis[72a,72b], M. De Santis[72a,72b], A. De Santo[154], K. De Vasconcelos Corga[100], J.B. De Vivie De Regie[130], C. Debenedetti[144], D.V. Dedovich[78], M. Del Gaudio[40b,40a], J. Del Peso[97], Y. Delabat Diaz[45], D. Delgove[130], F. Deliot[143], C.M. Delitzsch[7], M. Della Pietra[68a,68b], D. Della Volpe[53], A. Dell'Acqua[35], L. Dell'Asta[25], M. Delmastro[5], C. Delporte[130], P.A. Delsart[57], D.A. DeMarco[165], S. Demers[181], M. Demichev[78], S.P. Denisov[122], D. Denysiuk[119], L. D'Eramo[134], D. Derendarz[83], J.E. Derkaoui[34d], F. Derue[134], P. Dervan[89], K. Desch[24], C. Deterre[45], K. Dette[165], M.R. Devesa[30], P.O. Deviveiros[35], A. Dewhurst[142], S. Dhaliwal[26], F.A. Di Bello[53], A. Di Ciaccio[72a,72b], L. Di Ciaccio[5], W.K. Di Clemente[135], C. Di Donato[68a,68b], A. Di Girolamo[35], G. Di Gregorio[70a,70b], B. Di Micco[73a,73b], R. Di Nardo[101], K.F. Di Petrillo[58], R. Di Sipio[165], D. Di Valentino[33], C. Diaconu[100], F.A. Dias[39], T. Dias Do Vale[138a,138e], M.A. Diaz[145a], J. Dickinson[18], E.B. Diehl[104], J. Dietrich[19], S. Díez Cornell[45], A. Dimitrievska[18], J. Dingfelder[24], F. Dittus[35], F. Djama[100], T. Djobava[157b], J.I. Djuvsland[17], M.A.B. Do Vale[79c], M. Dobre[27b], D. Dodsworth[26], C. Doglioni[95], J. Dolejsi[141], Z. Dolezal[141], M. Donadelli[79d], J. Donini[37], A. D'onofrio[91], M. D'Onofrio[89], J. Dopke[142], A. Doria[68a], M.T. Dova[87], A.T. Doyle[56], E. Drechsler[150], E. Dreyer[150], T. Dreyer[52], Y. Du[59b], Y. Duan[59b], F. Dubinin[109], M. Dubovsky[28a], A. Dubreuil[53], E. Duchovni[178], G. Duckeck[113], A. Ducourthial[134], O.A. Ducu[108,w], D. Duda[114], A. Dudarev[35], A.C. Dudder[98], E.M. Duffield[18], L. Duflot[130], M. Dührssen[35], C. Dülsen[180], M. Dumancic[178], A.E. Dumitriu[27b], A.K. Duncan[56], M. Dunford[60a], A. Duperrin[100], H. Duran Yildiz[4a], M. Düren[55], A. Durglishvili[157b], D. Duschinger[47], B. Dutta[45], D. Duvnjak[1], G. Dyckes[135], M. Dyndal[45], S. Dysch[99], B.S. Dziedzic[83], K.M. Ecker[114], R.C. Edgar[104], T. Eifert[35], G. Eigen[17], K. Einsweiler[18], T. Ekelof[170], M. El Kacimi[34c], R. El Kosseifi[100], V. Ellajosyula[170], M. Ellert[170], F. Ellinghaus[180], A.A. Elliot[91], N. Ellis[35], J. Elmsheuser[29], M. Elsing[35], D. Emeliyanov[142], A. Emerman[38], Y. Enari[161], J.S. Ennis[176], M.B. Epland[48], J. Erdmann[46], A. Ereditato[20], M. Escalier[130], C. Escobar[172], O. Estrada Pastor[172], A.I. Etienvre[143], E. Etzion[159], H. Evans[64], A. Ezhilov[136], M. Ezzi[34e], F. Fabbri[56], L. Fabbri[23b,23a], V. Fabiani[118], G. Facini[93], R.M. Faisca Rodrigues Pereira[138a], R.M. Fakhrutdinov[122], S. Falciano[71a], P.J. Falke[5], S. Falke[5], J. Faltova[141], Y. Fang[15a], Y. Fang[15a], G. Fanourakis[43], M. Fanti[67a,67b], A. Farbin[8], A. Farilla[73a], E.M. Farina[69a,69b], T. Farooque[105], S. Farrell[18], S.M. Farrington[176], P. Farthouat[35], F. Fassi[34e], P. Fassnacht[35], D. Fassouliotis[9], M. Faucci Giannelli[49], W.J. Fawcett[31], L. Fayard[130], O.L. Fedin[136,p], W. Fedorko[173], M. Feickert[41], S. Feigl[132], L. Feligioni[100], C. Feng[59b], E.J. Feng[35], M. Feng[48], M.J. Fenton[56], A.B. Fenyuk[122], J. Ferrando[45], A. Ferrari[170], P. Ferrari[119], R. Ferrari[69a], D.E. Ferreira de Lima[60b], A. Ferrer[172], D. Ferrere[53], C. Ferretti[104], F. Fiedler[98], A. Filipčič[90], F. Filthaut[118], K.D. Finelli[25], M.C.N. Fiolhais[138a,138c,a], L. Fiorini[172], C. Fischer[14], W.C. Fisher[105], I. Fleck[149], P. Fleischmann[104], R.R.M. Fletcher[135], T. Flick[180], B.M. Flierl[113], L.M. Flores[135], L.R. Flores Castillo[62a], F.M. Follega[74a,74b], N. Fomin[17], G.T. Forcolin[74a,74b], A. Formica[143], F.A. Förster[14], A.C. Forti[99], A.G. Foster[21], D. Fournier[130], H. Fox[88], S. Fracchia[147], P. Francavilla[70a,70b], S. Francescato[71b], M. Franchini[23b,23a], S. Franchino[60a], D. Francis[35], L. Franconi[144], M. Franklin[58], M. Frate[169], A.N. Fray[91], B. Freund[108], W.S. Freund[79b], E.M. Freundlich[46], D.C. Frizzell[126], D. Froidevaux[35], J.A. Frost[133], C. Fukunaga[162], E. Fullana Torregrosa[172], E. Fumagalli[54b,54a], T. Fusayasu[115], J. Fuster[172], A. Gabrielli[23b,23a], A. Gabrielli[18], G.P. Gach[82a], S. Gadatsch[53], P. Gadow[114], G. Gagliardi[54b,54a], L.G. Gagnon[108], C. Galea[27b], B. Galhardo[138a,138c], E.J. Gallas[133], B.J. Gallop[142], P. Gallus[140], G. Galster[39], R. Gamboa Goni[91], K.K. Gan[124], S. Ganguly[178], J. Gao[59a], Y. Gao[89],

Y.S. Gao[151,m], C. García[172], J.E. García Navarro[172], J.A. García Pascual[15a], C. Garcia-Argos[51], M. Garcia-Sciveres[18], R.W. Gardner[36], N. Garelli[151], S. Gargiulo[51], V. Garonne[132], A. Gaudiello[54b,54a], G. Gaudio[69a], I.L. Gavrilenko[109], A. Gavrilyuk[110], C. Gay[173], G. Gaycken[24], E.N. Gazis[10], C.N.P. Gee[142], J. Geisen[52], M. Geisen[98], M.P. Geisler[60a], C. Gemme[54b], M.H. Genest[57], C. Geng[104], S. Gentile[71a,71b], S. George[92], T. Geralis[43], D. Gerbaudo[14], G. Gessner[46], S. Ghasemi[149], M. Ghasemi Bostanabad[174], M. Ghneimat[24], A. Ghosh[76], B. Giacobbe[23b], S. Giagu[71a,71b], N. Giangiacomi[23b,23a], P. Giannetti[70a], A. Giannini[68a,68b], S.M. Gibson[92], M. Gignac[144], D. Gillberg[33], G. Gilles[180], D.M. Gingrich[3,av], M.P. Giordani[65a,65c], F.M. Giorgi[23b], P.F. Giraud[143], G. Giugliarelli[65a,65c], D. Giugni[67a], F. Giuli[133], M. Giulini[60b], S. Gkaitatzis[160], I. Gkialas[9,j], E.L. Gkougkousis[14], P. Gkountoumis[10], L.K. Gladilin[112], C. Glasman[97], J. Glatzer[14], P.C.F. Glaysher[45], A. Glazov[45], M. Goblirsch-Kolb[26], S. Goldfarb[103], T. Golling[53], D. Golubkov[122], A. Gomes[138a,138b], R. Goncalves Gama[52], R. Gonçalo[138a,138b], G. Gonella[51], L. Gonella[21], A. Gongadze[78], F. Gonnella[21], J.L. Gonski[58], S. González de la Hoz[172], S. Gonzalez-Sevilla[53], G.R. Gonzalvo Rodriguez[172], L. Goossens[35], P.A. Gorbounov[110], H.A. Gordon[29], B. Gorini[35], E. Gorini[66a,66b], A. Gorišek[90], A.T. Goshaw[48], C. Gössling[46], M.I. Gostkin[78], C.A. Gottardo[24], C.R. Goudet[130], D. Goujdami[34c], A.G. Goussiou[146], N. Govender[32b,c], C. Goy[5], E. Gozani[158], I. Grabowska-Bold[82a], P.O.J. Gradin[170], E.C. Graham[89], J. Gramling[169], E. Gramstad[132], S. Grancagnolo[19], M. Grandi[154], V. Gratchev[136], P.M. Gravila[27f], F.G. Gravili[66a,66b], C. Gray[56], H.M. Gray[18], C. Grefe[24], K. Gregersen[95], I.M. Gregor[45], P. Grenier[151], K. Grevtsov[45], N.A. Grieser[126], J. Griffiths[8], A.A. Grillo[144], K. Grimm[151,b], S. Grinstein[14,x], J.-F. Grivaz[130], S. Groh[98], E. Gross[178], J. Grosse-Knetter[52], Z.J. Grout[93], C. Grud[104], A. Grummer[117], L. Guan[104], W. Guan[179], J. Guenther[35], A. Guerguichon[130], F. Guescini[166a], D. Guest[169], R. Gugel[51], B. Gui[124], T. Guillemin[5], S. Guindon[35], U. Gul[56], J. Guo[59c], W. Guo[104], Y. Guo[59a,s], Z. Guo[100], R. Gupta[45], S. Gurbuz[12c], G. Gustavino[126], P. Gutierrez[126], C. Gutschow[93], C. Guyot[143], M.P. Guzik[82a], C. Gwenlan[133], C.B. Gwilliam[89], A. Haas[123], C. Haber[18], H.K. Hadavand[8], N. Haddad[34e], A. Hadef[59a], S. Hageböck[35], M. Hagihara[167], M. Haleem[175], J. Haley[127], G. Halladjian[105], G.D. Hallewell[100], K. Hamacher[180], P. Hamal[128], K. Hamano[174], H. Hamdaoui[34e], G.N. Hamity[147], K. Han[59a,aj], L. Han[59a], S. Han[15d], K. Hanagaki[80,u], M. Hance[144], D.M. Handl[113], B. Haney[135], R. Hankache[134], P. Hanke[60a], E. Hansen[95], J.B. Hansen[39], J.D. Hansen[39], M.C. Hansen[24], P.H. Hansen[39], E.C. Hanson[99], K. Hara[167], A.S. Hard[179], T. Harenberg[180], S. Harkusha[106], P.F. Harrison[176], N.M. Hartmann[113], Y. Hasegawa[148], A. Hasib[49], S. Hassani[143], S. Haug[20], R. Hauser[105], L. Hauswald[47], L.B. Havener[38], M. Havranek[140], C.M. Hawkes[21], R.J. Hawkings[35], D. Hayden[105], C. Hayes[153], R.L. Hayes[173], C.P. Hays[133], J.M. Hays[91], H.S. Hayward[89], S.J. Haywood[142], F. He[59a], M.P. Heath[49], V. Hedberg[95], L. Heelan[8], S. Heer[24], K.K. Heidegger[51], J. Heilman[33], S. Heim[45], T. Heim[18], B. Heinemann[45,aq], J.J. Heinrich[113], L. Heinrich[123], C. Heinz[55], J. Hejbal[139], L. Helary[60b], A. Held[173], S. Hellesund[132], C.M. Helling[144], S. Hellman[44a,44b], C. Helsens[35], R.C.W. Henderson[88], Y. Heng[179], L. Henkelmann[60a], S. Henkelmann[173], A.M. Henriques Correia[35], G.H. Herbert[19], H. Herde[26], V. Herget[175], Y. Hernández Jiménez[32c], H. Herr[98], M.G. Herrmann[113], T. Herrmann[47], G. Herten[51], R. Hertenberger[113], L. Hervas[35], T.C. Herwig[135], G.G. Hesketh[93], N.P. Hessey[166a], A. Higashida[161], S. Higashino[80], E. Higón-Rodriguez[172], K. Hildebrand[36], E. Hill[174], J.C. Hill[31], K.K. Hill[29], K.H. Hiller[45], S.J. Hillier[21], M. Hils[47], I. Hinchliffe[18], F. Hinterkeuser[24], M. Hirose[131], D. Hirschbuehl[180], B. Hiti[90], O. Hladik[139], D.R. Hlaluku[32c], X. Hoad[49], J. Hobbs[153], N. Hod[178], M.C. Hodgkinson[147], A. Hoecker[35], F. Hoenig[113], D. Hohn[51], D. Hohov[130], T.R. Holmes[36], M. Holzbock[113], L.B.A.H Hommels[31], S. Honda[167], T. Honda[80], T.M. Hong[137], A. Hönle[114], B.H. Hooberman[171], W.H. Hopkins[6], Y. Horii[116], P. Horn[47], A.J. Horton[150], L.A. Horyn[36], J-Y. Hostachy[57], A. Hostiuc[146], S. Hou[156], A. Hoummada[34a], J. Howarth[99], J. Hoya[87], M. Hrabovsky[128], J. Hrdinka[35], I. Hristova[19], J. Hrivnac[130], A. Hrynevich[107], T. Hryn'ova[5], P.J. Hsu[63], S.-C. Hsu[146], Q. Hu[29], S. Hu[59c], Y. Huang[15a], Z. Hubacek[140], F. Hubaut[100], M. Huebner[24], F. Huegging[24], T.B. Huffman[133], M. Huhtinen[35], R.F.H. Hunter[33], P. Huo[153], A.M. Hupe[33], N. Huseynov[78,ae], J. Huston[105], J. Huth[58], R. Hyneman[104], G. Iacobucci[53], G. Iakovidis[29], I. Ibragimov[149],

L. Iconomidou-Fayard[130], Z. Idrissi[34e], P. Iengo[35], R. Ignazzi[39], O. Igonkina[119,z], R. Iguchi[161], T. Iizawa[53], Y. Ikegami[80], M. Ikeno[80], D. Iliadis[160], N. Ilic[118], F. Iltzsche[47], G. Introzzi[69a,69b], M. Iodice[73a], K. Iordanidou[38], V. Ippolito[71a,71b], M.F. Isacson[170], N. Ishijima[131], M. Ishino[161], M. Ishitsuka[163], W. Islam[127], C. Issever[133], S. Istin[158], F. Ito[167], J.M. Iturbe Ponce[62a], R. Iuppa[74a,74b], A. Ivina[178], H. Iwasaki[80], J.M. Izen[42], V. Izzo[68a], P. Jacka[139], P. Jackson[1], R.M. Jacobs[24], V. Jain[2], G. Jäkel[180], K.B. Jakobi[98], K. Jakobs[51], S. Jakobsen[75], T. Jakoubek[139], D.O. Jamin[127], R. Jansky[53], J. Janssen[24], M. Janus[52], P.A. Janus[82a], G. Jarlskog[95], N. Javadov[78,ae], T. Javůrek[35], M. Javurkova[51], F. Jeanneau[143], L. Jeanty[129], J. Jejelava[157a,af], A. Jelinskas[176], P. Jenni[51,d], J. Jeong[45], N. Jeong[45], S. Jézéquel[5], H. Ji[179], J. Jia[153], H. Jiang[77], Y. Jiang[59a], Z. Jiang[151,q], S. Jiggins[51], F.A. Jimenez Morales[37], J. Jimenez Pena[172], S. Jin[15c], A. Jinaru[27b], O. Jinnouchi[163], H. Jivan[32c], P. Johansson[147], K.A. Johns[7], C.A. Johnson[64], K. Jon-And[44a,44b], R.W.L. Jones[88], S.D. Jones[154], S. Jones[7], T.J. Jones[89], J. Jongmanns[60a], P.M. Jorge[138a,138b], J. Jovicevic[166a], X. Ju[18], J.J. Junggeburth[114], A. Juste Rozas[14,x], A. Kaczmarska[83], M. Kado[130], H. Kagan[124], M. Kagan[151], T. Kaji[177], E. Kajomovitz[158], C.W. Kalderon[95], A. Kaluza[98], A. Kamenshchikov[122], L. Kanjir[90], Y. Kano[161], V.A. Kantserov[111], J. Kanzaki[80], L.S. Kaplan[179], D. Kar[32c], M.J. Kareem[166b], E. Karentzos[10], S.N. Karpov[78], Z.M. Karpova[78], V. Kartvelishvili[88], A.N. Karyukhin[122], L. Kashif[179], R.D. Kass[124], A. Kastanas[44a,44b], Y. Kataoka[161], C. Kato[59d,59c], J. Katzy[45], K. Kawade[81], K. Kawagoe[86], T. Kawaguchi[116], T. Kawamoto[161], G. Kawamura[52], E.F. Kay[174], V.F. Kazanin[121b,121a], R. Keeler[174], R. Kehoe[41], J.S. Keller[33], E. Kellermann[95], J.J. Kempster[21], J. Kendrick[21], O. Kepka[139], S. Kersten[180], B.P. Kerševan[90], S. Ketabchi Haghighat[165], R.A. Keyes[102], M. Khader[171], F. Khalil-Zada[13], A. Khanov[127], A.G. Kharlamov[121b,121a], T. Kharlamova[121b,121a], E.E. Khoda[173], A. Khodinov[164], T.J. Khoo[53], E. Khramov[78], J. Khubua[157b], S. Kido[81], M. Kiehn[53], C.R. Kilby[92], Y.K. Kim[36], N. Kimura[65a,65c], O.M. Kind[19], B.T. King[89], D. Kirchmeier[47], J. Kirk[142], A.E. Kiryunin[114], T. Kishimoto[161], V. Kitali[45], O. Kivernyk[5], E. Kladiva[28b,*], T. Klapdor-Kleingrothaus[51], M.H. Klein[104], M. Klein[89], U. Klein[89], K. Kleinknecht[98], P. Klimek[120], A. Klimentov[29], T. Klingl[24], T. Klioutchnikova[35], F.F. Klitzner[113], P. Kluit[119], S. Kluth[114], E. Kneringer[75], E.B.F.G. Knoops[100], A. Knue[51], D. Kobayashi[86], T. Kobayashi[161], M. Kobel[47], M. Kocian[151], P. Kodys[141], P.T. Koenig[24], T. Koffas[33], N.M. Köhler[114], T. Koi[151], M. Kolb[60b], I. Koletsou[5], T. Kondo[80], N. Kondrashova[59c], K. Köneke[51], A.C. König[118], T. Kono[80], R. Konoplich[123,am], V. Konstantinides[93], N. Konstantinidis[93], B. Konya[95], R. Kopeliansky[64], S. Koperny[82a], K. Korcyl[83], K. Kordas[160], G. Koren[159], A. Korn[93], I. Korolkov[14], E.V. Korolkova[147], N. Korotkova[112], O. Kortner[114], S. Kortner[114], T. Kosek[141], V.V. Kostyukhin[24], A. Kotwal[48], A. Koulouris[10], A. Kourkoumeli-Charalampidi[69a,69b], C. Kourkoumelis[9], E. Kourlitis[147], V. Kouskoura[29], A.B. Kowalewska[83], R. Kowalewski[174], C. Kozakai[161], W. Kozanecki[143], A.S. Kozhin[122], V.A. Kramarenko[112], G. Kramberger[90], D. Krasnopevtsev[59a], M.W. Krasny[134], A. Krasznahorkay[35], D. Krauss[114], J.A. Kremer[82a], J. Kretzschmar[89], P. Krieger[165], K. Krizka[18], K. Kroeninger[46], H. Kroha[114], J. Kroll[139], J. Kroll[135], J. Krstic[16], U. Kruchonak[78], H. Krüger[24], N. Krumnack[77], M.C. Kruse[48], T. Kubota[103], S. Kuday[4b], J.T. Kuechler[45], S. Kuehn[35], A. Kugel[60a], T. Kuhl[45], V. Kukhtin[78], R. Kukla[100], Y. Kulchitsky[106,ai], S. Kuleshov[145b], Y.P. Kulinich[171], M. Kuna[57], T. Kunigo[84], A. Kupco[139], T. Kupfer[46], O. Kuprash[51], H. Kurashige[81], L.L. Kurchaninov[166a], Y.A. Kurochkin[106], A. Kurova[111], M.G. Kurth[15d], E.S. Kuwertz[35], M. Kuze[163], J. Kvita[128], T. Kwan[102], A. La Rosa[114], J.L. La Rosa Navarro[79d], L. La Rotonda[40b,40a], F. La Ruffa[40b,40a], C. Lacasta[172], F. Lacava[71a,71b], D.P.J. Lack[99], H. Lacker[19], D. Lacour[134], E. Ladygin[78], R. Lafaye[5], B. Laforge[134], T. Lagouri[32c], S. Lai[52], S. Lammers[64], W. Lampl[7], E. Lançon[29], U. Landgraf[51], M.P.J. Landon[91], M.C. Lanfermann[53], V.S. Lang[45], J.C. Lange[52], R.J. Langenberg[35], A.J. Lankford[169], F. Lanni[29], K. Lantzsch[24], A. Lanza[69a], A. Lapertosa[54b,54a], S. Laplace[134], J.F. Laporte[143], T. Lari[67a], F. Lasagni Manghi[23b,23a], M. Lassnig[35], T.S. Lau[62a], A. Laudrain[130], A. Laurier[33], M. Lavorgna[68a,68b], M. Lazzaroni[67a,67b], B. Le[103], O. Le Dortz[134], E. Le Guirriec[100], M. LeBlanc[7], T. LeCompte[6], F. Ledroit-Guillon[57], C.A. Lee[29], G.R. Lee[145a], L. Lee[58], S.C. Lee[156], S.J. Lee[33], B. Lefebvre[102], M. Lefebvre[174], F. Legger[113], C. Leggett[18], K. Lehmann[150],

N. Lehmann[180], G. Lehmann Miotto[35], W.A. Leight[45], A. Leisos[160,v], M.A.L. Leite[79d], R. Leitner[141], D. Lellouch[178], K.J.C. Leney[41], T. Lenz[24], B. Lenzi[35], R. Leone[7], S. Leone[70a], C. Leonidopoulos[49], A. Leopold[134], G. Lerner[154], C. Leroy[108], R. Les[165], C.G. Lester[31], M. Levchenko[136], J. Levêque[5], D. Levin[104], L.J. Levinson[178], B. Li[15b], B. Li[104], C-Q. Li[59a,al], H. Li[59a], H. Li[59b], K. Li[151], L. Li[59c], M. Li[15a], Q. Li[15d], Q.Y. Li[59a], S. Li[59d,59c], X. Li[59c], Y. Li[45], Z. Liang[15a], B. Liberti[72a], A. Liblong[165], K. Lie[62c], S. Liem[119], C.Y. Lin[31], K. Lin[105], T.H. Lin[98], R.A. Linck[64], J.H. Lindon[21], A.L. Lionti[53], E. Lipeles[135], A. Lipniacka[17], M. Lisovyi[60b], T.M. Liss[171,as], A. Lister[173], A.M. Litke[144], J.D. Little[8], B. Liu[77], B.L Liu[6], H.B. Liu[29], H. Liu[104], J.B. Liu[59a], J.K.K. Liu[133], K. Liu[134], M. Liu[59a], P. Liu[18], Y. Liu[15d], Y.L. Liu[59a], Y.W. Liu[59a], M. Livan[69a,69b], A. Lleres[57], J. Llorente Merino[15a], S.L. Lloyd[91], C.Y. Lo[62b], F. Lo Sterzo[41], E.M. Lobodzinska[45], P. Loch[7], T. Lohse[19], K. Lohwasser[147], M. Lokajicek[139], J.D. Long[171], R.E. Long[88], L. Longo[35], K.A. Looper[124], J.A. Lopez[145b], I. Lopez Paz[99], A. Lopez Solis[147], J. Lorenz[113], N. Lorenzo Martinez[5], M. Losada[22], P.J. Lösel[113], A. Lösle[51], X. Lou[45], X. Lou[15a], A. Lounis[130], J. Love[6], P.A. Love[88], J.J. Lozano Bahilo[172], H. Lu[62a], M. Lu[59a], Y.J. Lu[63], H.J. Lubatti[146], C. Luci[71a,71b], A. Lucotte[57], C. Luedtke[51], F. Luehring[64], I. Luise[134], L. Luminari[71a], B. Lund-Jensen[152], M.S. Lutz[101], D. Lynn[29], R. Lysak[139], E. Lytken[95], F. Lyu[15a], V. Lyubushkin[78], T. Lyubushkina[78], H. Ma[29], L.L. Ma[59b], Y. Ma[59b], G. Maccarrone[50], A. Macchiolo[114], C.M. Macdonald[147], J. Machado Miguens[135,138b], D. Madaffari[172], R. Madar[37], W.F. Mader[47], N. Madysa[47], J. Maeda[81], K. Maekawa[161], S. Maeland[17], T. Maeno[29], M. Maerker[47], A.S. Maevskiy[112], V. Magerl[51], N. Magini[77], D.J. Mahon[38], C. Maidantchik[79b], T. Maier[113], A. Maio[138a,138b,138d], O. Majersky[28a], S. Majewski[129], Y. Makida[80], N. Makovec[130], B. Malaescu[134], Pa. Malecki[83], V.P. Maleev[136], F. Malek[57], U. Mallik[76], D. Malon[6], C. Malone[31], S. Maltezos[10], S. Malyukov[35], J. Mamuzic[172], G. Mancini[50], I. Mandić[90], L. Manhaes de Andrade Filho[79a], I.M. Maniatis[160], J. Manjarres Ramos[47], K.H. Mankinen[95], A. Mann[113], A. Manousos[75], B. Mansoulie[143], I. Manthos[160], S. Manzoni[119], A. Marantis[160], G. Marceca[30], L. Marchese[133], G. Marchiori[134], M. Marcisovsky[139], C. Marcon[95], C.A. Marin Tobon[35], M. Marjanovic[37], F. Marroquim[79b], Z. Marshall[18], M.U.F Martensson[170], S. Marti-Garcia[172], C.B. Martin[124], T.A. Martin[176], V.J. Martin[49], B. Martin dit Latour[17], M. Martinez[14,x], V.I. Martinez Outschoorn[101], S. Martin-Haugh[142], V.S. Martoiu[27b], A.C. Martyniuk[93], A. Marzin[35], L. Masetti[98], T. Mashimo[161], R. Mashinistov[109], J. Masik[99], A.L. Maslennikov[121b,121a], L.H. Mason[103], L. Massa[72a,72b], P. Massarotti[68a,68b], P. Mastrandrea[70a,70b], A. Mastroberardino[40b,40a], T. Masubuchi[161], A. Matic[113], P. Mättig[24], J. Maurer[27b], B. Maček[90], S.J. Maxfield[89], D.A. Maximov[121b,121a], R. Mazini[156], I. Maznas[160], S.M. Mazza[144], S.P. Mc Kee[104], A. McCarn, Deiana[41], T.G. McCarthy[114], L.I. McClymont[93], W.P. McCormack[18], E.F. McDonald[103], J.A. Mcfayden[35], G. Mchedlidze[52], M.A. McKay[41], K.D. McLean[174], S.J. McMahon[142], P.C. McNamara[103], C.J. McNicol[176], R.A. McPherson[174,ac], J.E. Mdhluli[32c], Z.A. Meadows[101], S. Meehan[146], T.M. Megy[51], S. Mehlhase[113], A. Mehta[89], T. Meideck[57], B. Meirose[42], D. Melini[172], B.R. Mellado Garcia[32c], J.D. Mellenthin[52], M. Melo[28a], F. Meloni[45], A. Melzer[24], S.B. Menary[99], E.D. Mendes Gouveia[138a,138e], L. Meng[35], X.T. Meng[104], S. Menke[114], E. Meoni[40b,40a], S. Mergelmeyer[19], S.A.M. Merkt[137], C. Merlassino[20], P. Mermod[53], L. Merola[68a,68b], C. Meroni[67a], J.K.R. Meshreki[149], A. Messina[71a,71b], J. Metcalfe[6], A.S. Mete[169], C. Meyer[64], J. Meyer[158], J-P. Meyer[143], H. Meyer Zu Theenhausen[60a], F. Miano[154], R.P. Middleton[142], L. Mijović[49], G. Mikenberg[178], M. Mikestikova[139], M. Mikuž[90], M. Milesi[103], A. Milic[165], D.A. Millar[91], D.W. Miller[36], A. Milov[178], D.A. Milstead[44a,44b], R.A. Mina[151,q], A.A. Minaenko[122], M. Miñano Moya[172], I.A. Minashvili[157b], A.I. Mincer[123], B. Mindur[82a], M. Mineev[78], Y. Minegishi[161], Y. Ming[179], L.M. Mir[14], A. Mirto[66a,66b], K.P. Mistry[135], T. Mitani[177], J. Mitrevski[113], V.A. Mitsou[172], M. Mittal[59c], A. Miucci[20], P.S. Miyagawa[147], A. Mizukami[80], J.U. Mjörnmark[95], T. Mkrtchyan[182], M. Mlynarikova[141], T. Moa[44a,44b], K. Mochizuki[108], P. Mogg[51], S. Mohapatra[38], R. Moles-Valls[24], M.C. Mondragon[105], K. Mönig[45], J. Monk[39], E. Monnier[100], A. Montalbano[150], J. Montejo Berlingen[35], M. Montella[93], F. Monticelli[87], S. Monzani[67a], N. Morange[130], D. Moreno[22], M. Moreno Llácer[35], P. Morettini[54b], M. Morgenstern[119],

S. Morgenstern[47], D. Mori[150], M. Morii[58], M. Morinaga[177], V. Morisbak[132], A.K. Morley[35], G. Mornacchi[35], A.P. Morris[93], L. Morvaj[153], P. Moschovakos[10], M. Mosidze[157b], H.J. Moss[147], J. Moss[151,n], K. Motohashi[163], E. Mountricha[35], E.J.W. Moyse[101], S. Muanza[100], F. Mueller[114], J. Mueller[137], R.S.P. Mueller[113], D. Muenstermann[88], G.A. Mullier[95], F.J. Munoz Sanchez[99], P. Murin[28b], W.J. Murray[176,142], A. Murrone[67a,67b], M. Muškinja[90], C. Mwewa[32a], A.G. Myagkov[122,an], J. Myers[129], M. Myska[140], B.P. Nachman[18], O. Nackenhorst[46], K. Nagai[133], K. Nagano[80], Y. Nagasaka[61], M. Nagel[51], E. Nagy[100], A.M. Nairz[35], Y. Nakahama[116], K. Nakamura[80], T. Nakamura[161], I. Nakano[125], H. Nanjo[131], F. Napolitano[60a], R.F. Naranjo Garcia[45], R. Narayan[11], D.I. Narrias Villar[60a], I. Naryshkin[136], T. Naumann[45], G. Navarro[22], H.A. Neal[104,*], P.Y. Nechaeva[109], F. Nechansky[45], T.J. Neep[143], A. Negri[69a,69b], M. Negrini[23b], S. Nektarijevic[118], C. Nellist[52], M.E. Nelson[133], S. Nemecek[139], P. Nemethy[123], M. Nessi[35,f], M.S. Neubauer[171], M. Neumann[180], P.R. Newman[21], T.Y. Ng[62c], Y.S. Ng[19], Y.W.Y. Ng[169], H.D.N. Nguyen[100], T. Nguyen Manh[108], E. Nibigira[37], R.B. Nickerson[133], R. Nicolaidou[143], D.S. Nielsen[39], J. Nielsen[144], N. Nikiforou[11], V. Nikolaenko[122,an], I. Nikolic-Audit[134], K. Nikolopoulos[21], P. Nilsson[29], H.R. Nindhito[53], Y. Ninomiya[80], A. Nisati[71a], N. Nishu[59c], R. Nisius[114], I. Nitsche[46], T. Nitta[177], T. Nobe[161], Y. Noguchi[84], M. Nomachi[131], I. Nomidis[134], M.A. Nomura[29], M. Nordberg[35], N. Norjoharuddeen[133], T. Novak[90], O. Novgorodova[47], R. Novotny[140], L. Nozka[128], K. Ntekas[169], E. Nurse[93], F. Nuti[103], F.G. Oakham[33,av], H. Oberlack[114], J. Ocariz[134], A. Ochi[81], I. Ochoa[38], J.P. Ochoa-Ricoux[145a], K. O'Connor[26], S. Oda[86], S. Odaka[80], S. Oerdek[52], A. Ogrodnik[82a], A. Oh[99], S.H. Oh[48], C.C. Ohm[152], H. Oide[54b,54a], M.L. Ojeda[165], H. Okawa[167], Y. Okazaki[84], Y. Okumura[161], T. Okuyama[80], A. Olariu[27b], L.F. Oleiro Seabra[138a], S.A. Olivares Pino[145a], D. Oliveira Damazio[29], J.L. Oliver[1], M.J.R. Olsson[169], A. Olszewski[83], J. Olszowska[83], D.C. O'Neil[150], A. Onofre[138a,138e], K. Onogi[116], P.U.E. Onyisi[11], H. Oppen[132], M.J. Oreglia[36], G.E. Orellana[87], Y. Oren[159], D. Orestano[73a,73b], N. Orlando[14], R.S. Orr[165], B. Osculati[54b,54a,*], V. O'Shea[56], R. Ospanov[59a], G. Otero y Garzon[30], H. Otono[86], M. Ouchrif[34d], F. Ould-Saada[132], A. Ouraou[143], Q. Ouyang[15a], M. Owen[56], R.E. Owen[21], V.E. Ozcan[12c], N. Ozturk[8], J. Pacalt[128], H.A. Pacey[31], K. Pachal[48], A. Pacheco Pages[14], C. Padilla Aranda[14], S. Pagan Griso[18], M. Paganini[181], G. Palacino[64], S. Palazzo[49], S. Palestini[35], M. Palka[82b], D. Pallin[37], I. Panagoulias[10], C.E. Pandini[35], J.G. Panduro Vazquez[92], P. Pani[45], G. Panizzo[65a,65c], L. Paolozzi[53], K. Papageorgiou[9,j], A. Paramonov[6], D. Paredes Hernandez[62b], S.R. Paredes Saenz[133], B. Parida[164], T.H. Park[165], A.J. Parker[88], M.A. Parker[31], F. Parodi[54b,54a], E.W.P. Parrish[120], J.A. Parsons[38], U. Parzefall[51], L. Pascual Dominguez[134], V.R. Pascuzzi[165], J.M.P. Pasner[144], E. Pasqualucci[71a], S. Passaggio[54b], F. Pastore[92], P. Pasuwan[44a,44b], S. Pataraia[98], J.R. Pater[99], A. Pathak[179,k], T. Pauly[35], B. Pearson[114], M. Pedersen[132], L. Pedraza Diaz[118], R. Pedro[138a,138b], S.V. Peleganchuk[121b,121a], O. Penc[139], C. Peng[15a], H. Peng[59a], B.S. Peralva[79a], M.M. Perego[130], A.P. Pereira Peixoto[138a,138e], D.V. Perepelitsa[29], F. Peri[19], L. Perini[67a,67b], H. Pernegger[35], S. Perrella[68a,68b], V.D. Peshekhonov[78,*], K. Peters[45], R.F.Y. Peters[99], B.A. Petersen[35], T.C. Petersen[39], E. Petit[57], A. Petridis[1], C. Petridou[160], P. Petroff[130], M. Petrov[133], F. Petrucci[73a,73b], M. Pettee[181], N.E. Pettersson[101], K. Petukhova[141], A. Peyaud[143], R. Pezoa[145b], T. Pham[103], F.H. Phillips[105], P.W. Phillips[142], M.W. Phipps[171], G. Piacquadio[153], E. Pianori[18], A. Picazio[101], R.H. Pickles[99], R. Piegaia[30], J.E. Pilcher[36], A.D. Pilkington[99], M. Pinamonti[72a,72b], J.L. Pinfold[3], M. Pitt[178], L. Pizzimento[72a,72b], M.-A. Pleier[29], V. Pleskot[141], E. Plotnikova[78], D. Pluth[77], P. Podberezko[121b,121a], R. Poettgen[95], R. Poggi[53], L. Poggioli[130], I. Pogrebnyak[105], D. Pohl[24], I. Pokharel[52], G. Polesello[69a], A. Poley[18], A. Policicchio[71a,71b], R. Polifka[35], A. Polini[23b], C.S. Pollard[45], V. Polychronakos[29], D. Ponomarenko[111], L. Pontecorvo[35], G.A. Popeneciu[27d], D.M. Portillo Quintero[134], S. Pospisil[140], K. Potamianos[45], I.N. Potrap[78], C.J. Potter[31], H. Potti[11], T. Poulsen[95], J. Poveda[35], T.D. Powell[147], M.E. Pozo Astigarraga[35], P. Pralavorio[100], S. Prell[77], D. Price[99], M. Primavera[66a], S. Prince[102], M.L. Proffitt[146], N. Proklova[111], K. Prokofiev[62c], F. Prokoshin[145b], S. Protopopescu[29], J. Proudfoot[6], M. Przybycien[82a], A. Puri[171], P. Puzo[130], J. Qian[104], Y. Qin[99], A. Quadt[52], M. Queitsch-Maitland[45],

A. Qureshi[1], P. Rados[103], F. Ragusa[67a,67b], G. Rahal[96], J.A. Raine[53], S. Rajagopalan[29], A. Ramirez Morales[91], K. Ran[15d], T. Rashid[130], S. Raspopov[5], M.G. Ratti[67a,67b], D.M. Rauch[45], F. Rauscher[113], S. Rave[98], B. Ravina[147], I. Ravinovich[178], J.H. Rawling[99], M. Raymond[35], A.L. Read[132], N.P. Readioff[57], M. Reale[66a,66b], D.M. Rebuzzi[69a,69b], A. Redelbach[175], G. Redlinger[29], R.G. Reed[32c], K. Reeves[42], L. Rehnisch[19], J. Reichert[135], D. Reikher[159], A. Reiss[98], A. Rej[149], C. Rembser[35], H. Ren[15a], M. Rescigno[71a], S. Resconi[67a], E.D. Resseguie[135], S. Rettie[173], E. Reynolds[21], O.L. Rezanova[121b,121a], P. Reznicek[141], E. Ricci[74a,74b], R. Richter[114], S. Richter[45], E. Richter-Was[82b], O. Ricken[24], M. Ridel[134], P. Rieck[114], C.J. Riegel[180], O. Rifki[45], M. Rijssenbeek[153], A. Rimoldi[69a,69b], M. Rimoldi[20], L. Rinaldi[23b], G. Ripellino[152], B. Ristić[88], E. Ritsch[35], I. Riu[14], J.C. Rivera Vergara[145a], F. Rizatdinova[127], E. Rizvi[91], C. Rizzi[14], R.T. Roberts[99], S.H. Robertson[102,ac], D. Robinson[31], J.E.M. Robinson[45], A. Robson[56], E. Rocco[98], C. Roda[70a,70b], Y. Rodina[100], S. Rodriguez Bosca[172], A. Rodriguez Perez[14], D. Rodriguez Rodriguez[172], A.M. Rodríguez Vera[166b], S. Roe[35], O. Røhne[132], R. Röhrig[114], C.P.A. Roland[64], J. Roloff[58], A. Romaniouk[111], M. Romano[23b,23a], N. Rompotis[89], M. Ronzani[123], L. Roos[134], S. Rosati[71a], K. Rosbach[51], N-A. Rosien[52], B.J. Rosser[135], E. Rossi[45], E. Rossi[73a,73b], E. Rossi[68a,68b], L.P. Rossi[54b], L. Rossini[67a,67b], J.H.N. Rosten[31], R. Rosten[14], M. Rotaru[27b], J. Rothberg[146], D. Rousseau[130], D. Roy[32c], A. Rozanov[100], Y. Rozen[158], X. Ruan[32c], F. Rubbo[151], F. Rühr[51], A. Ruiz-Martinez[172], Z. Rurikova[51], N.A. Rusakovich[78], H.L. Russell[102], L. Rustige[37,46], J.P. Rutherfoord[7], E.M. Rüttinger[45,l], Y.F. Ryabov[136], M. Rybar[38], G. Rybkin[130], S. Ryu[6], A. Ryzhov[122], G.F. Rzehorz[52], P. Sabatini[52], G. Sabato[119], S. Sacerdoti[130], H.F-W. Sadrozinski[144], R. Sadykov[78], F. Safai Tehrani[71a], P. Saha[120], M. Sahinsoy[60a], A. Sahu[180], M. Saimpert[45], M. Saito[161], T. Saito[161], H. Sakamoto[161], A. Sakharov[123,am], D. Salamani[53], G. Salamanna[73a,73b], J.E. Salazar Loyola[145b], P.H. Sales De Bruin[170], D. Salihagic[114,*], A. Salnikov[151], J. Salt[172], D. Salvatore[40b,40a], F. Salvatore[154], A. Salvucci[62a,62b,62c], A. Salzburger[35], J. Samarati[35], D. Sammel[51], D. Sampsonidis[160], D. Sampsonidou[160], J. Sánchez[172], A. Sanchez Pineda[65a,65c], H. Sandaker[132], C.O. Sander[45], M. Sandhoff[180], C. Sandoval[22], D.P.C. Sankey[142], M. Sannino[54b,54a], Y. Sano[116], A. Sansoni[50], C. Santoni[37], H. Santos[138a,138b], S.N. Santpur[18], A. Santra[172], A. Sapronov[78], J.G. Saraiva[138a,138d], O. Sasaki[80], K. Sato[167], E. Sauvan[5], P. Savard[165,av], N. Savic[114], R. Sawada[161], C. Sawyer[142], L. Sawyer[94,ak], C. Sbarra[23b], A. Sbrizzi[23a], T. Scanlon[93], J. Schaarschmidt[146], P. Schacht[114], B.M. Schachtner[113], D. Schaefer[36], L. Schaefer[135], J. Schaeffer[98], S. Schaepe[35], U. Schäfer[98], A.C. Schaffer[130], D. Schaile[113], R.D. Schamberger[153], N. Scharmberg[99], V.A. Schegelsky[136], D. Scheirich[141], F. Schenck[19], M. Schernau[169], C. Schiavi[54b,54a], S. Schier[144], L.K. Schildgen[24], Z.M. Schillaci[26], E.J. Schioppa[35], M. Schioppa[40b,40a], K.E. Schleicher[51], S. Schlenker[35], K.R. Schmidt-Sommerfeld[114], K. Schmieden[35], C. Schmitt[98], S. Schmitt[45], S. Schmitz[98], J.C. Schmoeckel[45], U. Schnoor[51], L. Schoeffel[143], A. Schoening[60b], E. Schopf[133], M. Schott[98], J.F.P. Schouwenberg[118], J. Schovancova[35], S. Schramm[53], A. Schulte[98], H-C. Schultz-Coulon[60a], M. Schumacher[51], B.A. Schumm[144], Ph. Schune[143], A. Schwartzman[151], T.A. Schwarz[104], Ph. Schwemling[143], R. Schwienhorst[105], A. Sciandra[24], G. Sciolla[26], M. Scornajenghi[40b,40a], F. Scuri[70a], F. Scutti[103], L.M. Scyboz[114], C.D. Sebastiani[71a,71b], P. Seema[19], S.C. Seidel[117], A. Seiden[144], T. Seiss[36], J.M. Seixas[79b], G. Sekhniaidze[68a], K. Sekhon[104], S.J. Sekula[41], N. Semprini-Cesari[23b,23a], S. Sen[48], S. Senkin[37], C. Serfon[75], L. Serin[130], L. Serkin[65a,65b], M. Sessa[59a], H. Severini[126], F. Sforza[168], A. Sfyrla[53], E. Shabalina[52], J.D. Shahinian[144], N.W. Shaikh[44a,44b], D. Shaked Renous[178], L.Y. Shan[15a], R. Shang[171], J.T. Shank[25], M. Shapiro[18], A.S. Sharma[1], A. Sharma[133], P.B. Shatalov[110], K. Shaw[154], S.M. Shaw[99], A. Shcherbakova[136], Y. Shen[126], N. Sherafati[33], A.D. Sherman[25], P. Sherwood[93], L. Shi[156,ar], S. Shimizu[80], C.O. Shimmin[181], Y. Shimogama[177], M. Shimojima[115], I.P.J. Shipsey[133], S. Shirabe[86], M. Shiyakova[78,aa], J. Shlomi[178], A. Shmeleva[109], M.J. Shochet[36], S. Shojaii[103], D.R. Shope[126], S. Shrestha[124], E. Shulga[111], P. Sicho[139], A.M. Sickles[171], P.E. Sidebo[152], E. Sideras Haddad[32c], O. Sidiropoulou[35], A. Sidoti[23b,23a], F. Siegert[47], Dj. Sijacki[16], J. Silva[138a], M. Silva Jr.[179], M.V. Silva Oliveira[79a], S.B. Silverstein[44a], S. Simion[130], E. Simioni[98], M. Simon[98], R. Simoniello[98], P. Sinervo[165], N.B. Sinev[129], M. Sioli[23b,23a],

I. Siral[104], S.Yu. Sivoklokov[112], J. Sjölin[44a,44b], E. Skorda[95], P. Skubic[126], M. Slawinska[83], K. Sliwa[168], R. Slovak[141], V. Smakhtin[178], B.H. Smart[5], J. Smiesko[28a], N. Smirnov[111], S.Yu. Smirnov[111], Y. Smirnov[111], L.N. Smirnova[112], O. Smirnova[95], J.W. Smith[52], M. Smizanska[88], K. Smolek[140], A. Smykiewicz[83], A.A. Snesarev[109], I.M. Snyder[129], S. Snyder[29], R. Sobie[174,ac], A.M. Soffa[169], A. Soffer[159], A. Søgaard[49], F. Sohns[52], G. Sokhrannyi[90], C.A. Solans Sanchez[35], E.Yu. Soldatov[111], U. Soldevila[172], A.A. Solodkov[122], A. Soloshenko[78], O.V. Solovyanov[122], V. Solovyev[136], P. Sommer[147], H. Son[168], W. Song[142], W.Y. Song[166b], A. Sopczak[140], F. Sopkova[28b], C.L. Sotiropoulou[70a,70b], S. Sottocornola[69a,69b], R. Soualah[65a,65c,i], A.M. Soukharev[121b,121a], D. South[45], S. Spagnolo[66a,66b], M. Spalla[114], M. Spangenberg[176], F. Spanò[92], D. Sperlich[19], T.M. Spieker[60a], R. Spighi[23b], G. Spigo[35], L.A. Spiller[103], D.P. Spiteri[56], M. Spousta[141], A. Stabile[67a,67b], B.L. Stamas[120], R. Stamen[60a], M. Stamenkovic[119], S. Stamm[19], E. Stanecka[83], R.W. Stanek[6], B. Stanislaus[133], M.M. Stanitzki[45], B. Stapf[119], E.A. Starchenko[122], G.H. Stark[144], J. Stark[57], S.H Stark[39], P. Staroba[139], P. Starovoitov[60a], S. Stärz[102], R. Staszewski[83], G. Stavropoulos[43], M. Stegler[45], P. Steinberg[29], B. Stelzer[150], H.J. Stelzer[35], O. Stelzer-Chilton[166a], H. Stenzel[55], T.J. Stevenson[154], G.A. Stewart[35], M.C. Stockton[35], G. Stoicea[27b], M. Stolarski[138a], P. Stolte[52], S. Stonjek[114], A. Straessner[47], J. Strandberg[152], S. Strandberg[44a,44b], M. Strauss[126], P. Strizenec[28b], R. Ströhmer[175], D.M. Strom[129], R. Stroynowski[41], A. Strubig[49], S.A. Stucci[29], B. Stugu[17], J. Stupak[126], N.A. Styles[45], D. Su[151], S. Suchek[60a], Y. Sugaya[131], V.V. Sulin[109], M.J. Sullivan[89], D.M.S. Sultan[53], S. Sultansoy[4c], T. Sumida[84], S. Sun[104], X. Sun[3], K. Suruliz[154], C.J.E. Suster[155], M.R. Sutton[154], S. Suzuki[80], M. Svatos[139], M. Swiatlowski[36], S.P. Swift[2], A. Sydorenko[98], I. Sykora[28a], M. Sykora[141], T. Sykora[141], D. Ta[98], K. Tackmann[45,y], J. Taenzer[159], A. Taffard[169], R. Tafirout[166a], E. Tahirovic[91], H. Takai[29], R. Takashima[85], K. Takeda[81], T. Takeshita[148], Y. Takubo[80], M. Talby[100], A.A. Talyshev[121b,121a], J. Tanaka[161], M. Tanaka[163], R. Tanaka[130], B.B. Tannenwald[124], S. Tapia Araya[171], S. Tapprogge[98], A. Tarek Abouelfadl Mohamed[134], S. Tarem[158], G. Tarna[27b,e], G.F. Tartarelli[67a], P. Tas[141], M. Tasevsky[139], T. Tashiro[84], E. Tassi[40b,40a], A. Tavares Delgado[138a,138b], Y. Tayalati[34e], A.J. Taylor[49], G.N. Taylor[103], P.T.E. Taylor[103], W. Taylor[166b], A.S. Tee[88], R. Teixeira De Lima[151], P. Teixeira-Dias[92], H. Ten Kate[35], J.J. Teoh[119], S. Terada[80], K. Terashi[161], J. Terron[97], S. Terzo[14], M. Testa[50], R.J. Teuscher[165,ac], S.J. Thais[181], T. Theveneaux-Pelzer[45], F. Thiele[39], D.W. Thomas[92], J.P. Thomas[21], A.S. Thompson[56], P.D. Thompson[21], L.A. Thomsen[181], E. Thomson[135], Y. Tian[38], R.E. Ticse Torres[52], V.O. Tikhomirov[109,ao], Yu.A. Tikhonov[121b,121a], S. Timoshenko[111], P. Tipton[181], S. Tisserant[100], K. Todome[163], S. Todorova-Nova[5], S. Todt[47], J. Tojo[86], S. Tokár[28a], K. Tokushuku[80], E. Tolley[124], K.G. Tomiwa[32c], M. Tomoto[116], L. Tompkins[151,q], K. Toms[117], B. Tong[58], P. Tornambe[51], E. Torrence[129], H. Torres[47], E. Torró Pastor[146], C. Tosciri[133], J. Toth[100,ab], D.R. Tovey[147], C.J. Treado[123], T. Trefzger[175], F. Tresoldi[154], A. Tricoli[29], I.M. Trigger[166a], S. Trincaz-Duvoid[134], W. Trischuk[165], B. Trocmé[57], A. Trofymov[130], C. Troncon[67a], M. Trovatelli[174], F. Trovato[154], L. Truong[32b], M. Trzebinski[83], A. Trzupek[83], F. Tsai[45], J.C-L. Tseng[133], P.V. Tsiareshka[106,ai], A. Tsirigotis[160], N. Tsirintanis[9], V. Tsiskaridze[153], E.G. Tskhadadze[157a], M. Tsopoulou[160], I.I. Tsukerman[110], V. Tsulaia[18], S. Tsuno[80], D. Tsybychev[153,164], Y. Tu[62b], A. Tudorache[27b], V. Tudorache[27b], T.T. Tulbure[27a], A.N. Tuna[58], S. Turchikhin[78], D. Turgeman[178], I. Turk Cakir[4b,t], R.J. Turner[21], R.T. Turra[67a], P.M. Tuts[38], S Tzamarias[160], E. Tzovara[98], G. Ucchielli[46], I. Ueda[80], M. Ughetto[44a,44b], F. Ukegawa[167], G. Unal[35], A. Undrus[29], G. Unel[169], F.C. Ungaro[103], Y. Unno[80], K. Uno[161], J. Urban[28b], P. Urquijo[103], G. Usai[8], J. Usui[80], L. Vacavant[100], V. Vacek[140], B. Vachon[102], K.O.H. Vadla[132], A. Vaidya[93], C. Valderanis[113], E. Valdes Santurio[44a,44b], M. Valente[53], S. Valentinetti[23b,23a], A. Valero[172], L. Valéry[45], R.A. Vallance[21], A. Vallier[5], J.A. Valls Ferrer[172], T.R. Van Daalen[14], P. Van Gemmeren[6], I. Van Vulpen[119], M. Vanadia[72a,72b], W. Vandelli[35], A. Vaniachine[164], R. Vari[71a], E.W. Varnes[7], C. Varni[54b,54a], T. Varol[41], D. Varouchas[130], K.E. Varvell[155], G.A. Vasquez[145b], J.G. Vasquez[181], F. Vazeille[37], D. Vazquez Furelos[14], T. Vazquez Schroeder[35], J. Veatch[52], V. Vecchio[73a,73b], L.M. Veloce[165], F. Veloso[138a,138c], S. Veneziano[71a], A. Ventura[66a,66b],

N. Venturi[35], A. Verbytskyi[114], V. Vercesi[69a], M. Verducci[73a,73b], C.M. Vergel Infante[77], C. Vergis[24], W. Verkerke[119], A.T. Vermeulen[119], J.C. Vermeulen[119], M.C. Vetterli[150,av], N. Viaux Maira[145b], M. Vicente Barreto Pinto[53], I. Vichou[171,*], T. Vickey[147], O.E. Vickey Boeriu[147], G.H.A. Viehhauser[133], L. Vigani[133], M. Villa[23b,23a], M. Villaplana Perez[67a,67b], E. Vilucchi[50], M.G. Vincter[33], V.B. Vinogradov[78], A. Vishwakarma[45], C. Vittori[23b,23a], I. Vivarelli[154], M. Vogel[180], P. Vokac[140], G. Volpi[14], S.E. von Buddenbrock[32c], E. Von Toerne[24], V. Vorobel[141], K. Vorobev[111], M. Vos[172], J.H. Vossebeld[89], N. Vranjes[16], M. Vranjes Milosavljevic[16], V. Vrba[140], M. Vreeswijk[119], T. Šfiligoj[90], R. Vuillermet[35], I. Vukotic[36], T. Ženiš[28a], L. Živković[16], P. Wagner[24], W. Wagner[180], J. Wagner-Kuhr[113], H. Wahlberg[87], S. Wahrmund[47], K. Wakamiya[81], V.M. Walbrecht[114], J. Walder[88], R. Walker[113], S.D. Walker[92], W. Walkowiak[149], V. Wallangen[44a,44b], A.M. Wang[58], C. Wang[59b], F. Wang[179], H. Wang[18], H. Wang[3], J. Wang[155], J. Wang[60b], P. Wang[41], Q. Wang[126], R.-J. Wang[134], R. Wang[59a], R. Wang[6], S.M. Wang[156], W.T. Wang[59a], W. Wang[15c,ad], W.X. Wang[59a,ad], Y. Wang[59a,al], Z. Wang[59c], C. Wanotayaroj[45], A. Warburton[102], C.P. Ward[31], D.R. Wardrope[93], A. Washbrook[49], A.T. Watson[21], M.F. Watson[21], G. Watts[146], B.M. Waugh[93], A.F. Webb[11], S. Webb[98], C. Weber[181], M.S. Weber[20], S.A. Weber[33], S.M. Weber[60a], A.R. Weidberg[133], J. Weingarten[46], M. Weirich[98], C. Weiser[51], P.S. Wells[35], T. Wenaus[29], T. Wengler[35], S. Wenig[35], N. Wermes[24], M.D. Werner[77], P. Werner[35], M. Wessels[60a], T.D. Weston[20], K. Whalen[129], N.L. Whallon[146], A.M. Wharton[88], A.S. White[104], A. White[8], M.J. White[1], R. White[145b], D. Whiteson[169], B.W. Whitmore[88], F.J. Wickens[142], W. Wiedenmann[179], M. Wielers[142], C. Wiglesworth[39], L.A.M. Wiik-Fuchs[51], F. Wilk[99], H.G. Wilkens[35], L.J. Wilkins[92], H.H. Williams[135], S. Williams[31], C. Willis[105], S. Willocq[101], J.A. Wilson[21], I. Wingerter-Seez[5], E. Winkels[154], F. Winklmeier[129], O.J. Winston[154], B.T. Winter[51], M. Wittgen[151], M. Wobisch[94], A. Wolf[98], T.M.H. Wolf[119], R. Wolff[100], J. Wollrath[51], M.W. Wolter[83], H. Wolters[138a,138c], V.W.S. Wong[173], N.L. Woods[144], S.D. Worm[21], B.K. Wosiek[83], K.W. Woźniak[83], K. Wraight[56], S.L. Wu[179], X. Wu[53], Y. Wu[59a], T.R. Wyatt[99], B.M. Wynne[49], S. Xella[39], Z. Xi[104], L. Xia[176], D. Xu[15a], H. Xu[59a,e], L. Xu[29], T. Xu[143], W. Xu[104], Z. Xu[151], B. Yabsley[155], S. Yacoob[32a], K. Yajima[131], D.P. Yallup[93], D. Yamaguchi[163], Y. Yamaguchi[163], A. Yamamoto[80], T. Yamanaka[161], F. Yamane[81], M. Yamatani[161], T. Yamazaki[161], Y. Yamazaki[81], Z. Yan[25], H.J. Yang[59c,59d], H.T. Yang[18], S. Yang[76], Y. Yang[161], Z. Yang[17], W-M. Yao[18], Y.C. Yap[45], Y. Yasu[80], E. Yatsenko[59c,59d], J. Ye[41], S. Ye[29], I. Yeletskikh[78], E. Yigitbasi[25], E. Yildirim[98], K. Yorita[177], K. Yoshihara[135], C.J.S. Young[35], C. Young[151], J. Yu[77], X. Yue[60a], S.P.Y. Yuen[24], B. Zabinski[83], G. Zacharis[10], E. Zaffaroni[53], R. Zaidan[14], A.M. Zaitsev[122,an], T. Zakareishvili[157b], N. Zakharchuk[33], S. Zambito[58], D. Zanzi[35], D.R. Zaripovas[56], S.V. Zeißner[46], C. Zeitnitz[180], G. Zemaityte[133], J.C. Zeng[171], O. Zenin[122], D. Zerwas[130], M. Zgubič[133], D.F. Zhang[15b], F. Zhang[179], G. Zhang[59a], G. Zhang[15b], H. Zhang[15c], J. Zhang[6], L. Zhang[15c], L. Zhang[59a], M. Zhang[171], R. Zhang[59a], R. Zhang[24], X. Zhang[59b], Y. Zhang[15d], Z. Zhang[62a], Z. Zhang[130], P. Zhao[48], Y. Zhao[59b], Z. Zhao[59a], A. Zhemchugov[78], Z. Zheng[104], D. Zhong[171], B. Zhou[104], C. Zhou[179], M.S. Zhou[15d], M. Zhou[153], N. Zhou[59c], Y. Zhou[7], C.G. Zhu[59b], H.L. Zhu[59a], H. Zhu[15a], J. Zhu[104], Y. Zhu[59a], X. Zhuang[15a], K. Zhukov[109], V. Zhulanov[121b,121a], D. Zieminska[64], N.I. Zimine[78], S. Zimmermann[51], Z. Zinonos[114], M. Ziolkowski[149], G. Zobernig[179], A. Zoccoli[23b,23a], K. Zoch[52], T.G. Zorbas[147], R. Zou[36], L. Zwalinski[35].

[1]Department of Physics, University of Adelaide, Adelaide; Australia.
[2]Physics Department, SUNY Albany, Albany NY; United States of America.
[3]Department of Physics, University of Alberta, Edmonton AB; Canada.
[4(a)]Department of Physics, Ankara University, Ankara;[(b)]Istanbul Aydin University, Istanbul;[(c)]Division of Physics, TOBB University of Economics and Technology, Ankara; Turkey.
[5]LAPP, Université Grenoble Alpes, Université Savoie Mont Blanc, CNRS/IN2P3, Annecy; France.
[6]High Energy Physics Division, Argonne National Laboratory, Argonne IL; United States of America.
[7]Department of Physics, University of Arizona, Tucson AZ; United States of America.

[8]Department of Physics, University of Texas at Arlington, Arlington TX; United States of America.
[9]Physics Department, National and Kapodistrian University of Athens, Athens; Greece.
[10]Physics Department, National Technical University of Athens, Zografou; Greece.
[11]Department of Physics, University of Texas at Austin, Austin TX; United States of America.
[12(a)]Bahcesehir University, Faculty of Engineering and Natural Sciences, Istanbul;[(b)]Istanbul Bilgi University, Faculty of Engineering and Natural Sciences, Istanbul;[(c)]Department of Physics, Bogazici University, Istanbul;[(d)]Department of Physics Engineering, Gaziantep University, Gaziantep; Turkey.
[13]Institute of Physics, Azerbaijan Academy of Sciences, Baku; Azerbaijan.
[14]Institut de Física d'Altes Energies (IFAE), Barcelona Institute of Science and Technology, Barcelona; Spain.
[15(a)]Institute of High Energy Physics, Chinese Academy of Sciences, Beijing;[(b)]Physics Department, Tsinghua University, Beijing;[(c)]Department of Physics, Nanjing University, Nanjing;[(d)]University of Chinese Academy of Science (UCAS), Beijing; China.
[16]Institute of Physics, University of Belgrade, Belgrade; Serbia.
[17]Department for Physics and Technology, University of Bergen, Bergen; Norway.
[18]Physics Division, Lawrence Berkeley National Laboratory and University of California, Berkeley CA; United States of America.
[19]Institut für Physik, Humboldt Universität zu Berlin, Berlin; Germany.
[20]Albert Einstein Center for Fundamental Physics and Laboratory for High Energy Physics, University of Bern, Bern; Switzerland.
[21]School of Physics and Astronomy, University of Birmingham, Birmingham; United Kingdom.
[22]Facultad de Ciencias y Centro de Investigaciónes, Universidad Antonio Nariño, Bogota; Colombia.
[23(a)]INFN Bologna and Universita' di Bologna, Dipartimento di Fisica;[(b)]INFN Sezione di Bologna; Italy.
[24]Physikalisches Institut, Universität Bonn, Bonn; Germany.
[25]Department of Physics, Boston University, Boston MA; United States of America.
[26]Department of Physics, Brandeis University, Waltham MA; United States of America.
[27(a)]Transilvania University of Brasov, Brasov;[(b)]Horia Hulubei National Institute of Physics and Nuclear Engineering, Bucharest;[(c)]Department of Physics, Alexandru Ioan Cuza University of Iasi, Iasi;[(d)]National Institute for Research and Development of Isotopic and Molecular Technologies, Physics Department, Cluj-Napoca;[(e)]University Politehnica Bucharest, Bucharest;[(f)]West University in Timisoara, Timisoara; Romania.
[28(a)]Faculty of Mathematics, Physics and Informatics, Comenius University, Bratislava;[(b)]Department of Subnuclear Physics, Institute of Experimental Physics of the Slovak Academy of Sciences, Kosice; Slovak Republic.
[29]Physics Department, Brookhaven National Laboratory, Upton NY; United States of America.
[30]Departamento de Física, Universidad de Buenos Aires, Buenos Aires; Argentina.
[31]Cavendish Laboratory, University of Cambridge, Cambridge; United Kingdom.
[32(a)]Department of Physics, University of Cape Town, Cape Town;[(b)]Department of Mechanical Engineering Science, University of Johannesburg, Johannesburg;[(c)]School of Physics, University of the Witwatersrand, Johannesburg; South Africa.
[33]Department of Physics, Carleton University, Ottawa ON; Canada.
[34(a)]Faculté des Sciences Ain Chock, Réseau Universitaire de Physique des Hautes Energies - Université Hassan II, Casablanca;[(b)]Centre National de l'Energie des Sciences Techniques Nucleaires (CNESTEN), Rabat;[(c)]Faculté des Sciences Semlalia, Université Cadi Ayyad, LPHEA-Marrakech;[(d)]Faculté des Sciences, Université Mohamed Premier and LPTPM, Oujda;[(e)]Faculté des sciences, Université Mohammed V, Rabat; Morocco.
[35]CERN, Geneva; Switzerland.

[36]Enrico Fermi Institute, University of Chicago, Chicago IL; United States of America.
[37]LPC, Université Clermont Auvergne, CNRS/IN2P3, Clermont-Ferrand; France.
[38]Nevis Laboratory, Columbia University, Irvington NY; United States of America.
[39]Niels Bohr Institute, University of Copenhagen, Copenhagen; Denmark.
[40(a)]Dipartimento di Fisica, Università della Calabria, Rende;[(b)]INFN Gruppo Collegato di Cosenza, Laboratori Nazionali di Frascati; Italy.
[41]Physics Department, Southern Methodist University, Dallas TX; United States of America.
[42]Physics Department, University of Texas at Dallas, Richardson TX; United States of America.
[43]National Centre for Scientific Research "Demokritos", Agia Paraskevi; Greece.
[44(a)]Department of Physics, Stockholm University;[(b)]Oskar Klein Centre, Stockholm; Sweden.
[45]Deutsches Elektronen-Synchrotron DESY, Hamburg and Zeuthen; Germany.
[46]Lehrstuhl für Experimentelle Physik IV, Technische Universität Dortmund, Dortmund; Germany.
[47]Institut für Kern- und Teilchenphysik, Technische Universität Dresden, Dresden; Germany.
[48]Department of Physics, Duke University, Durham NC; United States of America.
[49]SUPA - School of Physics and Astronomy, University of Edinburgh, Edinburgh; United Kingdom.
[50]INFN e Laboratori Nazionali di Frascati, Frascati; Italy.
[51]Physikalisches Institut, Albert-Ludwigs-Universität Freiburg, Freiburg; Germany.
[52]II. Physikalisches Institut, Georg-August-Universität Göttingen, Göttingen; Germany.
[53]Département de Physique Nucléaire et Corpusculaire, Université de Genève, Genève; Switzerland.
[54(a)]Dipartimento di Fisica, Università di Genova, Genova;[(b)]INFN Sezione di Genova; Italy.
[55]II. Physikalisches Institut, Justus-Liebig-Universität Giessen, Giessen; Germany.
[56]SUPA - School of Physics and Astronomy, University of Glasgow, Glasgow; United Kingdom.
[57]LPSC, Université Grenoble Alpes, CNRS/IN2P3, Grenoble INP, Grenoble; France.
[58]Laboratory for Particle Physics and Cosmology, Harvard University, Cambridge MA; United States of America.
[59(a)]Department of Modern Physics and State Key Laboratory of Particle Detection and Electronics, University of Science and Technology of China, Hefei;[(b)]Institute of Frontier and Interdisciplinary Science and Key Laboratory of Particle Physics and Particle Irradiation (MOE), Shandong University, Qingdao;[(c)]School of Physics and Astronomy, Shanghai Jiao Tong University, KLPPAC-MoE, SKLPPC, Shanghai;[(d)]Tsung-Dao Lee Institute, Shanghai; China.
[60(a)]Kirchhoff-Institut für Physik, Ruprecht-Karls-Universität Heidelberg, Heidelberg;[(b)]Physikalisches Institut, Ruprecht-Karls-Universität Heidelberg, Heidelberg; Germany.
[61]Faculty of Applied Information Science, Hiroshima Institute of Technology, Hiroshima; Japan.
[62(a)]Department of Physics, Chinese University of Hong Kong, Shatin, N.T., Hong Kong;[(b)]Department of Physics, University of Hong Kong, Hong Kong;[(c)]Department of Physics and Institute for Advanced Study, Hong Kong University of Science and Technology, Clear Water Bay, Kowloon, Hong Kong; China.
[63]Department of Physics, National Tsing Hua University, Hsinchu; Taiwan.
[64]Department of Physics, Indiana University, Bloomington IN; United States of America.
[65(a)]INFN Gruppo Collegato di Udine, Sezione di Trieste, Udine;[(b)]ICTP, Trieste;[(c)]Dipartimento Politecnico di Ingegneria e Architettura, Università di Udine, Udine; Italy.
[66(a)]INFN Sezione di Lecce;[(b)]Dipartimento di Matematica e Fisica, Università del Salento, Lecce; Italy.
[67(a)]INFN Sezione di Milano;[(b)]Dipartimento di Fisica, Università di Milano, Milano; Italy.
[68(a)]INFN Sezione di Napoli;[(b)]Dipartimento di Fisica, Università di Napoli, Napoli; Italy.
[69(a)]INFN Sezione di Pavia;[(b)]Dipartimento di Fisica, Università di Pavia, Pavia; Italy.
[70(a)]INFN Sezione di Pisa;[(b)]Dipartimento di Fisica E. Fermi, Università di Pisa, Pisa; Italy.
[71(a)]INFN Sezione di Roma;[(b)]Dipartimento di Fisica, Sapienza Università di Roma, Roma; Italy.
[72(a)]INFN Sezione di Roma Tor Vergata;[(b)]Dipartimento di Fisica, Università di Roma Tor Vergata, Roma;

Italy.
[73(a)]INFN Sezione di Roma Tre;[(b)]Dipartimento di Matematica e Fisica, Università Roma Tre, Roma; Italy.
[74(a)]INFN-TIFPA;[(b)]Università degli Studi di Trento, Trento; Italy.
[75]Institut für Astro- und Teilchenphysik, Leopold-Franzens-Universität, Innsbruck; Austria.
[76]University of Iowa, Iowa City IA; United States of America.
[77]Department of Physics and Astronomy, Iowa State University, Ames IA; United States of America.
[78]Joint Institute for Nuclear Research, Dubna; Russia.
[79(a)]Departamento de Engenharia Elétrica, Universidade Federal de Juiz de Fora (UFJF), Juiz de Fora;[(b)]Universidade Federal do Rio De Janeiro COPPE/EE/IF, Rio de Janeiro;[(c)]Universidade Federal de São João del Rei (UFSJ), São João del Rei;[(d)]Instituto de Física, Universidade de São Paulo, São Paulo; Brazil.
[80]KEK, High Energy Accelerator Research Organization, Tsukuba; Japan.
[81]Graduate School of Science, Kobe University, Kobe; Japan.
[82(a)]AGH University of Science and Technology, Faculty of Physics and Applied Computer Science, Krakow;[(b)]Marian Smoluchowski Institute of Physics, Jagiellonian University, Krakow; Poland.
[83]Institute of Nuclear Physics Polish Academy of Sciences, Krakow; Poland.
[84]Faculty of Science, Kyoto University, Kyoto; Japan.
[85]Kyoto University of Education, Kyoto; Japan.
[86]Research Center for Advanced Particle Physics and Department of Physics, Kyushu University, Fukuoka ; Japan.
[87]Instituto de Física La Plata, Universidad Nacional de La Plata and CONICET, La Plata; Argentina.
[88]Physics Department, Lancaster University, Lancaster; United Kingdom.
[89]Oliver Lodge Laboratory, University of Liverpool, Liverpool; United Kingdom.
[90]Department of Experimental Particle Physics, Jožef Stefan Institute and Department of Physics, University of Ljubljana, Ljubljana; Slovenia.
[91]School of Physics and Astronomy, Queen Mary University of London, London; United Kingdom.
[92]Department of Physics, Royal Holloway University of London, Egham; United Kingdom.
[93]Department of Physics and Astronomy, University College London, London; United Kingdom.
[94]Louisiana Tech University, Ruston LA; United States of America.
[95]Fysiska institutionen, Lunds universitet, Lund; Sweden.
[96]Centre de Calcul de l'Institut National de Physique Nucléaire et de Physique des Particules (IN2P3), Villeurbanne; France.
[97]Departamento de Física Teorica C-15 and CIAFF, Universidad Autónoma de Madrid, Madrid; Spain.
[98]Institut für Physik, Universität Mainz, Mainz; Germany.
[99]School of Physics and Astronomy, University of Manchester, Manchester; United Kingdom.
[100]CPPM, Aix-Marseille Université, CNRS/IN2P3, Marseille; France.
[101]Department of Physics, University of Massachusetts, Amherst MA; United States of America.
[102]Department of Physics, McGill University, Montreal QC; Canada.
[103]School of Physics, University of Melbourne, Victoria; Australia.
[104]Department of Physics, University of Michigan, Ann Arbor MI; United States of America.
[105]Department of Physics and Astronomy, Michigan State University, East Lansing MI; United States of America.
[106]B.I. Stepanov Institute of Physics, National Academy of Sciences of Belarus, Minsk; Belarus.
[107]Research Institute for Nuclear Problems of Byelorussian State University, Minsk; Belarus.
[108]Group of Particle Physics, University of Montreal, Montreal QC; Canada.
[109]P.N. Lebedev Physical Institute of the Russian Academy of Sciences, Moscow; Russia.
[110]Institute for Theoretical and Experimental Physics of the National Research Centre Kurchatov Institute,

Moscow; Russia.
[111]National Research Nuclear University MEPhI, Moscow; Russia.
[112]D.V. Skobeltsyn Institute of Nuclear Physics, M.V. Lomonosov Moscow State University, Moscow; Russia.
[113]Fakultät für Physik, Ludwig-Maximilians-Universität München, München; Germany.
[114]Max-Planck-Institut für Physik (Werner-Heisenberg-Institut), München; Germany.
[115]Nagasaki Institute of Applied Science, Nagasaki; Japan.
[116]Graduate School of Science and Kobayashi-Maskawa Institute, Nagoya University, Nagoya; Japan.
[117]Department of Physics and Astronomy, University of New Mexico, Albuquerque NM; United States of America.
[118]Institute for Mathematics, Astrophysics and Particle Physics, Radboud University Nijmegen/Nikhef, Nijmegen; Netherlands.
[119]Nikhef National Institute for Subatomic Physics and University of Amsterdam, Amsterdam; Netherlands.
[120]Department of Physics, Northern Illinois University, DeKalb IL; United States of America.
[121(a)]Budker Institute of Nuclear Physics and NSU, SB RAS, Novosibirsk;[(b)]Novosibirsk State University Novosibirsk; Russia.
[122]Institute for High Energy Physics of the National Research Centre Kurchatov Institute, Protvino; Russia.
[123]Department of Physics, New York University, New York NY; United States of America.
[124]Ohio State University, Columbus OH; United States of America.
[125]Faculty of Science, Okayama University, Okayama; Japan.
[126]Homer L. Dodge Department of Physics and Astronomy, University of Oklahoma, Norman OK; United States of America.
[127]Department of Physics, Oklahoma State University, Stillwater OK; United States of America.
[128]Palacký University, RCPTM, Joint Laboratory of Optics, Olomouc; Czech Republic.
[129]Center for High Energy Physics, University of Oregon, Eugene OR; United States of America.
[130]LAL, Université Paris-Sud, CNRS/IN2P3, Université Paris-Saclay, Orsay; France.
[131]Graduate School of Science, Osaka University, Osaka; Japan.
[132]Department of Physics, University of Oslo, Oslo; Norway.
[133]Department of Physics, Oxford University, Oxford; United Kingdom.
[134]LPNHE, Sorbonne Université, Paris Diderot Sorbonne Paris Cité, CNRS/IN2P3, Paris; France.
[135]Department of Physics, University of Pennsylvania, Philadelphia PA; United States of America.
[136]Konstantinov Nuclear Physics Institute of National Research Centre "Kurchatov Institute", PNPI, St. Petersburg; Russia.
[137]Department of Physics and Astronomy, University of Pittsburgh, Pittsburgh PA; United States of America.
[138(a)]Laboratório de Instrumentação e Física Experimental de Partículas - LIP;[(b)]Departamento de Física, Faculdade de Ciências, Universidade de Lisboa, Lisboa;[(c)]Departamento de Física, Universidade de Coimbra, Coimbra;[(d)]Centro de Física Nuclear da Universidade de Lisboa, Lisboa;[(e)]Departamento de Física, Universidade do Minho, Braga;[(f)]Universidad de Granada, Granada (Spain);[(g)]Dep Física and CEFITEC of Faculdade de Ciências e Tecnologia, Universidade Nova de Lisboa, Caparica; Portugal.
[139]Institute of Physics of the Czech Academy of Sciences, Prague; Czech Republic.
[140]Czech Technical University in Prague, Prague; Czech Republic.
[141]Charles University, Faculty of Mathematics and Physics, Prague; Czech Republic.
[142]Particle Physics Department, Rutherford Appleton Laboratory, Didcot; United Kingdom.
[143]IRFU, CEA, Université Paris-Saclay, Gif-sur-Yvette; France.
[144]Santa Cruz Institute for Particle Physics, University of California Santa Cruz, Santa Cruz CA; United

States of America.
[145](a)Departamento de Física, Pontificia Universidad Católica de Chile, Santiago;(b)Departamento de Física, Universidad Técnica Federico Santa María, Valparaíso; Chile.
[146]Department of Physics, University of Washington, Seattle WA; United States of America.
[147]Department of Physics and Astronomy, University of Sheffield, Sheffield; United Kingdom.
[148]Department of Physics, Shinshu University, Nagano; Japan.
[149]Department Physik, Universität Siegen, Siegen; Germany.
[150]Department of Physics, Simon Fraser University, Burnaby BC; Canada.
[151]SLAC National Accelerator Laboratory, Stanford CA; United States of America.
[152]Physics Department, Royal Institute of Technology, Stockholm; Sweden.
[153]Departments of Physics and Astronomy, Stony Brook University, Stony Brook NY; United States of America.
[154]Department of Physics and Astronomy, University of Sussex, Brighton; United Kingdom.
[155]School of Physics, University of Sydney, Sydney; Australia.
[156]Institute of Physics, Academia Sinica, Taipei; Taiwan.
[157](a)E. Andronikashvili Institute of Physics, Iv. Javakhishvili Tbilisi State University, Tbilisi;(b)High Energy Physics Institute, Tbilisi State University, Tbilisi; Georgia.
[158]Department of Physics, Technion, Israel Institute of Technology, Haifa; Israel.
[159]Raymond and Beverly Sackler School of Physics and Astronomy, Tel Aviv University, Tel Aviv; Israel.
[160]Department of Physics, Aristotle University of Thessaloniki, Thessaloniki; Greece.
[161]International Center for Elementary Particle Physics and Department of Physics, University of Tokyo, Tokyo; Japan.
[162]Graduate School of Science and Technology, Tokyo Metropolitan University, Tokyo; Japan.
[163]Department of Physics, Tokyo Institute of Technology, Tokyo; Japan.
[164]Tomsk State University, Tomsk; Russia.
[165]Department of Physics, University of Toronto, Toronto ON; Canada.
[166](a)TRIUMF, Vancouver BC;(b)Department of Physics and Astronomy, York University, Toronto ON; Canada.
[167]Division of Physics and Tomonaga Center for the History of the Universe, Faculty of Pure and Applied Sciences, University of Tsukuba, Tsukuba; Japan.
[168]Department of Physics and Astronomy, Tufts University, Medford MA; United States of America.
[169]Department of Physics and Astronomy, University of California Irvine, Irvine CA; United States of America.
[170]Department of Physics and Astronomy, University of Uppsala, Uppsala; Sweden.
[171]Department of Physics, University of Illinois, Urbana IL; United States of America.
[172]Instituto de Física Corpuscular (IFIC), Centro Mixto Universidad de Valencia - CSIC, Valencia; Spain.
[173]Department of Physics, University of British Columbia, Vancouver BC; Canada.
[174]Department of Physics and Astronomy, University of Victoria, Victoria BC; Canada.
[175]Fakultät für Physik und Astronomie, Julius-Maximilians-Universität Würzburg, Würzburg; Germany.
[176]Department of Physics, University of Warwick, Coventry; United Kingdom.
[177]Waseda University, Tokyo; Japan.
[178]Department of Particle Physics, Weizmann Institute of Science, Rehovot; Israel.
[179]Department of Physics, University of Wisconsin, Madison WI; United States of America.
[180]Fakultät für Mathematik und Naturwissenschaften, Fachgruppe Physik, Bergische Universität Wuppertal, Wuppertal; Germany.
[181]Department of Physics, Yale University, New Haven CT; United States of America.
[182]Yerevan Physics Institute, Yerevan; Armenia.

[a] Also at Borough of Manhattan Community College, City University of New York, NY; United States of America.
[b] Also at California State University, East Bay; United States of America.
[c] Also at Centre for High Performance Computing, CSIR Campus, Rosebank, Cape Town; South Africa.
[d] Also at CERN, Geneva; Switzerland.
[e] Also at CPPM, Aix-Marseille Université, CNRS/IN2P3, Marseille; France.
[f] Also at Département de Physique Nucléaire et Corpusculaire, Université de Genève, Genève; Switzerland.
[g] Also at Departament de Fisica de la Universitat Autonoma de Barcelona, Barcelona; Spain.
[h] Also at Departamento de Física, Instituto Superior Técnico, Universidade de Lisboa, Lisboa; Portugal.
[i] Also at Department of Applied Physics and Astronomy, University of Sharjah, Sharjah; United Arab Emirates.
[j] Also at Department of Financial and Management Engineering, University of the Aegean, Chios; Greece.
[k] Also at Department of Physics and Astronomy, University of Louisville, Louisville, KY; United States of America.
[l] Also at Department of Physics and Astronomy, University of Sheffield, Sheffield; United Kingdom.
[m] Also at Department of Physics, California State University, Fresno CA; United States of America.
[n] Also at Department of Physics, California State University, Sacramento CA; United States of America.
[o] Also at Department of Physics, King's College London, London; United Kingdom.
[p] Also at Department of Physics, St. Petersburg State Polytechnical University, St. Petersburg; Russia.
[q] Also at Department of Physics, Stanford University, Stanford CA; United States of America.
[r] Also at Department of Physics, University of Fribourg, Fribourg; Switzerland.
[s] Also at Department of Physics, University of Michigan, Ann Arbor MI; United States of America.
[t] Also at Giresun University, Faculty of Engineering, Giresun; Turkey.
[u] Also at Graduate School of Science, Osaka University, Osaka; Japan.
[v] Also at Hellenic Open University, Patras; Greece.
[w] Also at Horia Hulubei National Institute of Physics and Nuclear Engineering, Bucharest; Romania.
[x] Also at Institucio Catalana de Recerca i Estudis Avancats, ICREA, Barcelona; Spain.
[y] Also at Institut für Experimentalphysik, Universität Hamburg, Hamburg; Germany.
[z] Also at Institute for Mathematics, Astrophysics and Particle Physics, Radboud University Nijmegen/Nikhef, Nijmegen; Netherlands.
[aa] Also at Institute for Nuclear Research and Nuclear Energy (INRNE) of the Bulgarian Academy of Sciences, Sofia; Bulgaria.
[ab] Also at Institute for Particle and Nuclear Physics, Wigner Research Centre for Physics, Budapest; Hungary.
[ac] Also at Institute of Particle Physics (IPP); Canada.
[ad] Also at Institute of Physics, Academia Sinica, Taipei; Taiwan.
[ae] Also at Institute of Physics, Azerbaijan Academy of Sciences, Baku; Azerbaijan.
[af] Also at Institute of Theoretical Physics, Ilia State University, Tbilisi; Georgia.
[ag] Also at Instituto de Física Teórica de la Universidad Autónoma de Madrid; Spain.
[ah] Also at Istanbul University, Dept. of Physics, Istanbul; Turkey.
[ai] Also at Joint Institute for Nuclear Research, Dubna; Russia.
[aj] Also at LAL, Université Paris-Sud, CNRS/IN2P3, Université Paris-Saclay, Orsay; France.
[ak] Also at Louisiana Tech University, Ruston LA; United States of America.
[al] Also at LPNHE, Sorbonne Université, Paris Diderot Sorbonne Paris Cité, CNRS/IN2P3, Paris; France.
[am] Also at Manhattan College, New York NY; United States of America.
[an] Also at Moscow Institute of Physics and Technology State University, Dolgoprudny; Russia.

[ao] Also at National Research Nuclear University MEPhI, Moscow; Russia.
[ap] Also at Physics Dept, University of South Africa, Pretoria; South Africa.
[aq] Also at Physikalisches Institut, Albert-Ludwigs-Universität Freiburg, Freiburg; Germany.
[ar] Also at School of Physics, Sun Yat-sen University, Guangzhou; China.
[as] Also at The City College of New York, New York NY; United States of America.
[at] Also at The Collaborative Innovation Center of Quantum Matter (CICQM), Beijing; China.
[au] Also at Tomsk State University, Tomsk, and Moscow Institute of Physics and Technology State University, Dolgoprudny; Russia.
[av] Also at TRIUMF, Vancouver BC; Canada.
[aw] Also at Universita di Napoli Parthenope, Napoli; Italy.
[*] Deceased